X-ray imaging using lenses

Oak Ridge/Argonne
National School on Neutron and X-ray Scattering
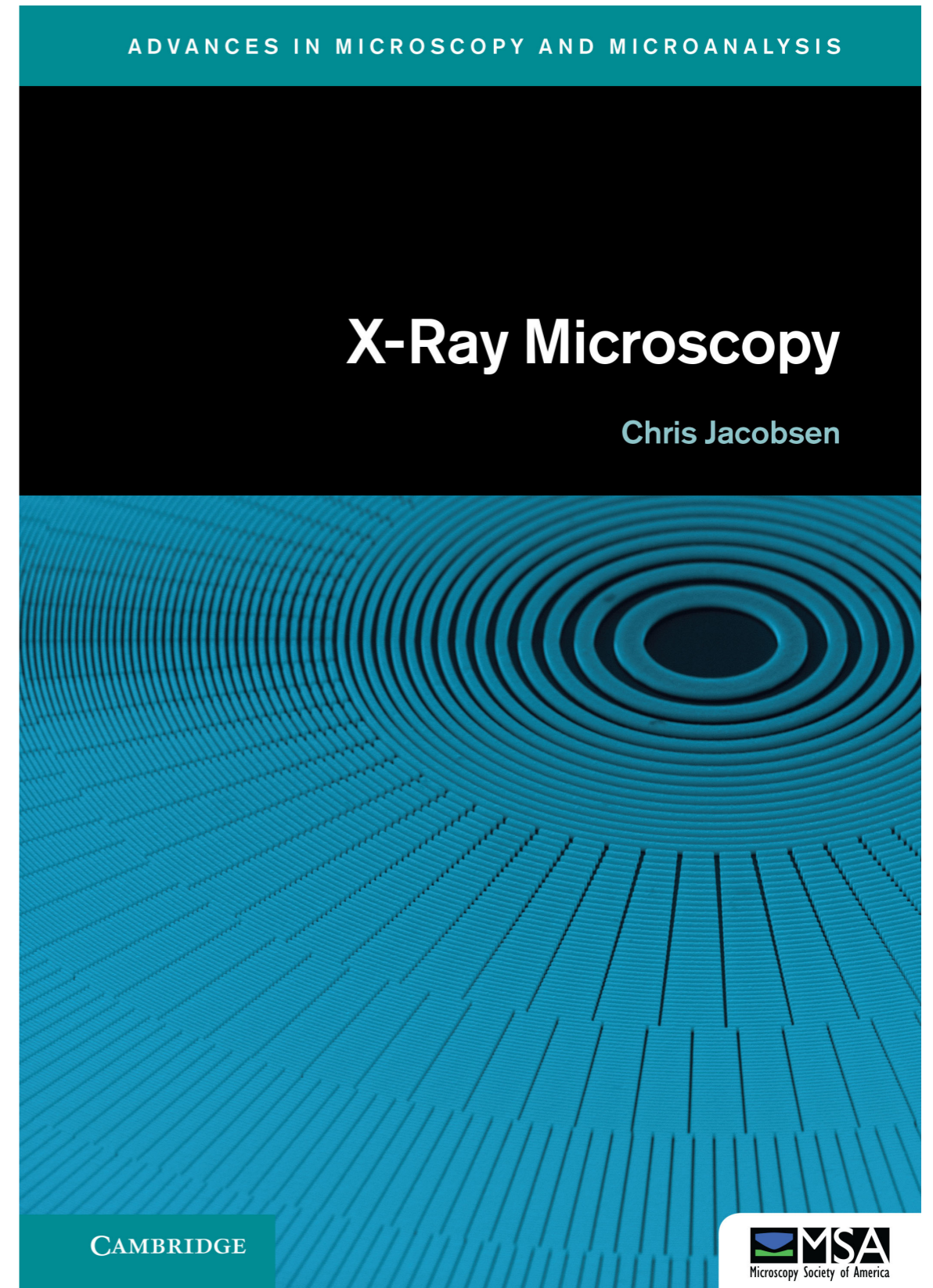
These slides:
https://tinyurl.com/yc79s6tu

Chris Jacobsen
Research Professor
Dept. Physics & Astronomy
Northwestern University

Shameful plug…

- Cambridge University Press, 2020.
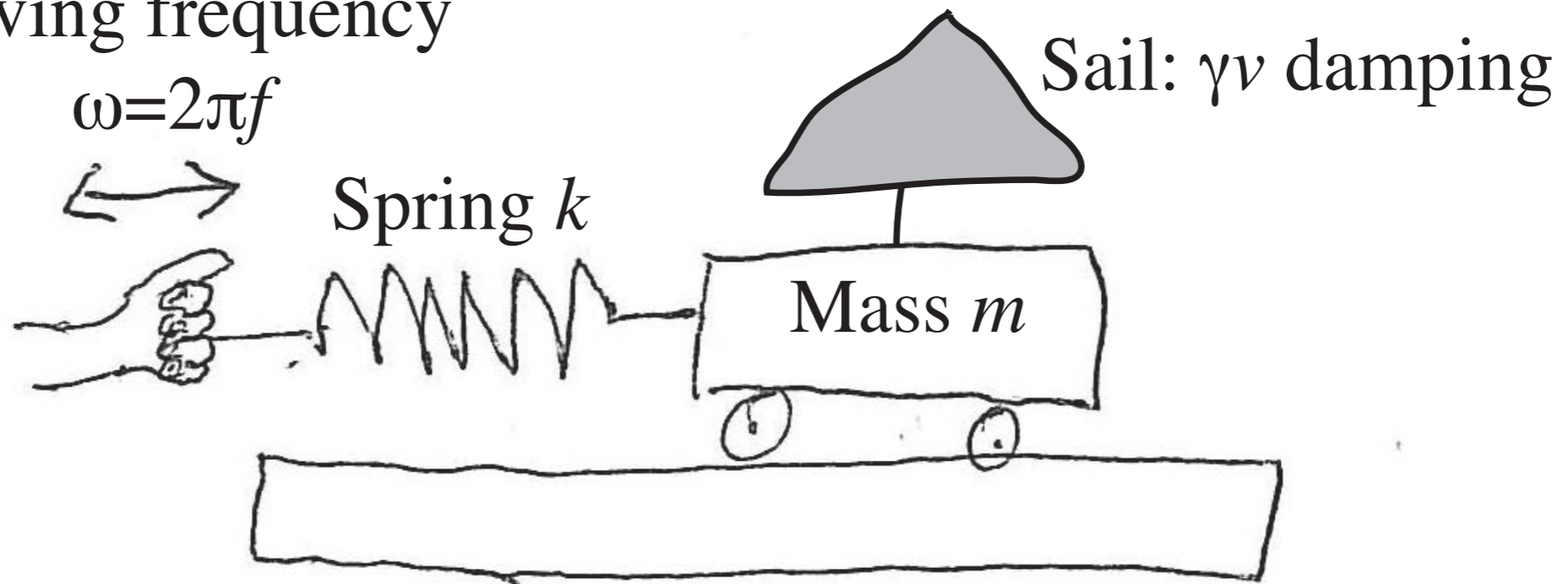- See www.cambridge.org/Jacobsen

ADVANCES IN MICROSCOPY AND MICROANALYSIS

X-Ray Microscopy

Chris Jacobsen

CAMBRIDGE

The refractive index

- Damped, driven harmonic oscillator

Driving frequency
$\omega = 2\pi f$

Spring k

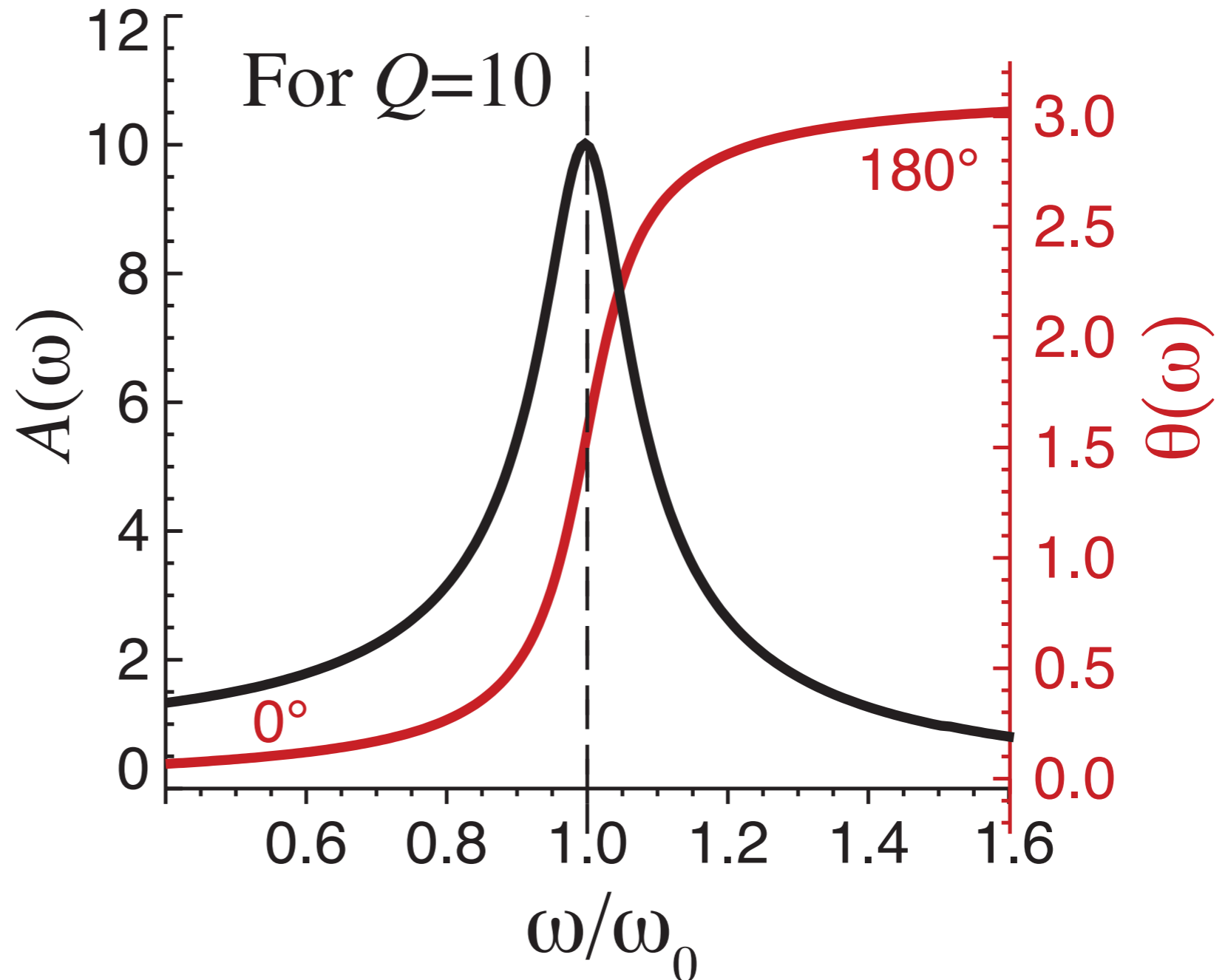Sail: γv damping

Mass m

- Damped: scattering, absorption
- Driven: incident electromagnetic wave ω
- Harmonic oscillator: electronic quantum state with energy

$$\hbar\omega = \hbar\sqrt{k/m}$$

Damped, driven harmonic oscillator

- Single resonance: absorption peak, phase shift across resonance

$$Q = \omega_0 / \gamma$$

Refractive index: 1902 Drude model

- General form:

$$n = 1 - \frac{n_a e^2}{2 m_e \epsilon_0} \sum_j \frac{(\omega^2 - \omega_j^2 + i\gamma_j\omega)\, g_j}{(\omega_j^2 - \omega^2)^2 + \gamma_j^2 \omega^2}$$

- Low frequency limit ($w << w_j$)

$$n = 1 + \left(\frac{n_a e^2}{2 m_e \epsilon_0} \sum_j \frac{g_j}{\omega_j^2} \right) + \omega^2 \left(\frac{n_a e^2}{2 m_e \epsilon_0} \sum_j \frac{g_j}{\omega_j^4} \right)$$

$$n = 1 + A(1 + \frac{B}{\lambda^2})$$

- High frequency limit ($w >> w_j$)

$$n = 1 - \frac{n_a e^2}{2 m_e \epsilon_0} \frac{1}{\omega^2} \sum_j g_j \left(1 + i\gamma_j/\omega\right)$$

$$n = 1 - \frac{r_e}{2\pi} n_a \lambda^2 (f_1 + i f_2)$$
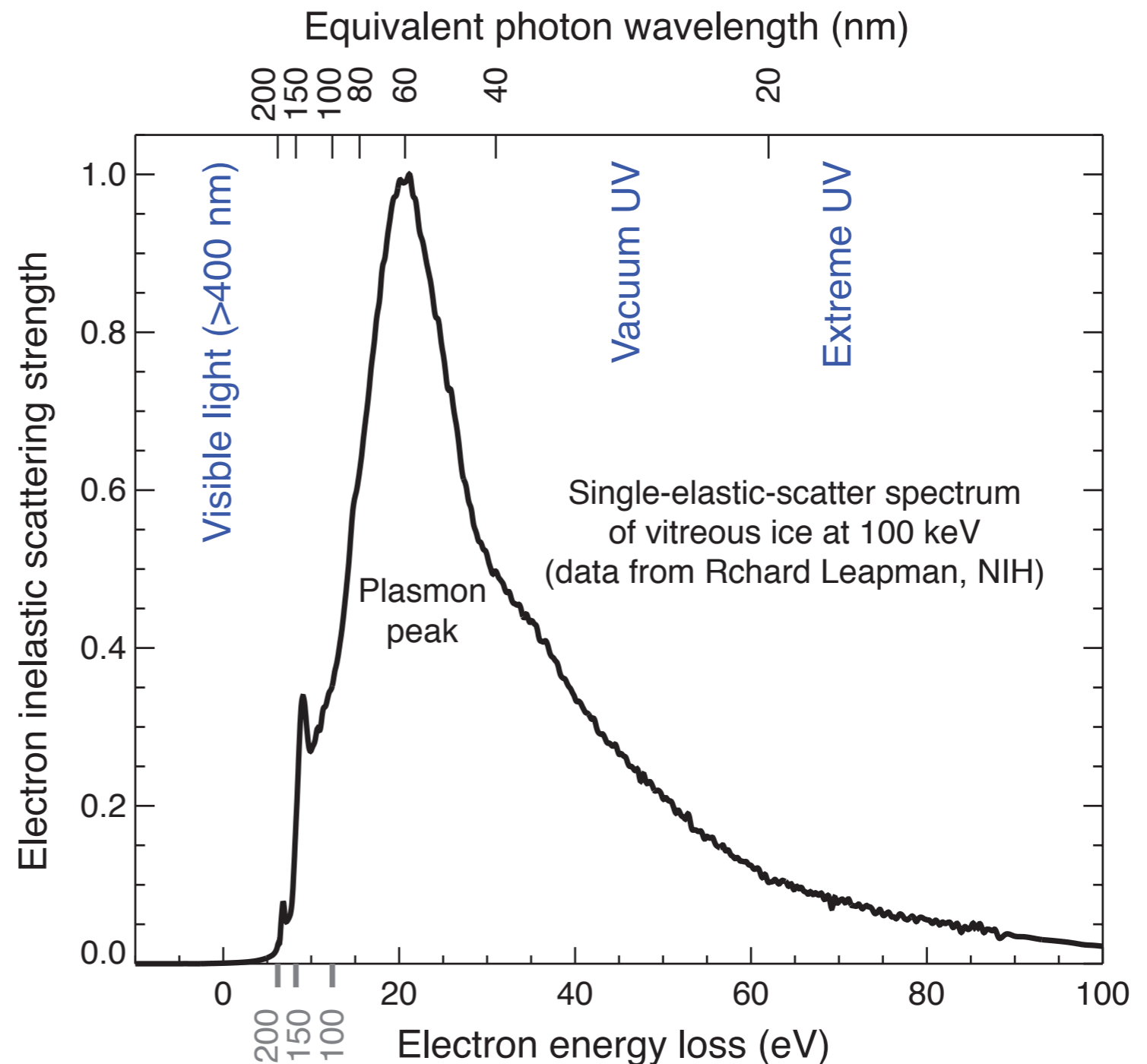
Also written as
$$f_1 + i f_2 \rightarrow f_0(\vec{q}) + \Delta f' + i \Delta f_{\prime\prime}$$

X-rays: the high frequency limit?

What's the dividing line between low and high frequency limits of refractive index? At what frequency are most of the oscillators?

Plasmon frequency

$\omega_p = (4\pi c^2 n_a r_e)^{1/2}$

Equivalent photon wavelength (nm)

Single-elastic-scatter spectrum of vitreous ice at 100 keV (data from Rchard Leapman, NIH)

Plasmon peak

Electron inelastic scattering strength

Electron energy loss (eV)

Visible light (>400 nm)

Vacuum UV

Extreme UV

Mysteries of the x-ray refractive index

Write refractive index as

$$n = 1 - \frac{n_a r_e}{2\pi}\lambda^2(f_1 + if_2)$$

$$= 1 - \alpha\lambda^2(f_1 + if_2)$$

where n_a=# atoms/volume, and

r_e=2.818x10^{-15} m is the classical radius of the electron. Assumes exp[$-i(kx-\omega t)$] for forward propagation.

Also written as n=1-δ-iβ

Phase velocity is

$$v_p = \frac{\omega}{k} \simeq c(1 + \alpha\lambda^2 f_1)$$

Group velocity is

$$v_g = \frac{d\omega}{dk} \simeq c(1 - \alpha\lambda^2 f_1)$$

Vor einigen Tagen erhielt ich von Herrn Prof. A. KÖHLER (Wiesbaden) eine kurze Arbeit[1], in welcher eine auffallende Erscheinung bei Röntgenaufnahmen geschildert ist, die sich bisher nicht hat deuten lassen. Die reproduzierten Aufnahmen — zumeist menschliche Gliedmaßen darstellend — zeigen an der Kontur einen hellen Saum von etwa 1 mm Breite, in welchem die Platte heller bestrahlt zu sein scheint als in der (nicht beschatteten) Umgebung des Röntgenbildes.

Ich möchte die Fachgenossen auf diese Erscheinung hinweisen und beifügen, daß die Erscheinung wahrscheinlich auf Total-reflexion beruht. Nach der klassischen Dispersionstheorie müssen wir erwarten, daß der Brechungsexponent n für Röntgenstrahlen nahe an 1 liegt, aber im allgemeinen doch von 1 verschieden ist. n wird kleiner bzw. größer als 1 sein, je nachdem der Einfluß derjenigen Elektronen auf die Dispersion überwiegt, deren Eigenfrequenz kleiner oder größer ist als die Frequenz der Röntgenstrahlen. Die Schwierigkeit einer Bestimmung von n liegt darin, daß $(n-1)$ sehr klein ist (etwa 10^{-5}). Es ist aber leicht einzusehen, daß bei nahezu streifender Inzidenz der Röntgenstrahlen im Falle $n < 1$ eine nachweisbare Totalreflexion auftreten muß.
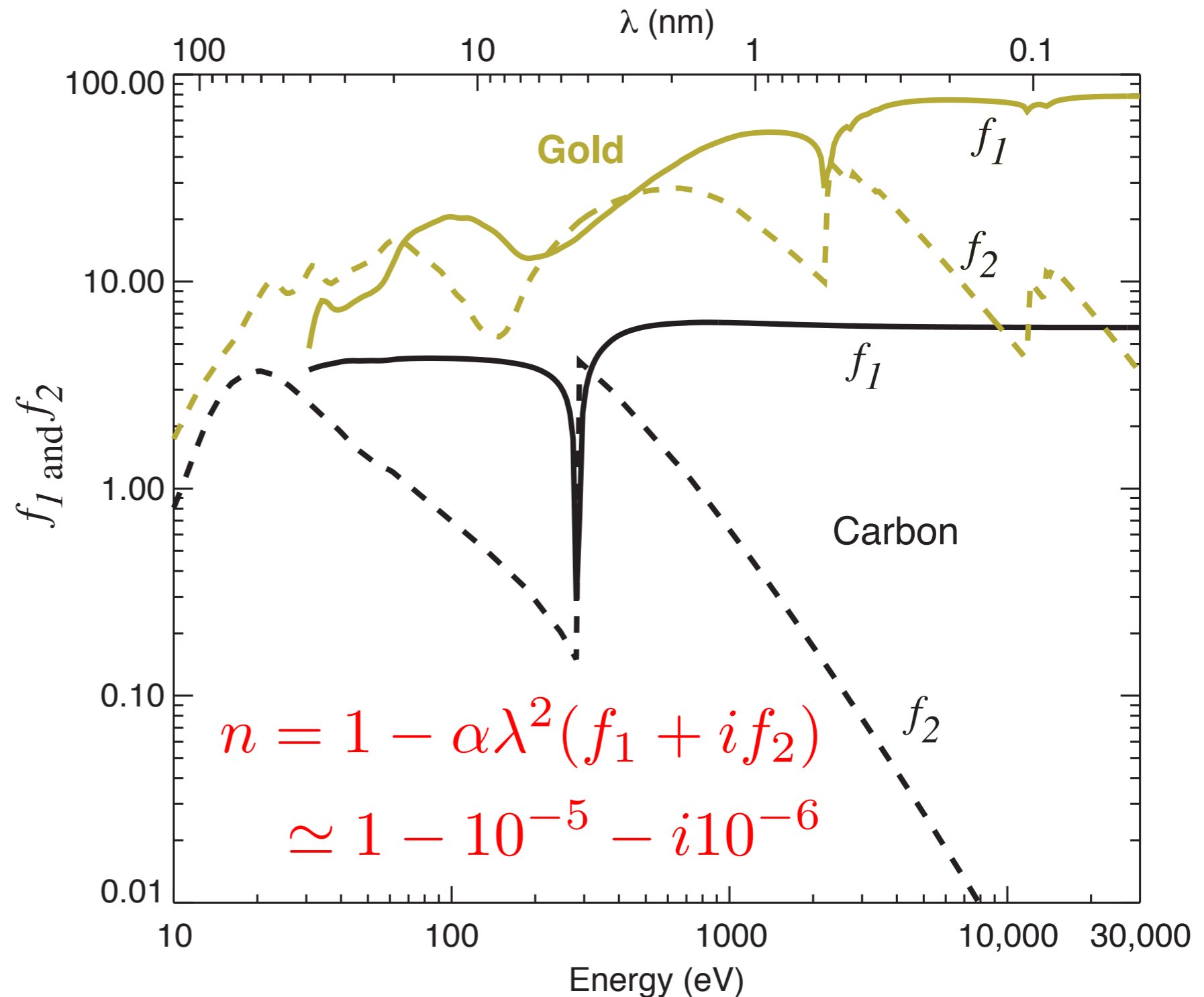
X-ray refractive index

Refractive index of
$n=1-\alpha\lambda^2(f_1+if_2)$

Real part of oscillator strength f_1 tends towards atomic number Z

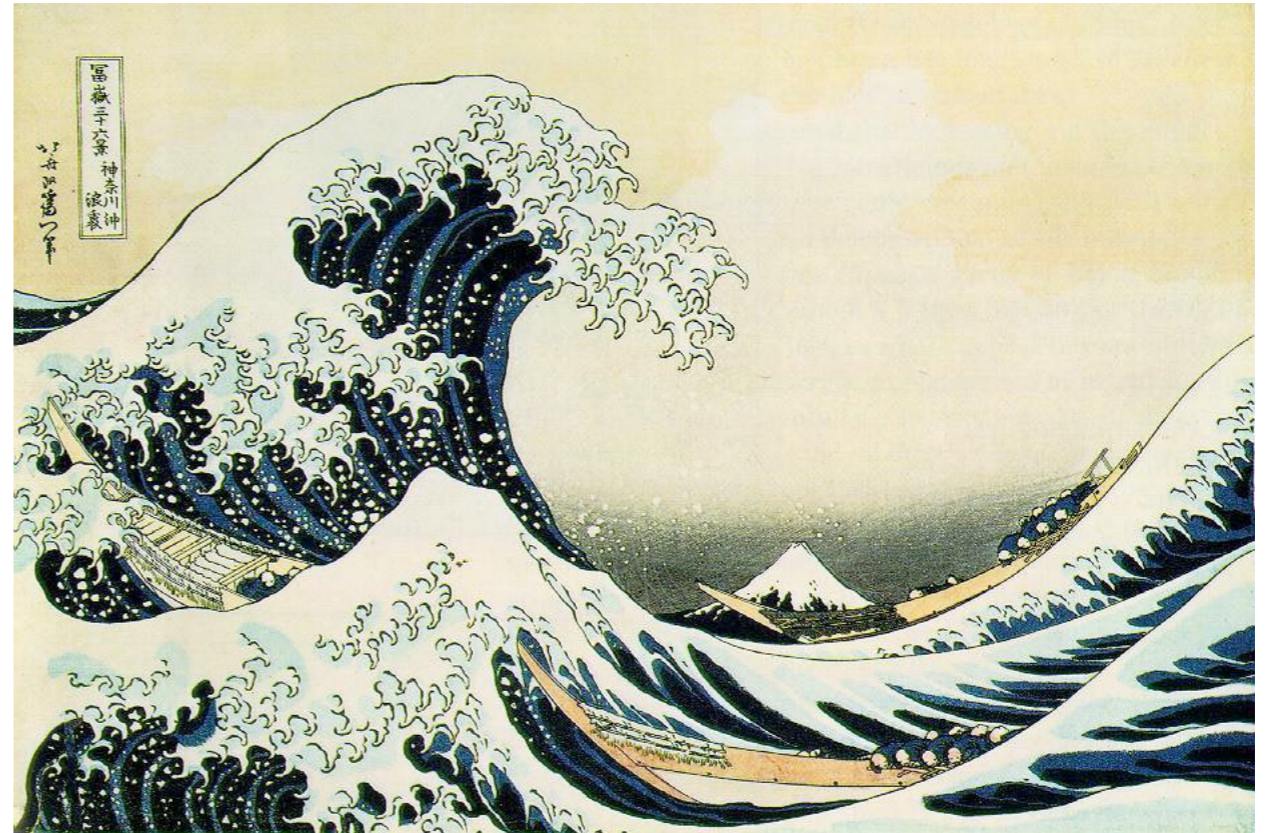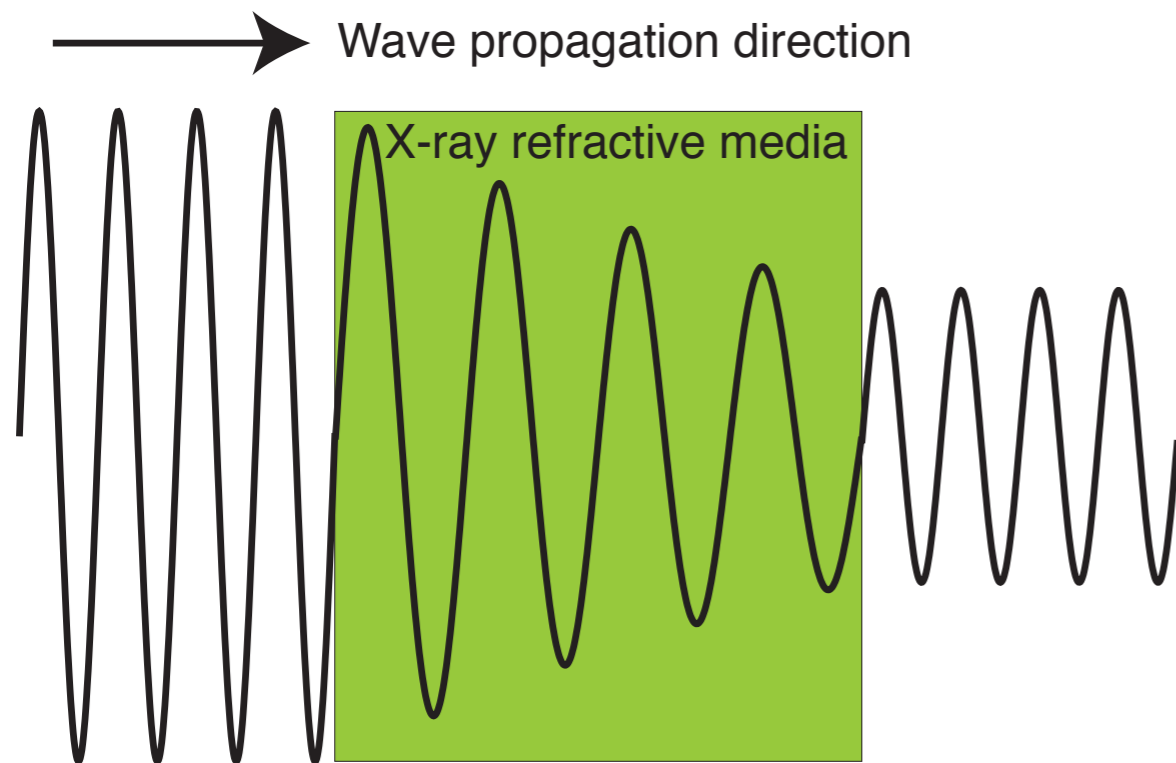Imaginary part of oscillator strength f_2 declines as E^{-2}

Phase exp[$-ink$] is advanced relative to vacuum by $2\pi\alpha\lambda f_1$
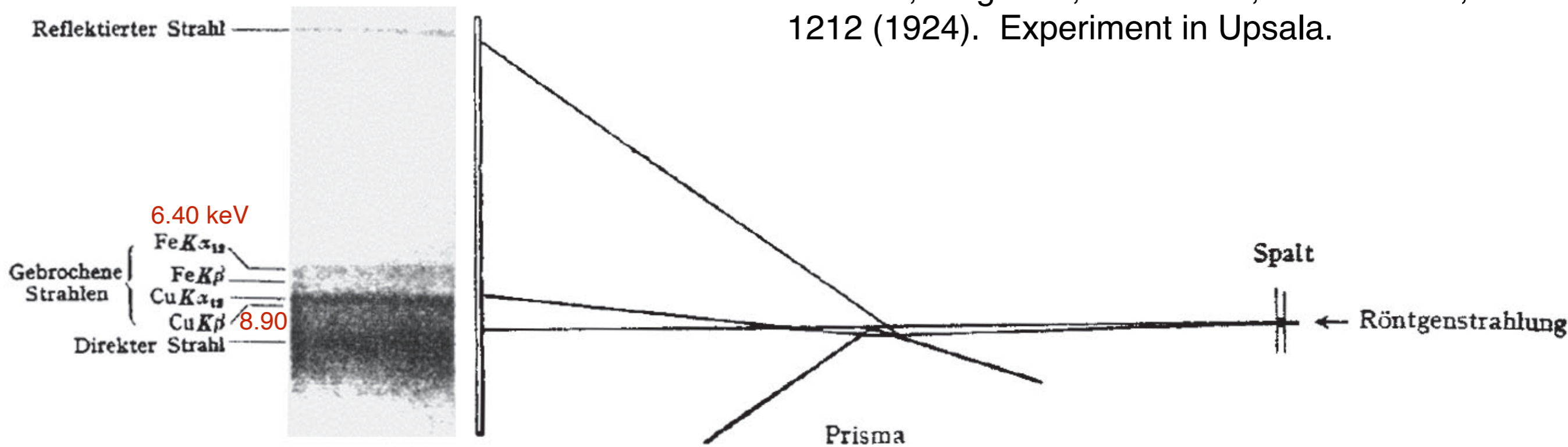
Intensity is decreased as exp[$-4\pi\alpha\lambda f_2$]

$$n = 1 - \alpha\lambda^2(f_1 + if_2)$$
$$\simeq 1 - 10^{-5} - i10^{-6}$$

Data from http://henke.lbl.gov/optical_constants/

X rays in media

Wave propagation direction

X-ray refractive media

X-ray refraction

Larsson, Siegbahn, and Waller, *Naturwis*. **12**, 1212 (1924). Experiment in Upsala.

Reflektierter Strahl

6.40 keV

Gebrochene Strahlen

FeKα₁₂
FeKβ
CuKα₁₂
CuKβ 8.90

Direkter Strahl

Spalt

Röntgenstrahlung

Prisma

X-ray mirrors use total internal reflection!

- Snell's law: $n_1 \sin(\theta_1) = n_2 \sin(\theta_2)$

- Total internal reflection at critical angle θ_c happens when $\theta_1 = 90°$, giving
$$\sin(\theta_c) = n_1/n_2$$
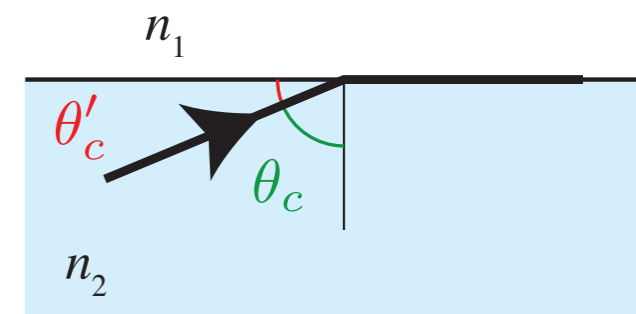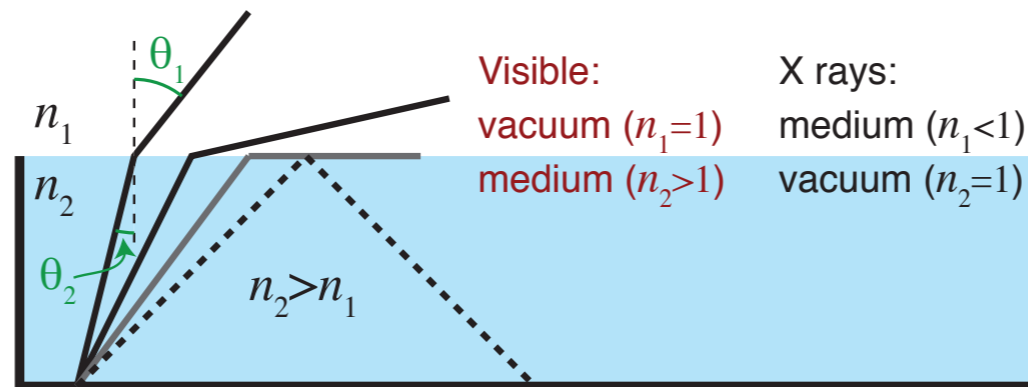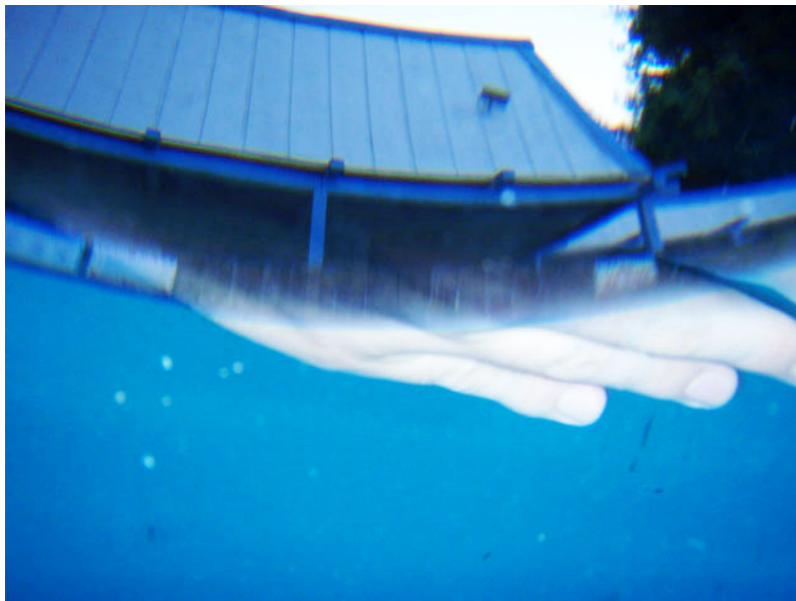
- For small $n = 1 - \delta$, switch to grazing angles $\theta' = 90° - \theta$. Critical angle:
$$\cos(\theta'_c) = (1 - \delta)/1 \quad \text{or} \quad 1 - (\theta_c)^2/2 \simeq 1 - \delta$$

- Thus critical angle is
$$\theta'_c \simeq \sqrt{2\delta} = \lambda\sqrt{2\alpha f_1}$$

- Note diffraction resolution limit of $\theta'_c/\lambda = \sqrt{2\alpha f_1}$ is (almost) independent of wavelength!
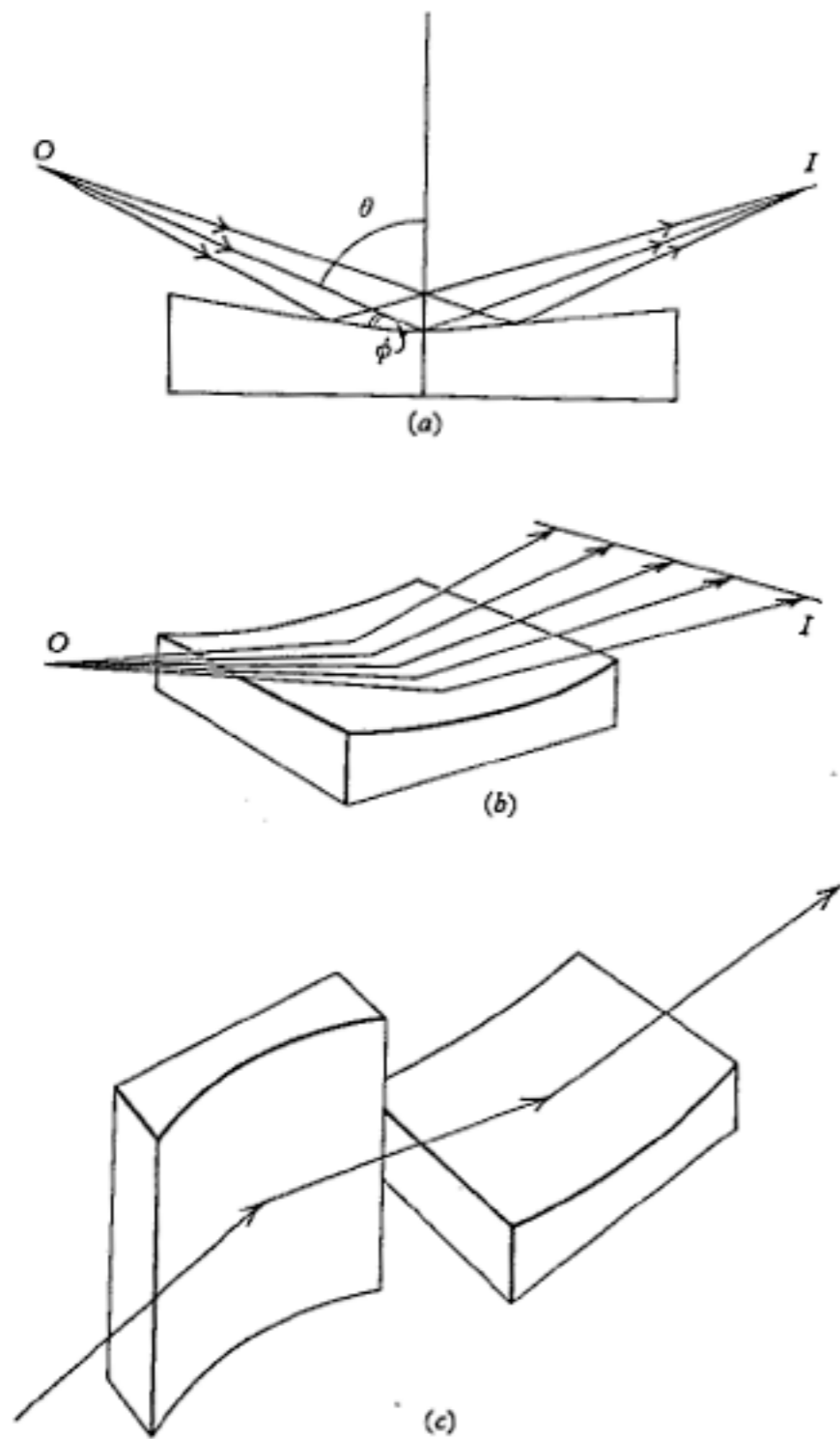
Paul Kirkpatrick and Albert Baez, 1948

Fig. 1.2. Reflexion X-ray microscopy. (a) and (b) X-rays diverging from a source O are focused by a cylindrical surface to form an astigmatic image I; (c) arrangement of two cylindrical mirrors for eliminating astigmatism. (Kirkpatrick & Pattee, 1953.)
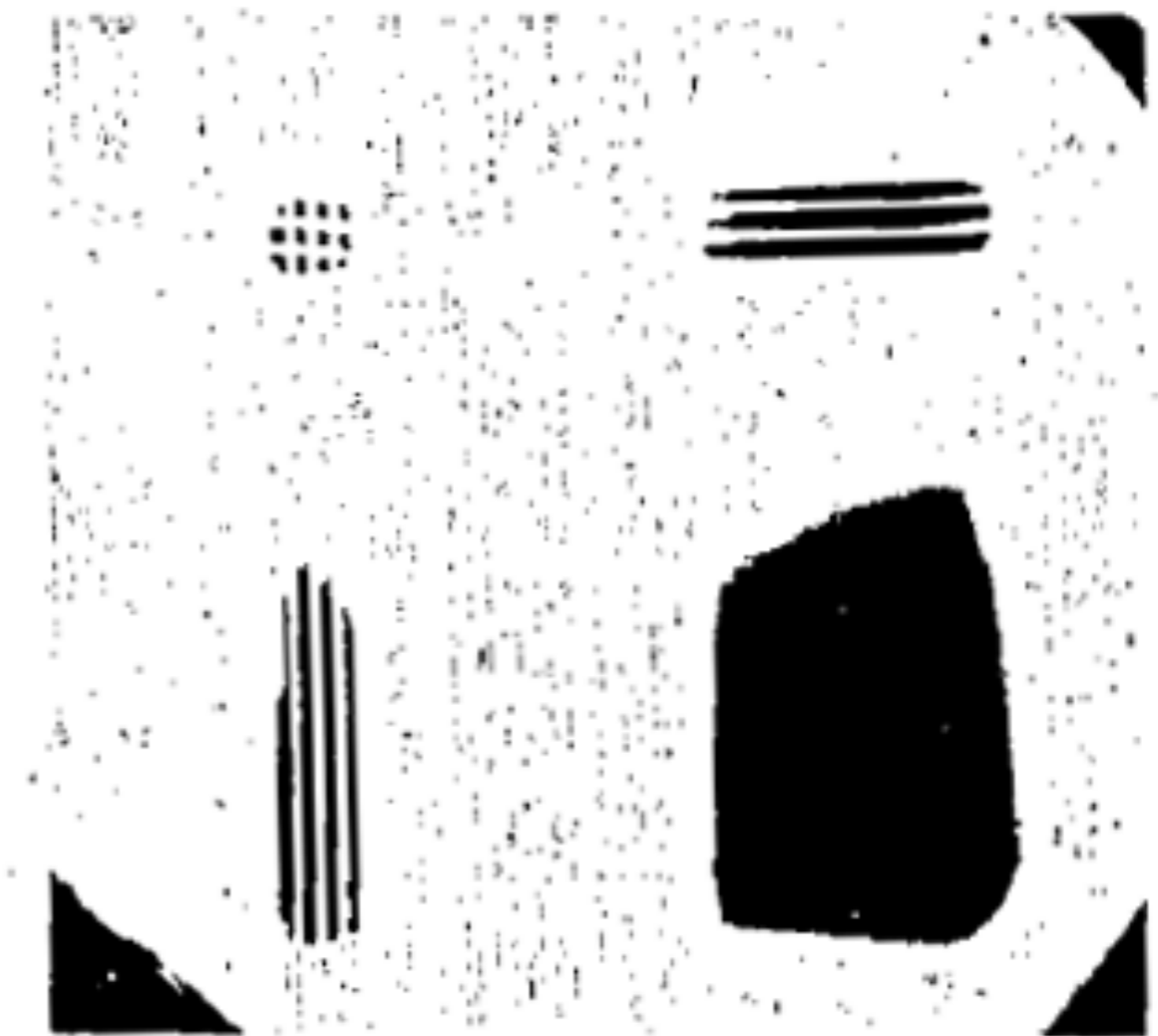

FIG. 12. Pattern produced by mirrors arranged as in Fig. 11. Object was a monel screen having 350 meshes per linear inch. In addition to the full image of the screen two partial images, each formed by one mirror, and a large spot caused by direct radiation appear above.

Albert Baez's famous daughter

ROCK&ROLL HALL OF FAME

TICKETS   VISIT   EXHIBITS   EVENTS   INDUCTEES   MISSION   MEMBERSHIP   SHOP   ENGLISH

JOAN BAEZ

< CLASS OF 2017   ALL INDUCTEES >

YEAR
2017

INDUCTED BY

Joan Baez breathed new life into folk music in the 1960s, powering rock music's turn toward social and political consciousness.

Baez's unwavering dedication to activism shows that volume isn't the only way to be loud—and totally rock and roll.

SCIENTIFIC AMERICAN

Established 1845

CONTENTS FOR MARCH 1949   VOLUME 180, NUMBER 3
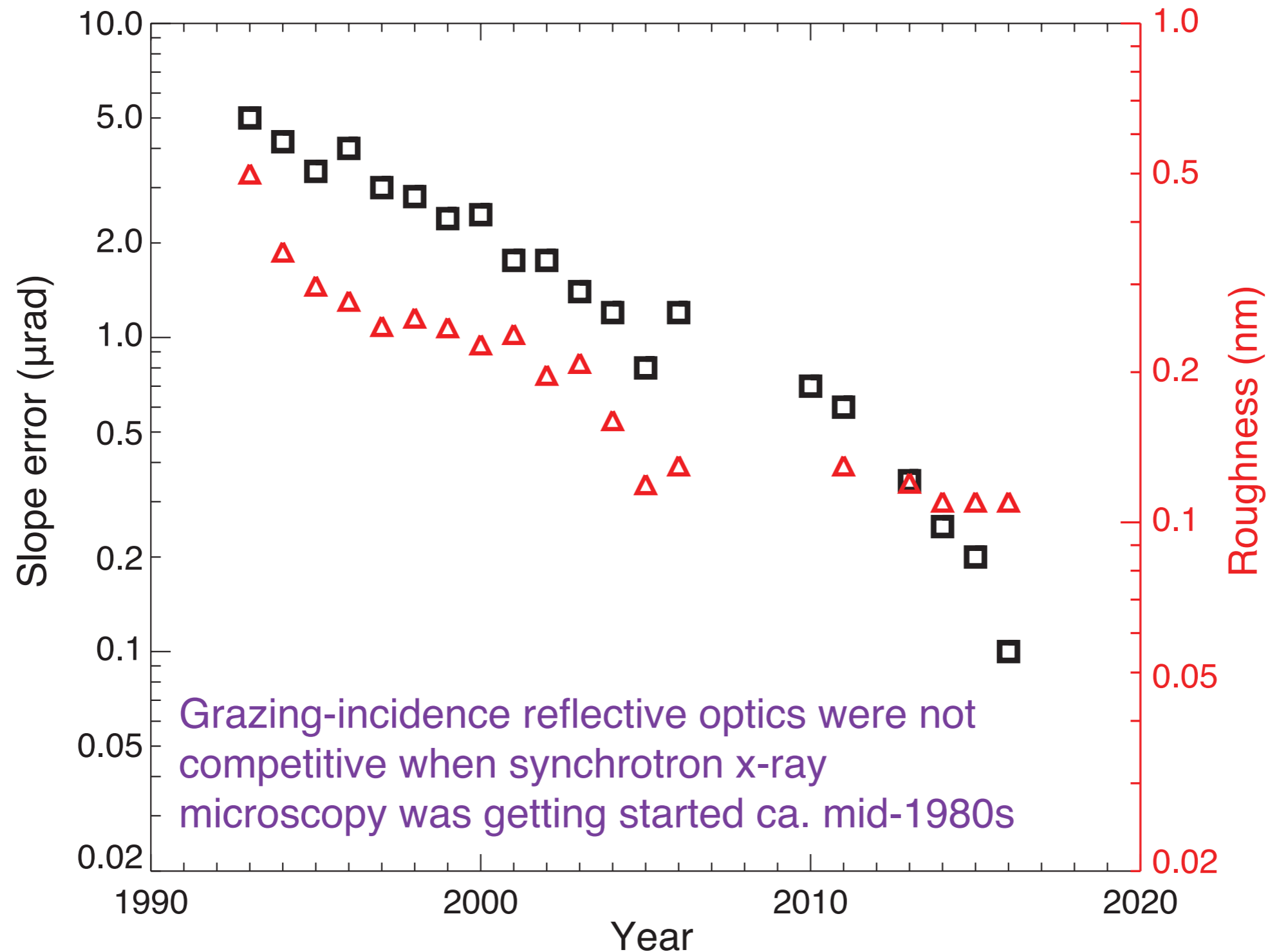
Kirkpatrick and Pattee, 1953
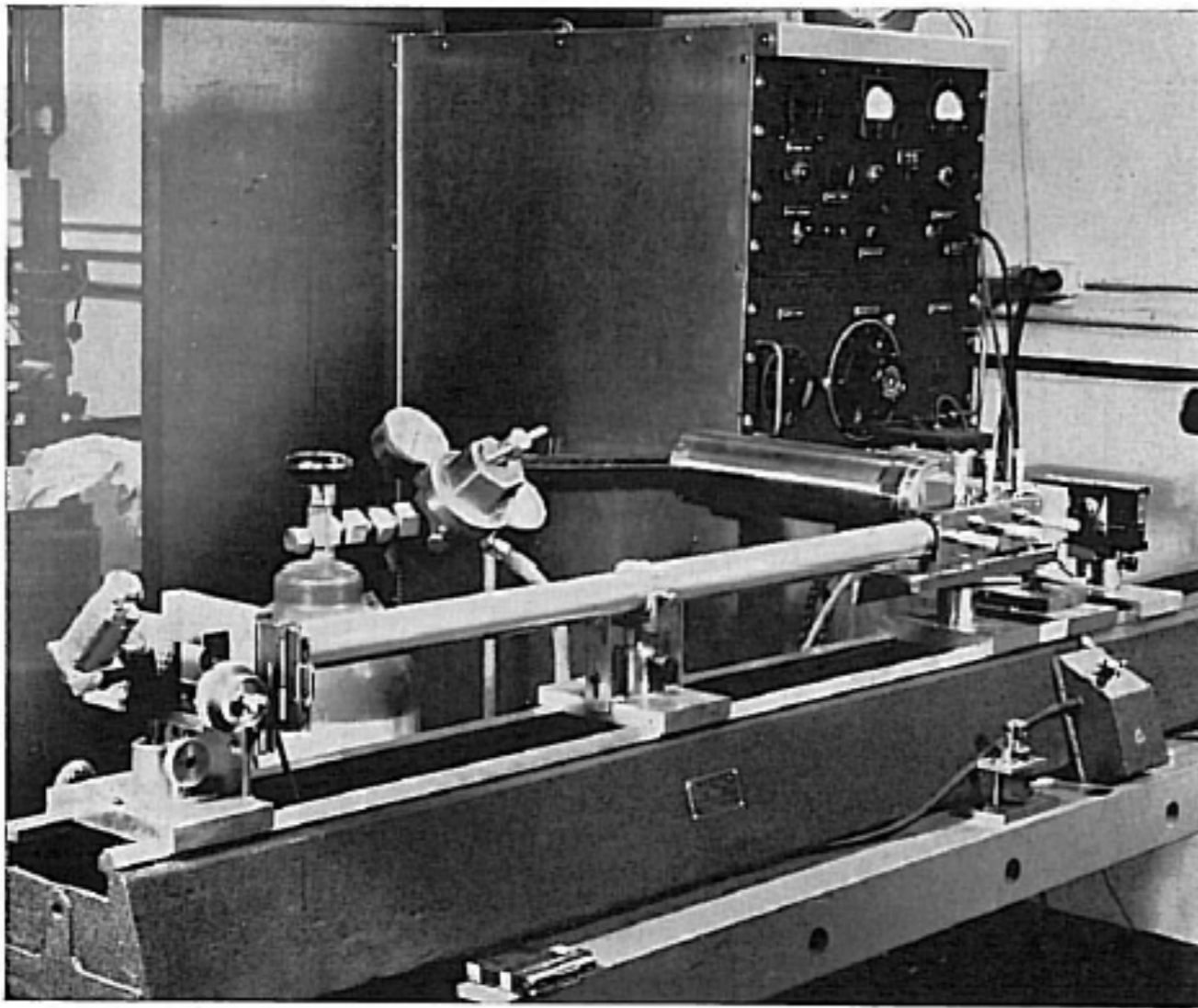
Reflexion X-ray microscope of Kirkpatrick and Pattee, incorporating two pairs of mirrors. (Kirkpatrick & Pattee, 1953.)
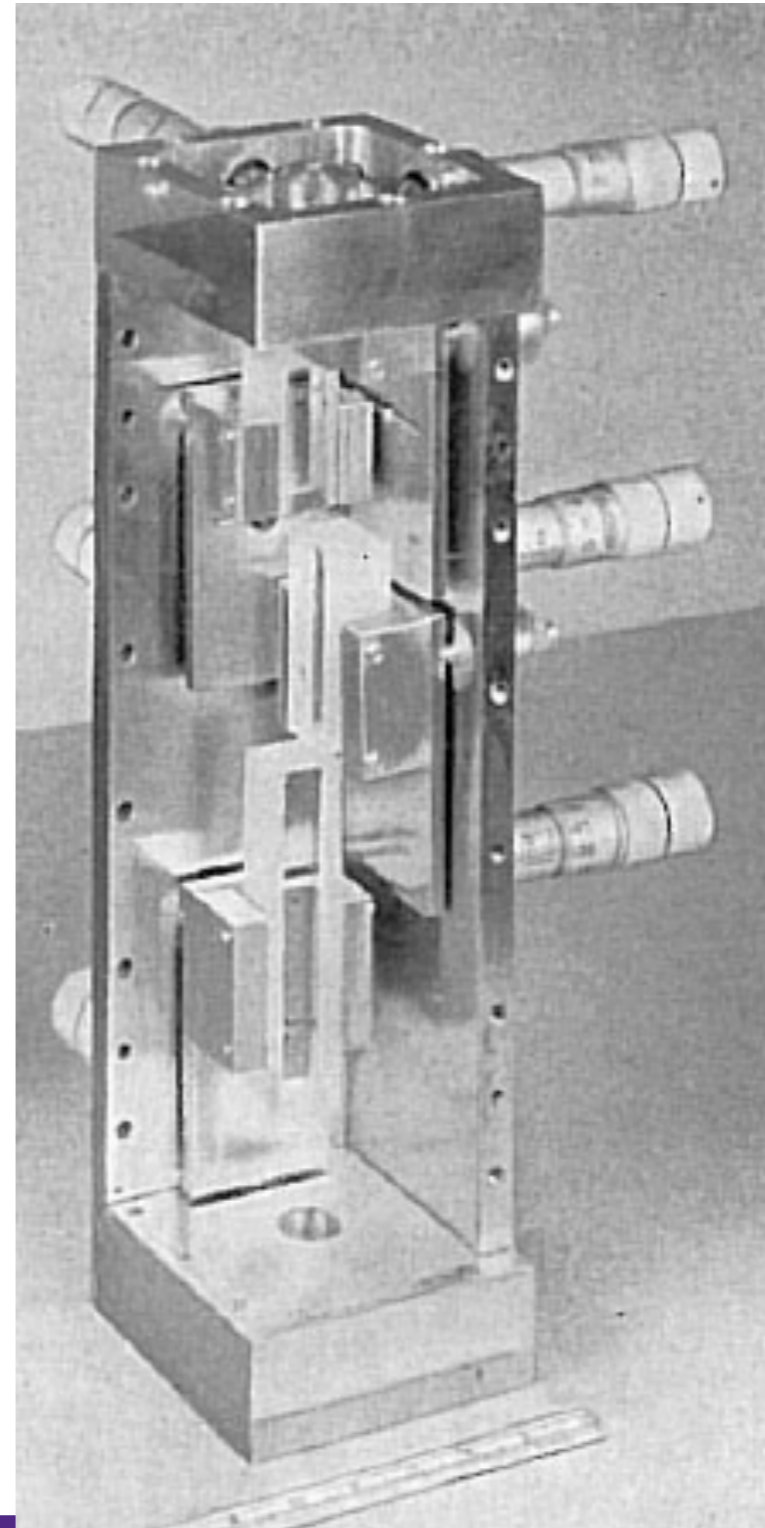
Improving the figure and roughness of mirrors

- Data provided by Lahsen Assoufid, head of the Optics Group at the APS

Grazing-incidence reflective optics were not competitive when synchrotron x-ray microscopy was getting started ca. mid-1980s

Osaka University: Yamauchi group

Precision Engineering **9**, 123 (1987)

Elastic emission machining

Y. Mori, K. Yamauchi and K. Endo*

Numerically controlled ultra-precision machining, which can easily finish the workpiece into an arbitrary shape, utilizing elastic fracture of the order of atomic size, has been realized. Ultra-fine powder particles are employed as a tool. Powder particles and water are mixed, and by utilizing the state of fluid lubrication of the slurry, only the powder particles are made to act on the material surface. Consequently, minute atomic size removal is achieved with no damage. The mechanism of metal removal is considered from the standpoint of the interaction between the metal surface and the surfaces of the powder particles. It is suggested that the removal of the surface atoms of the substrate is carried out through a very similar process to chemical etching.

Rev. Sci. Instrum. **60**, 2120 (1989)

New machining method for making precise and very smooth mirror surfaces made from Cu and Al alloys for synchrotron radiation optics

Y. Higashi, T. Meike, and J. Suzuki

Mechanical Engineering Center, National Laboratory for High Energy Physics, Ohho 1-1, Tsukuba, Ibaragi 305, Japan

Y. Mori, K. Yamauchi, and K. Endo

*Faculty of Engineering, University of Osaka, Osaka, Japan*

H. Namba

Faculty of Science, University of Tokyo, Tokyo, Japan

(Presented on 29 August 1988)

A combined machining method of diamond turning and numerically controlled elastic emission machining has been developed for finishing metal mirror surfaces made from Cu and Al alloys. A mirror surface can be polished without any stress by this method. Shape and roughness of the mirror surface examined in different machining methods are compared and discussed. A precisely shaped mirror with a roughness less than 2-nm R_{max} was obtained. A copper mirror was installed in a VUV beamline of the Photon Factory. It is confirmed that the metal mirror finished by the present method has good optical characteristics for synchrotron radiation beamlines.

JTEC Corporation high-precision X-ray mirror

High-precision X-ray mirrors are used in large synchrotron radiation facilities as one of the important optical instruments that reflect the synchrotron radiation beam to the target. There are different types of collector mirrors and spectroscopic mirrors depending on the purpose. High-precision X-ray mirrors contribute to many research achievements in fields, such as life science, materials science, earth science, and environmental science.
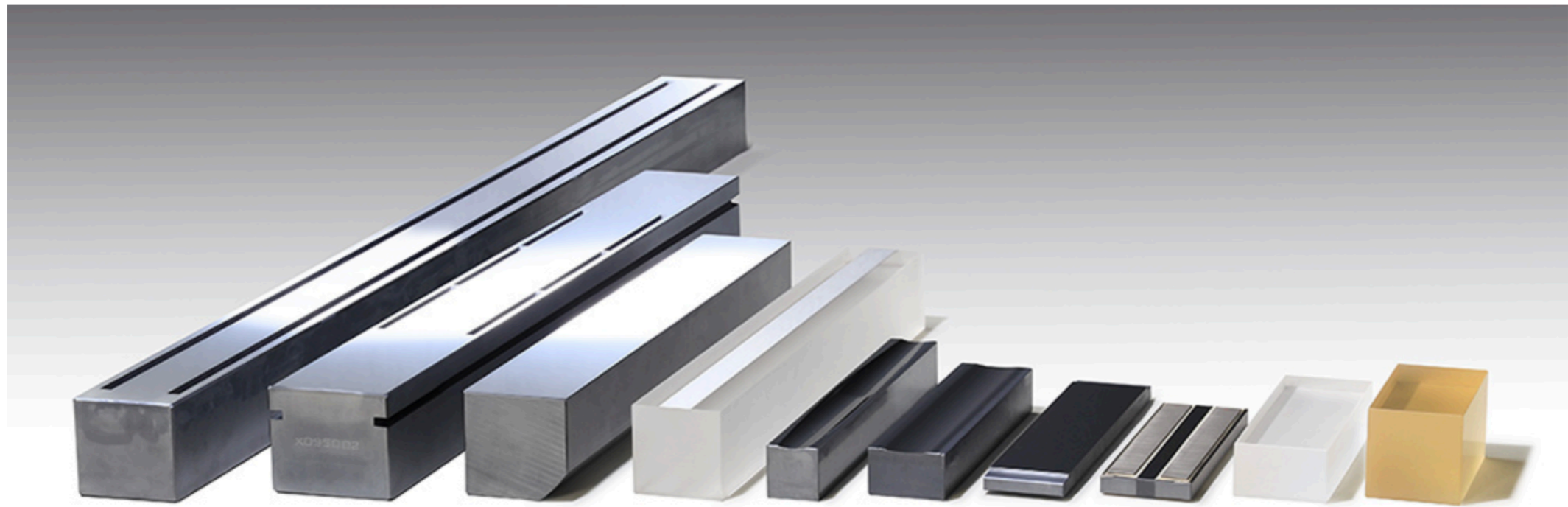

JTEC Corporation provides a maximum of 1 m long X-ray mirrors with a shape error of ±1 nm. For example, if a railroad is laid between Tokyo and Osaka 500 km, this is equivalent to ±0.5 mm of height difference. As our advantage, we can provide not only flat shapes but also free curved surfaces, such as elliptical, cylindrical, toroidal and ellipsoidal surfaces.

https://www.j-tec.co.jp/english/optical/high-precision-x-ray-mirror/

Nanofocusing with multilayer-coated KB mirrors

- da Silva, Pacureanu, Yang, Bohic, Morawe, Barrett, and Cloetens, *Optica* **4**, 492 (2017)

- FWHM of 12.0 nm (H) and 12.6 nm (V) at 34 keV (similar at 17 keV)

  - Multilayer coated, so not energy tunable.

 - Scanning microscopy, diverging beam in-line holography.
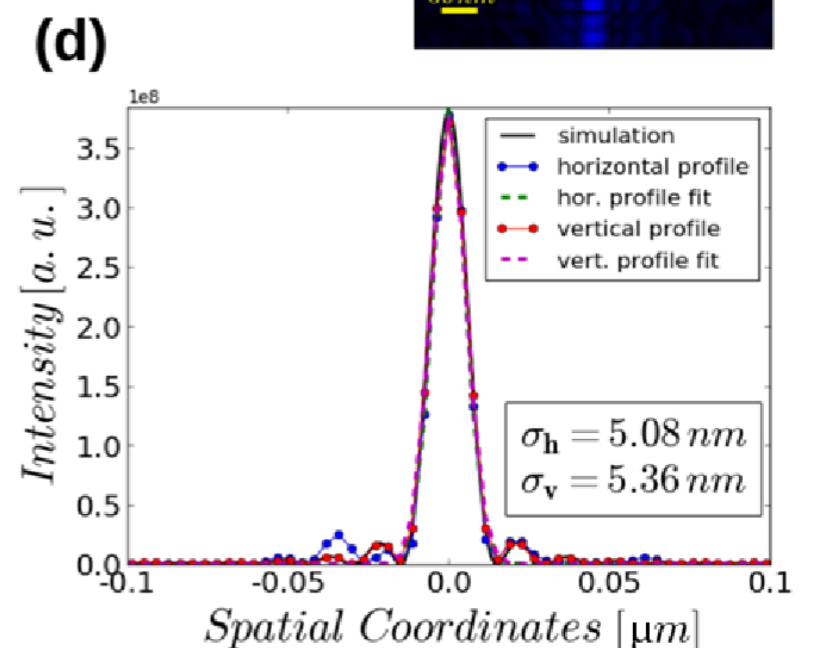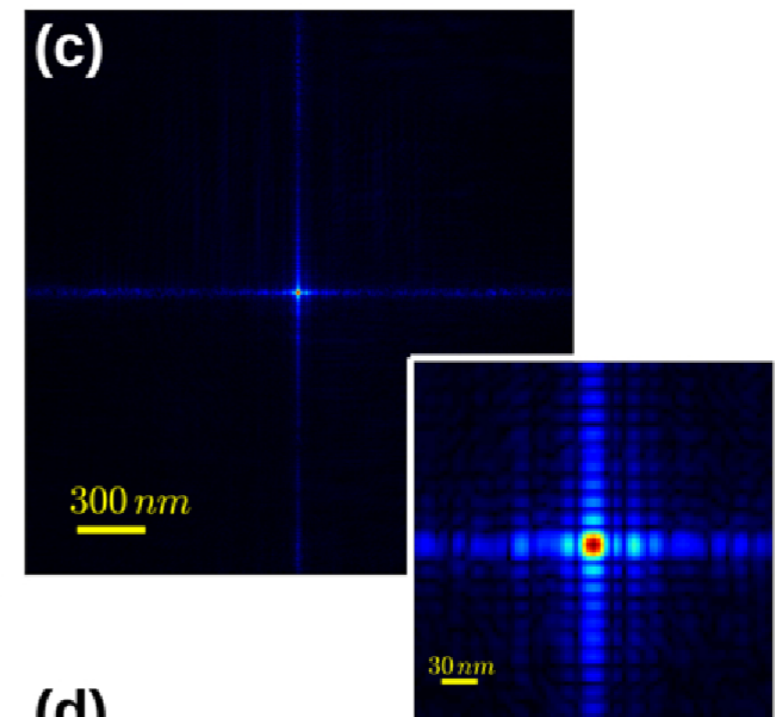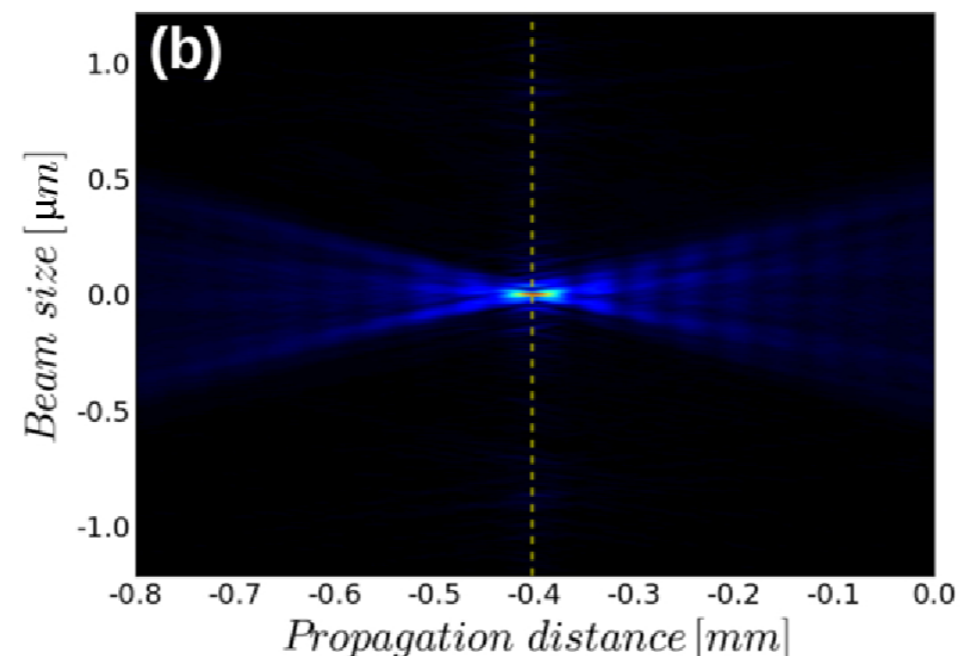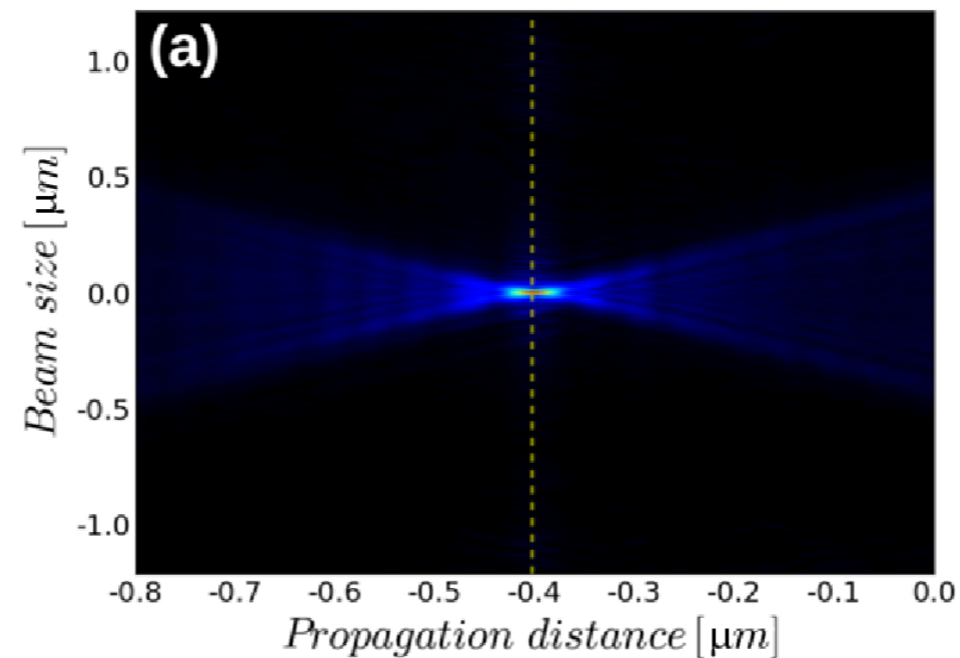
Compound refractive lenses

- Röntgen tried to make lenses, but found no focusing.

- Focal length of one lens is long – so combine many lenses! Tomie; Snigirev *et al.*, *Nature* **384**, 49 (1996); Lengeler *et al.*, *J. Synch. Rad.* **9**, 119 (2002).

- Resolution approaching 60 nm at 5-10 keV with parabolic beryllium lenses.

- Refractive lenses are especially good at 20 keV and higher.

a

X-rays

$$F = \frac{R}{2\delta}$$

R

$\times N$

b

X-rays

d

R

$$F = \frac{R}{2N\delta}$$

N

σ

ring

core
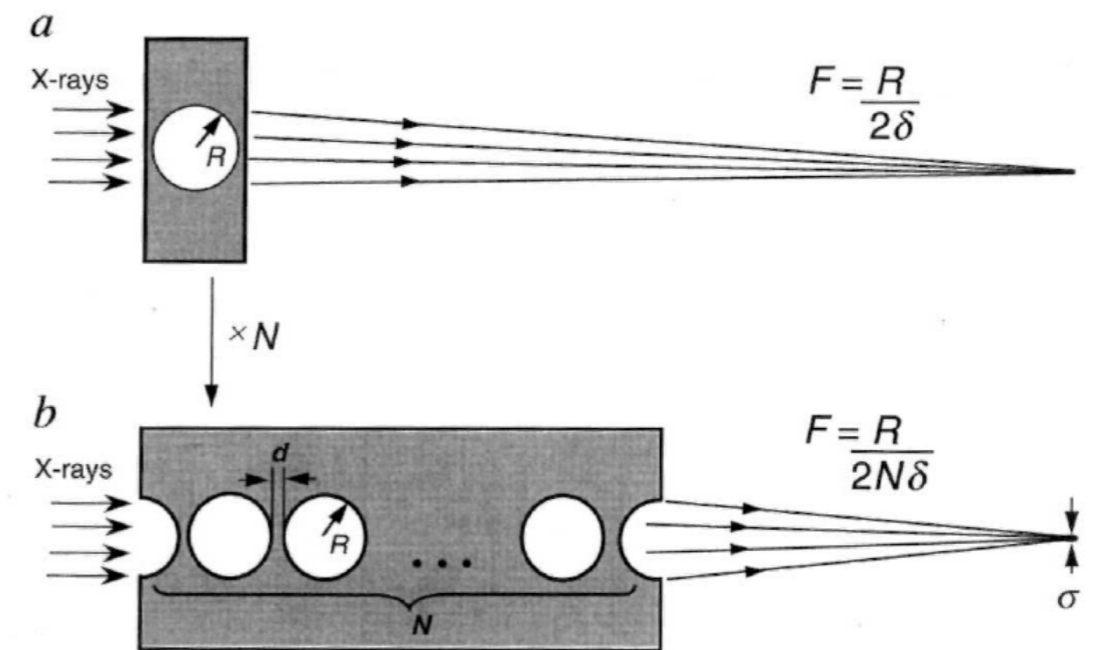
Compound refractive lenses at Universität Aachen; later rxoptics.de

N pieces
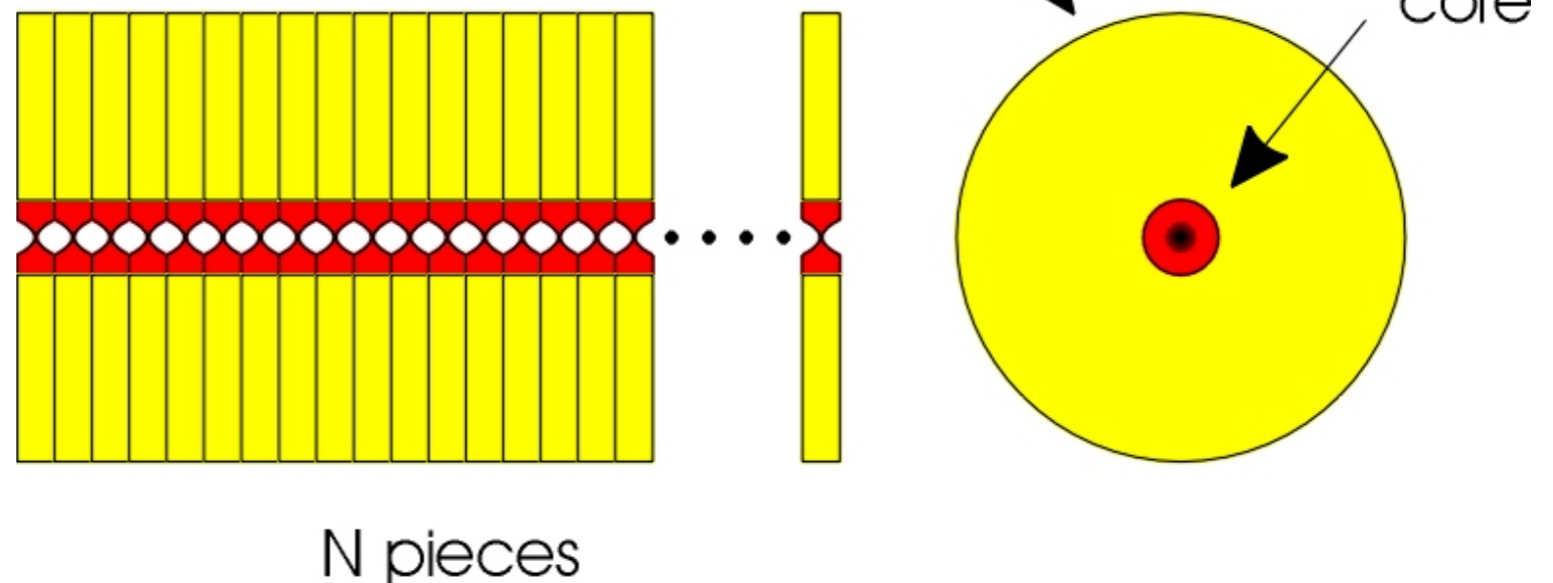
WELCOME TO RXOPTICS

The world leading producer
of refractive x-ray optics

WELCOME TO RXOPTICS

Our refractive optical devices are used as focusing and imaging components in all techniques based on synchrotron radiation, like microscopy, diffraction, spectroscopy, reflection, and coherent scattering, at storage rings as well as x-ray free electron laser facilities. They have been **established as popular and reliable working horses** in almost all synchrotron radiation facilities worldwide.

Our optical devices have the following **outstanding properties**:

- Parabolic lens shape: imaging practically **free of aberrations**
- Metallic lens material:
  - High **resistance to radiation damage**
  - **Thermal stability** in the beam due to high heat conductivity
- Appropriate for a **very wide energy range** (roughly from 2 keV to 150 keV)

- Handling and adjustment:
  - **Robust and compact** components
  - **Quick and easy** installation, **alignment** (typically 15 minutes), and removal
  - **Relatively insensitive** to misorientation, vibrations, and contamination
  - **Focus stays on axis**
  - **Comfortable working distance** between optics and sample

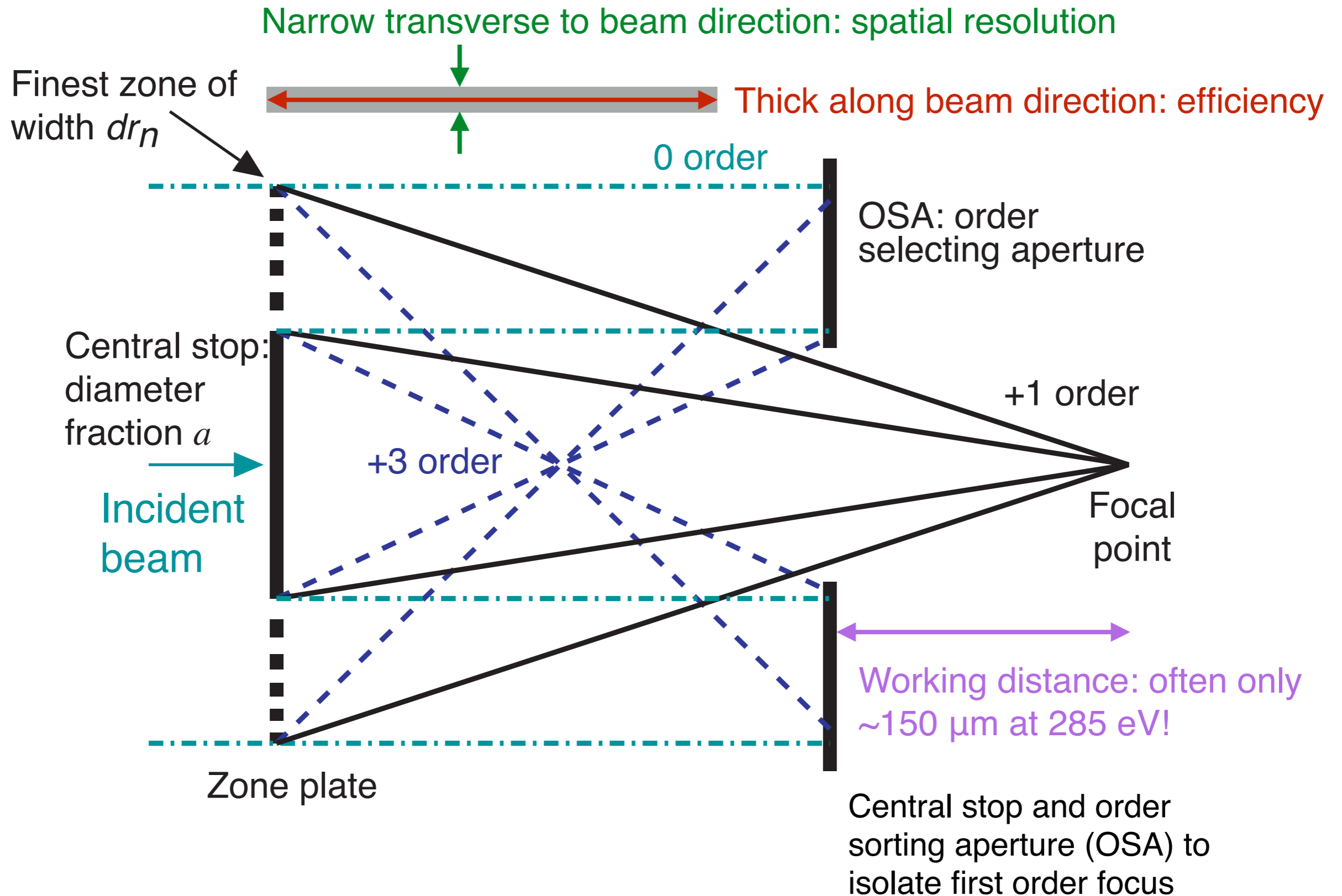# Diffractive focusing: Fresnel zone plates

- Fresnel zone construction: block out (or phase shift) every other $\lambda/2$

- Largest diffraction angle is given by outermost (finest) zone width dr_N as $\theta = \lambda/(2 dr_N)$

- Rayleigh resolution is 0.61 $\lambda/(\theta) = 1.22 dr_N$

- Zones must be positioned to $\sim 1/3$ width over diameter (10 nm in 100 μm, or $1:10^4$)

- Diameters tend to be $\sim$100 μm, and focal lengths tend to be $\sim$1 mm at 300 eV and few cm at 10 keV.

Diameter d, outermost zone width dr_N, focal length f, wavelength λ:

$$d \; dr_N = f \, \lambda$$

$$\left.\begin{matrix} (n+1)\lambda \\ (n+\dfrac{1}{2})\lambda \end{matrix}\right\} n = 0, 1 \ldots$$

X-ray focusing: Fresnel zone plates

Narrow transverse to beam direction: spatial resolution

Thick along beam direction: efficiency

Finest zone of width dr_n

0 order

OSA: order selecting aperture

Central stop: diameter fraction a

Incident beam

+3 order

+1 order

Focal point

Working distance: often only ~150 μm at 285 eV!

Zone plate
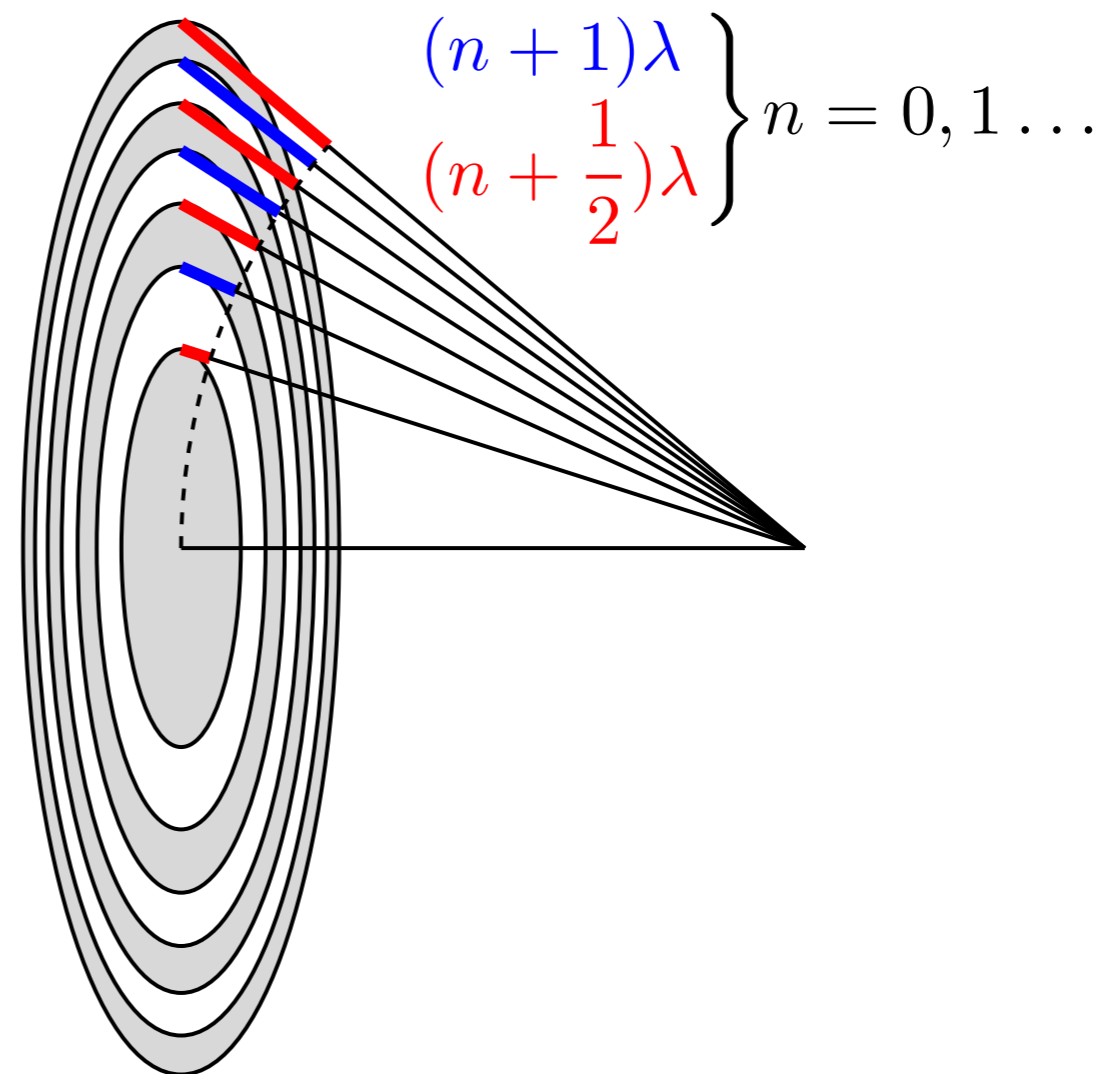
Central stop and order sorting aperture (OSA) to isolate first order focus

Zone plate efficiency and thickness

For binary zones, 1:1 mark:space ratio.
See Kirz, *J. Opt. Soc. Am.* **64**, 301 (1974)
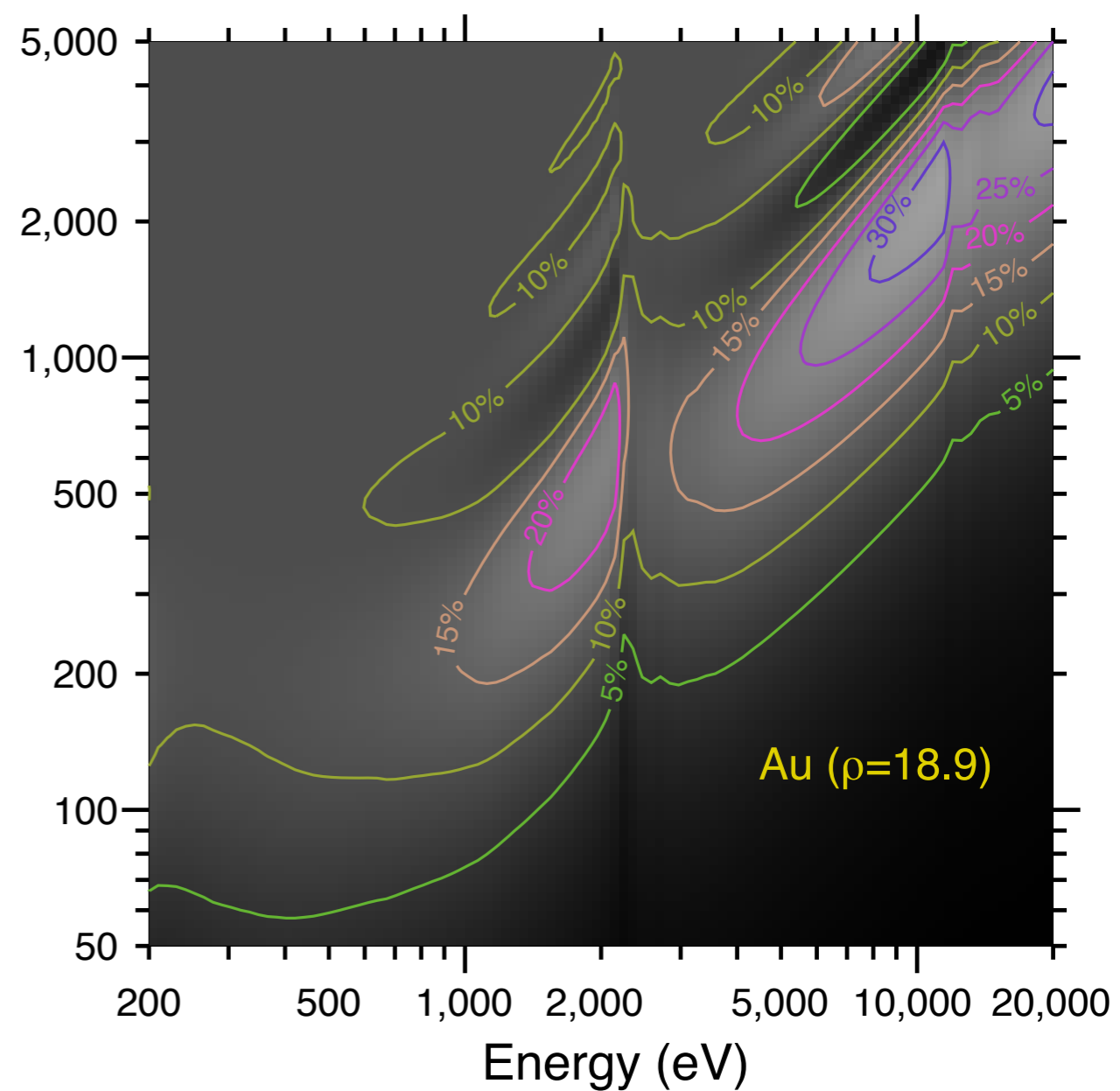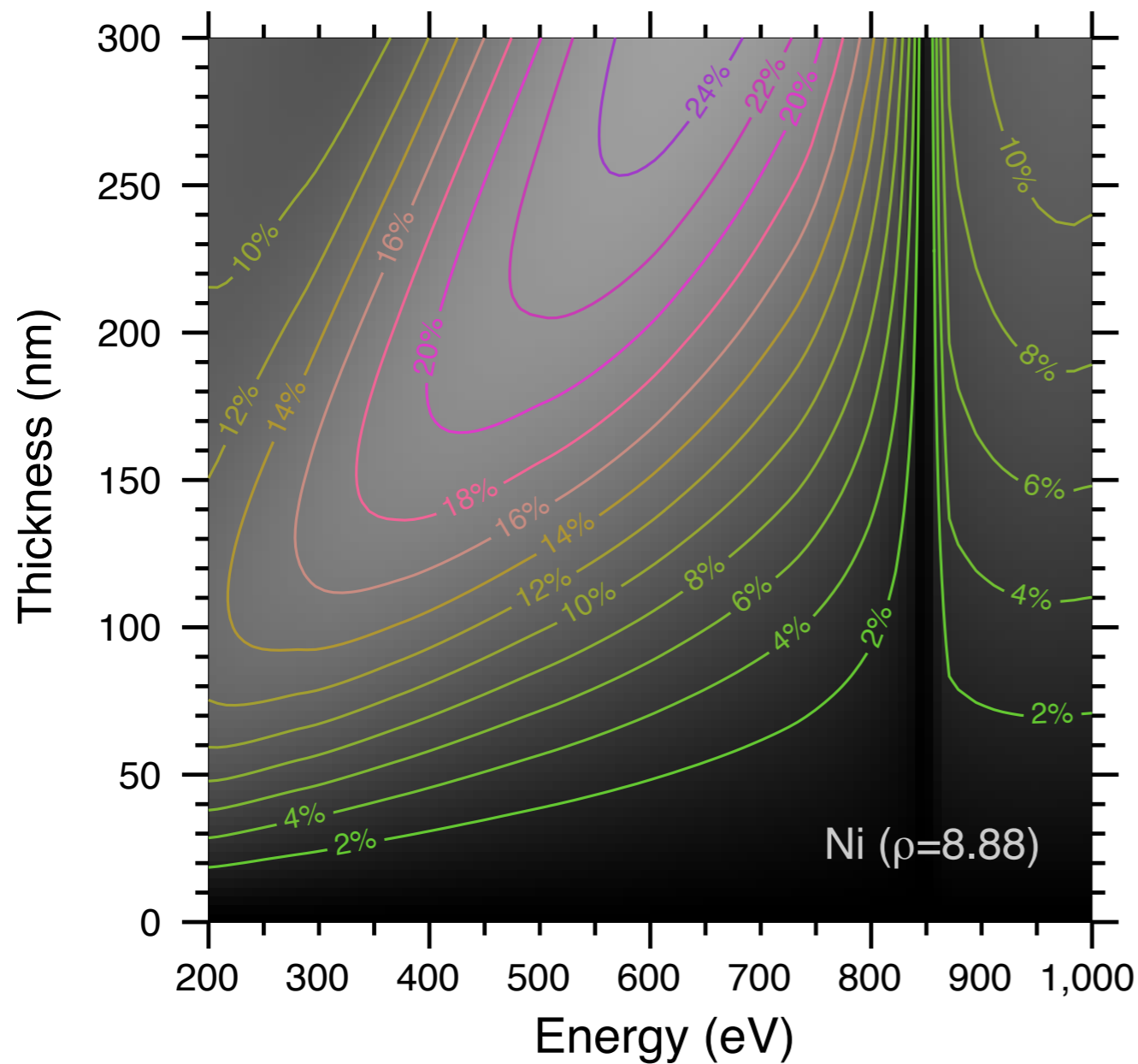
Zone plates by electron beam lithography

- Electron beam lithography: produces the finest possible structures (other than what nature can be persuaded to make by itself)
    - Example: JEOL JBX-9300FS: 1 nA into 4 nm spot, 1.2 nm over 500 μm, 100 keV
- Electrons scatter within resist, so highest resolution is only within ~100 nm thickness.
- Use directional etching methods like reactive ion etching for thick structures

1. E-beam expose, develop

E-beam resist
Hard mask
Plating mold
Plating base
Window
Si frame
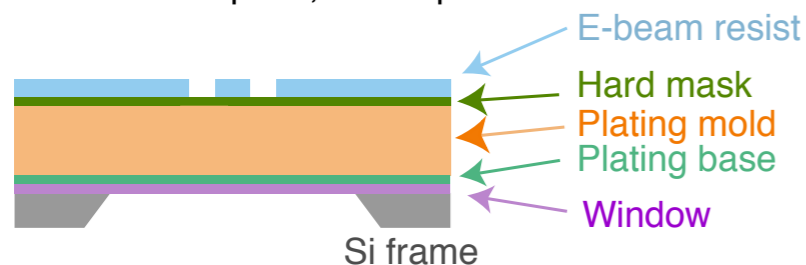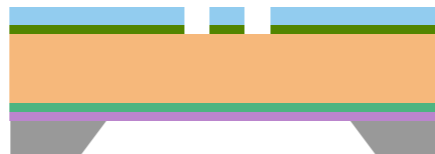
2. Etch hard mask

3. Etch plating mold; strip hard mask

4. Metal plating

A. Stein and JBX-9300FS

Improving single zone plates: zone doubling

1) Substrate preparation

500 nm HSQ resist

200 nm Si_3N_4 membrane

2) 100 keV electron-beam lithography exposure

3) Development and critical point drying

4) Iridium coating by atomic layer deposition

Ir layer

Jefimovs et al., Phys. Rev. Lett. 99, 264801 (2007).
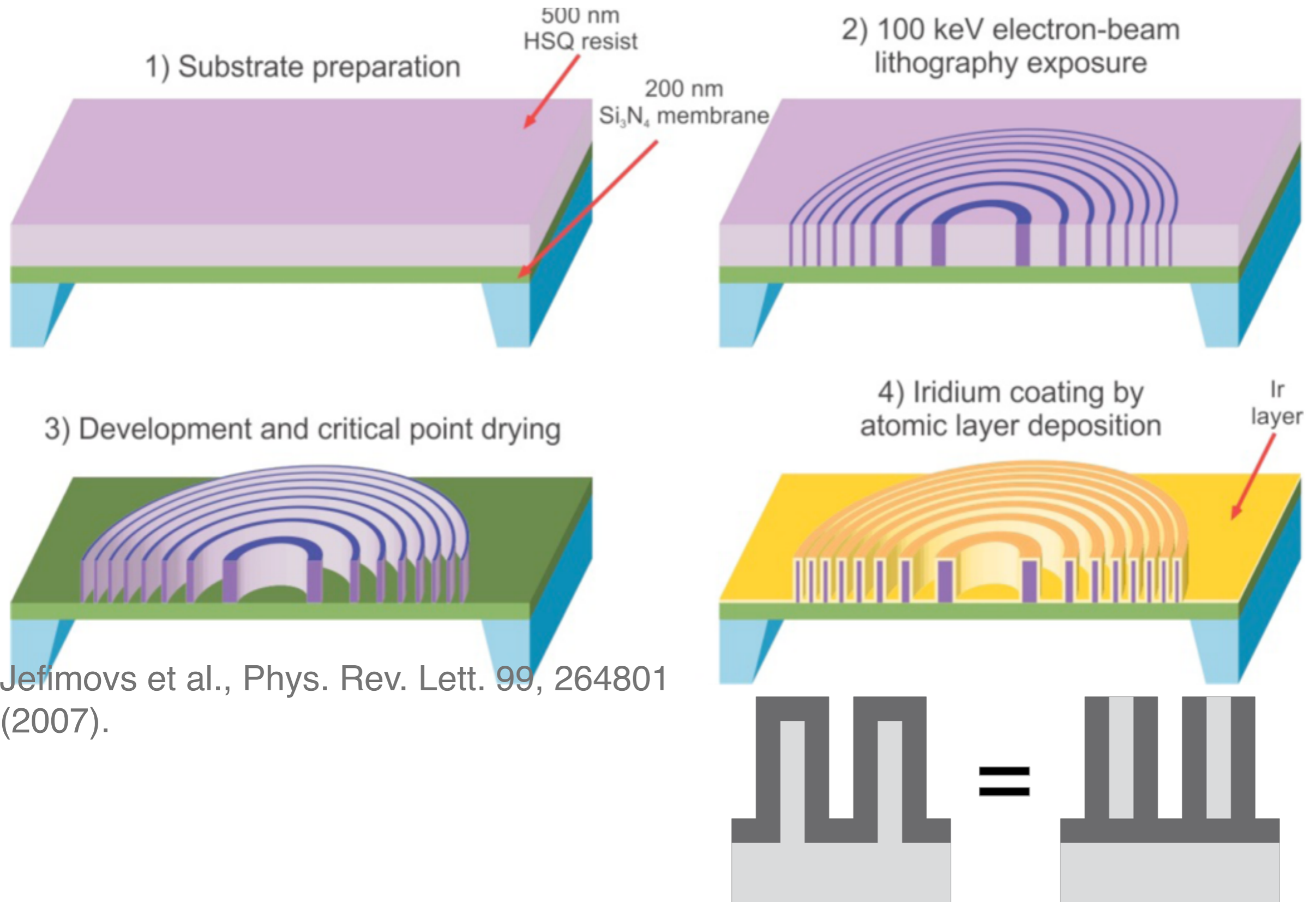
Fresnel zone plates for hard x-ray nanofocusing

14 nm zone width in Pt, up to 8 µm tall (aspect ratio=500).

Kenan Li, M. Wojcik, R. Divan, L. Ocola, B. Shi, D. Rosenmann, and C. Jacobsen, *J. Vac. Sci. Tech. B* **35**, 06G901 (2017)
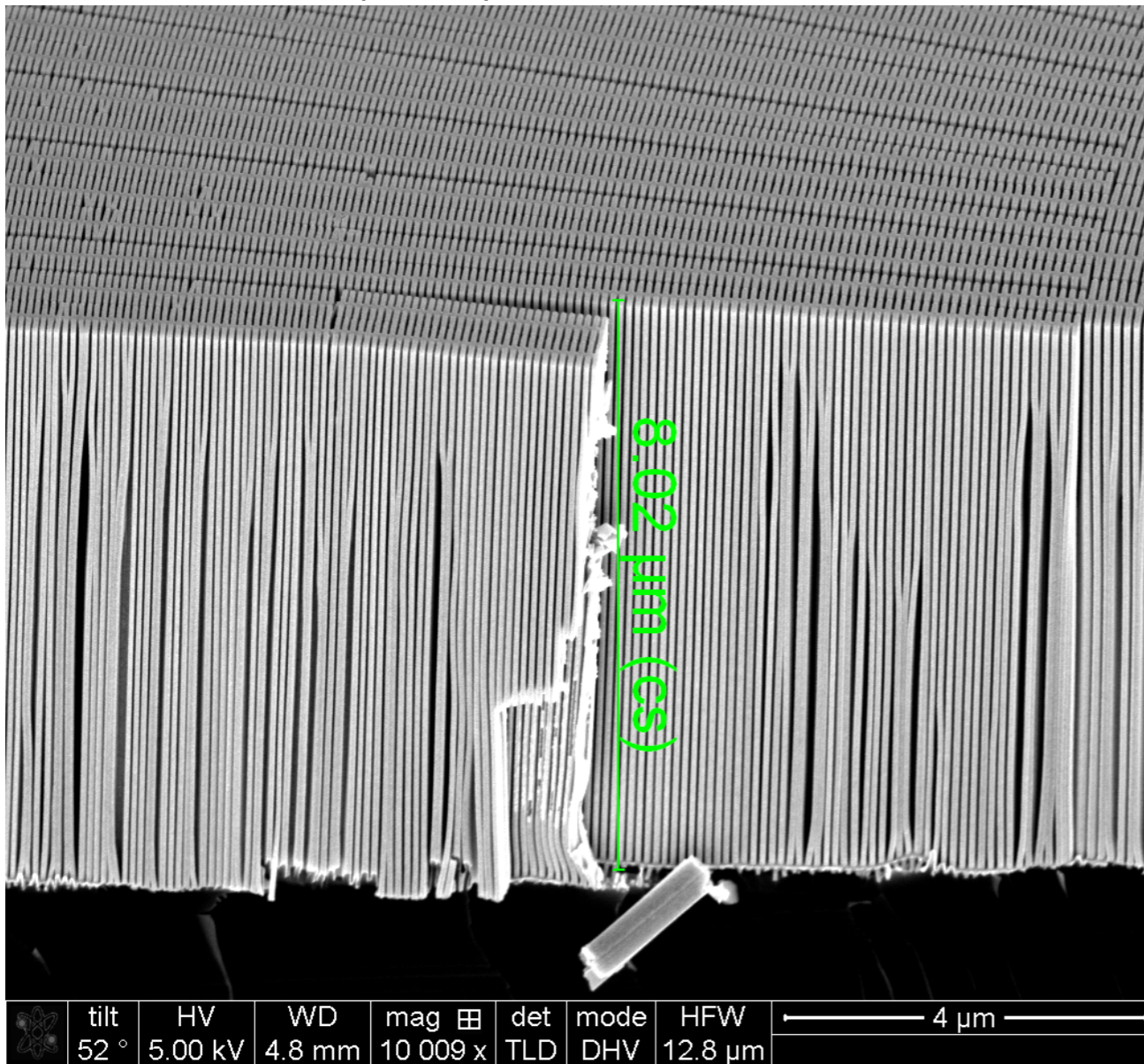
Metal-assisted chemical etching of silicon and atomic layer deposition to produce Pt zones.
14 nm wide zones that are 8 µm tall!
Aspect ratio>500

8.02 µm (cs)

62.5 nm (s)

13.8 nm (s)

	tilt	HV	WD	mag ⊞	det	mode	HFW	⊢——— 4 µm ———⊣
	52 °	5.00 kV	4.8 mm	10 009 x	TLD	DHV	12.8 µm	

	tilt	HV	WD	mag ⊞	det	mode	HFW	⊢— 200 nm —⊣
	52 °	5.00 kV	4.8 mm	200 000 x	TLD	DHV	640 nm	
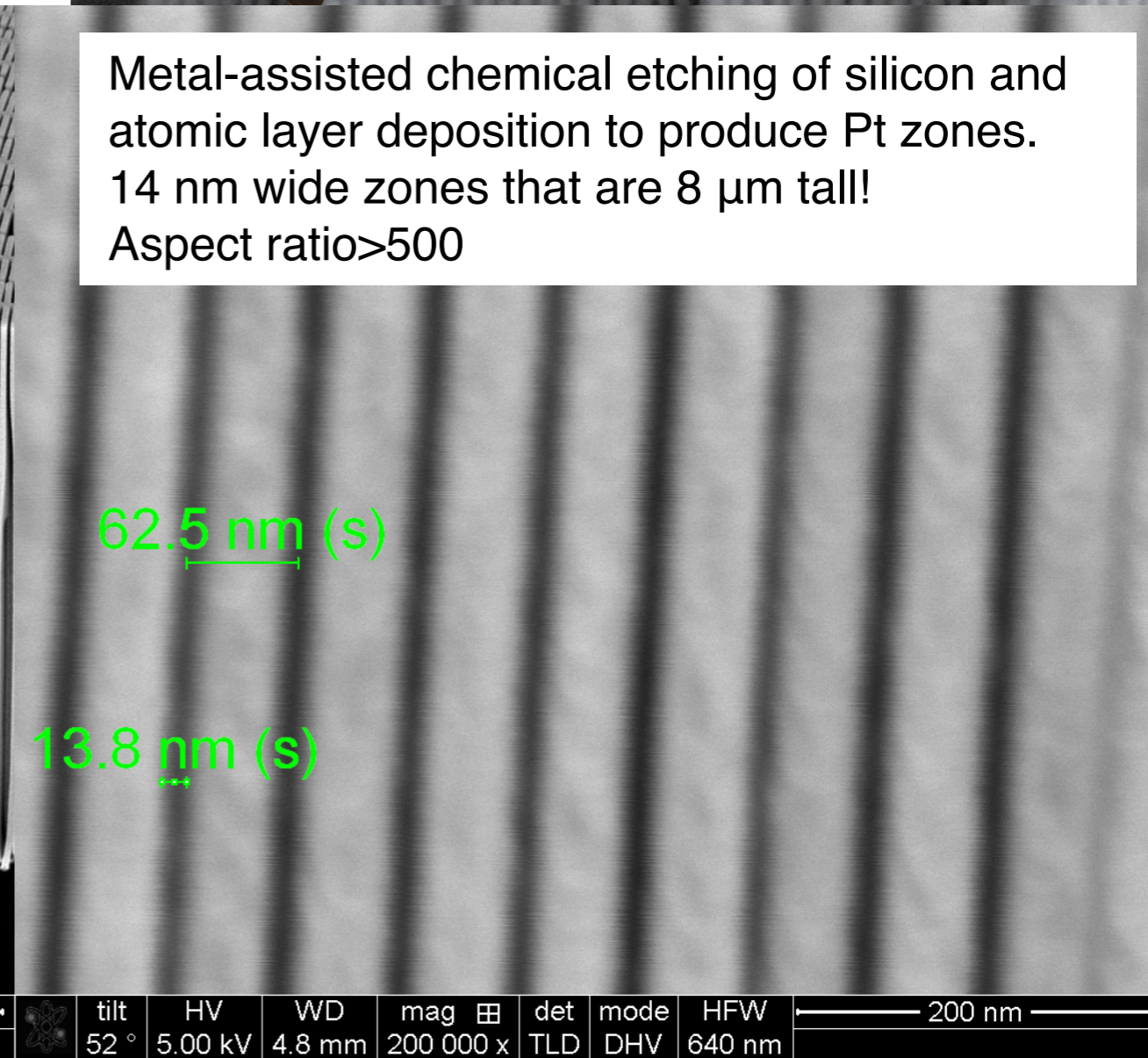
Not perfect, but still effective!

- Transmission x-ray microscope tomography: etching degrades with depth

- Phase contrast image shows 14 nm resolution with 6.2% efficiency at 10 keV.

Etch depth | 0.15 μm etch depth | 1.08 μm etch depth
1.57 μm etch depth | 2.30 μm etch depth | 4.21 μm etch depth

- K. Li, S. Ali, M. Wojcik, V. De Andrade, X. Huang, H. Yan, Y. Chu, E. Nazaretski, A. Pattammattel, and C. Jacobsen, *Optica* **7**, 410 (2020)

Siemens star phase-contrast image

200 nm

X-ray nanofocusing approaches are improving

- Visible light microscopy: better than 30 nm using centroid of Rayleigh blur of sparse/switchable emitters

- Electron microscopy: aberration-corrected microscopes reach below 0.1 nm resolution

- X-ray microscopy: reaching 10 nm resolution for demonstrations on robust samples

Zone plate >1 keV

Zone plate <1 keV

MLL (1D)

Mirrors (1D)

X-ray nanofocusing has improved over time - but resolution in most practical experiments is still limited to 20-30 nm
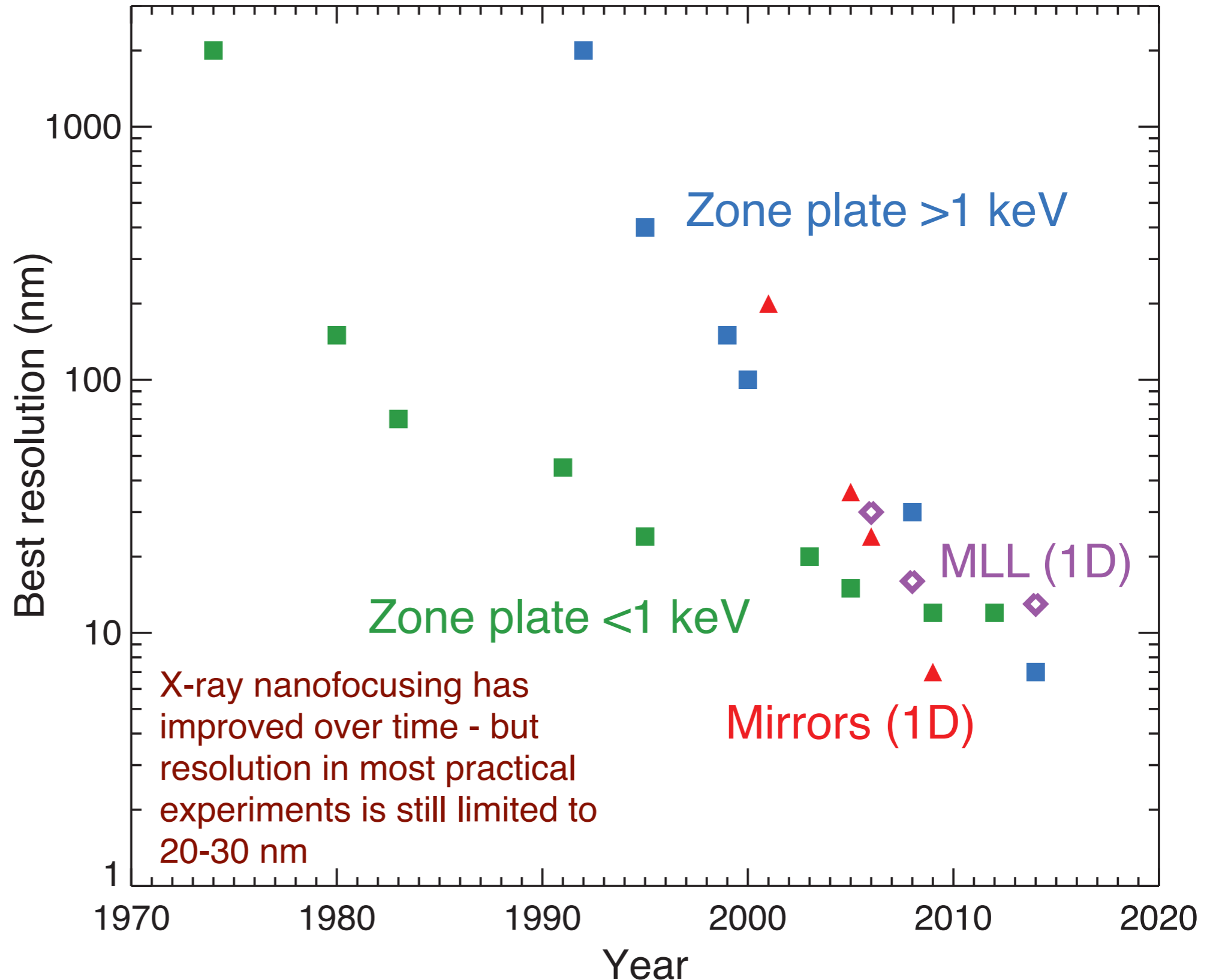
Zone plate microscopes

- Full-field: transmission x-ray microscope (TXM)

- Incoherent illumination; works well with a bending magnet or a laboratory source

- Inefficient zone plate is after the sample (higher radiation dose)

- Faster (pixels in parallel)

- Transmission or reflection imaging

- TXM spectromicroscopy: see *e.g.,* Guttmann… Schneider, *Nature Photonics* **6**, 25 (2011)

- Scanning transmission x-ray microscope (STXM)

- Coherent illumination; works best with an undulator

- Inefficient zone plate is before the sample (lower radiation dose)

- Slower (pixels one-by-one)

- Flexible modalities: fluorescence etc.

- Unlimited field of view and magnification (scanning stages)

TXM: transmission x-ray microscope
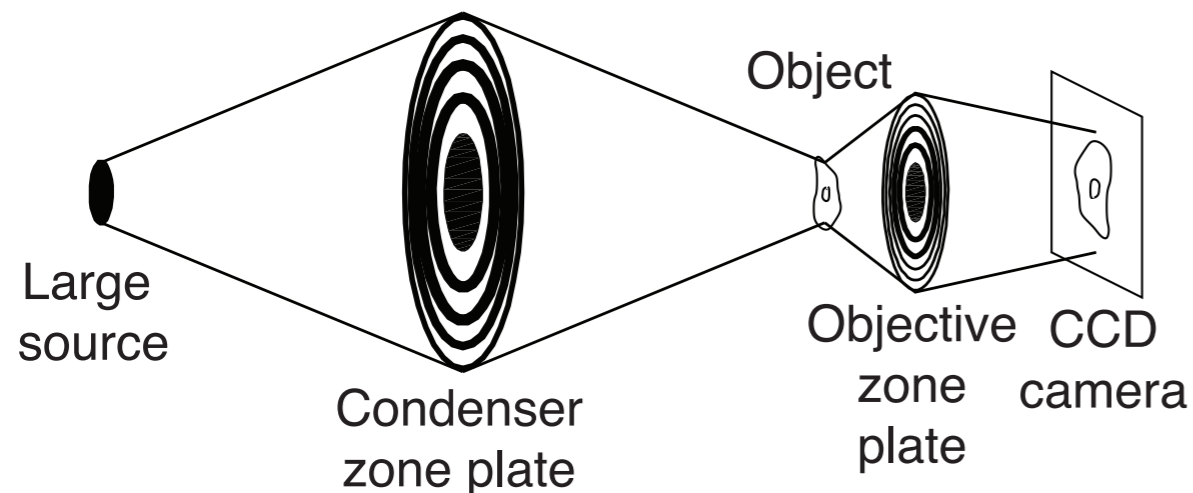
STXM: scanning transmission x-ray microscope
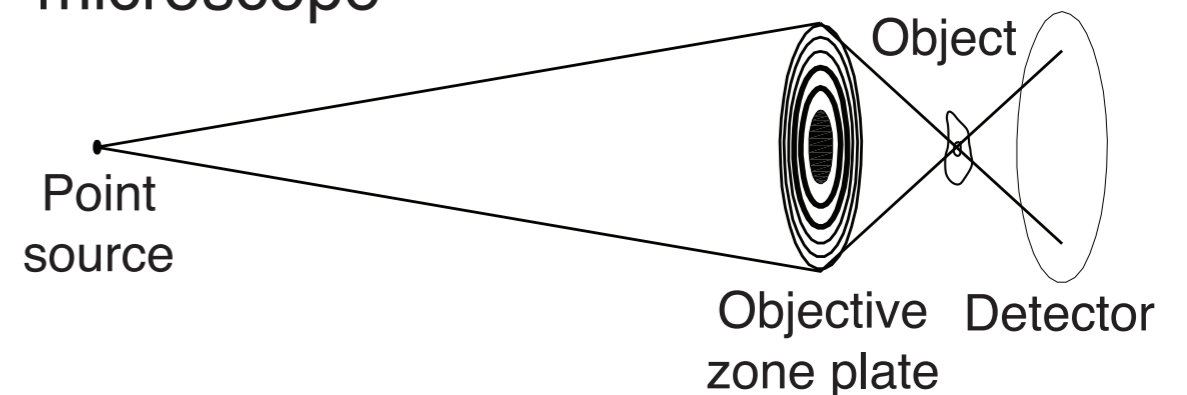
Transmission x-ray microscope: APS 32-ID

- Phase ring provides Zernike phase contrast
- Sub-10 nm resolution using MACE/ALD zone plates from Kenan Li
- Rotation stage for tomographic imaging
- V. De Andrade *et al.*, *Advanced Materials* **33**, 2008653 (2021)

Depth of focus

- Numerical aperture: semi-angle of lens θ

- Transverse resolution δ_r is

$$\delta_r = 0.61\frac{\lambda}{\theta}$$

- Depth of focus DOF is

$$\text{DOF} = 2\frac{\lambda}{\theta^2}$$
$$= 5.4\frac{\delta_r^2}{\lambda}$$

δ_r: transverse resolution

Depth of focus DOF (μm) vs Energy (keV), with lines labeled δ_r=1000 nm, δ_r=500 nm, δ_r=200 nm, δ_r=100 nm, δ_r=50 nm, δ_r=20 nm, δ_r=10 nm, δ_r=5 nm, δ_r=2 nm
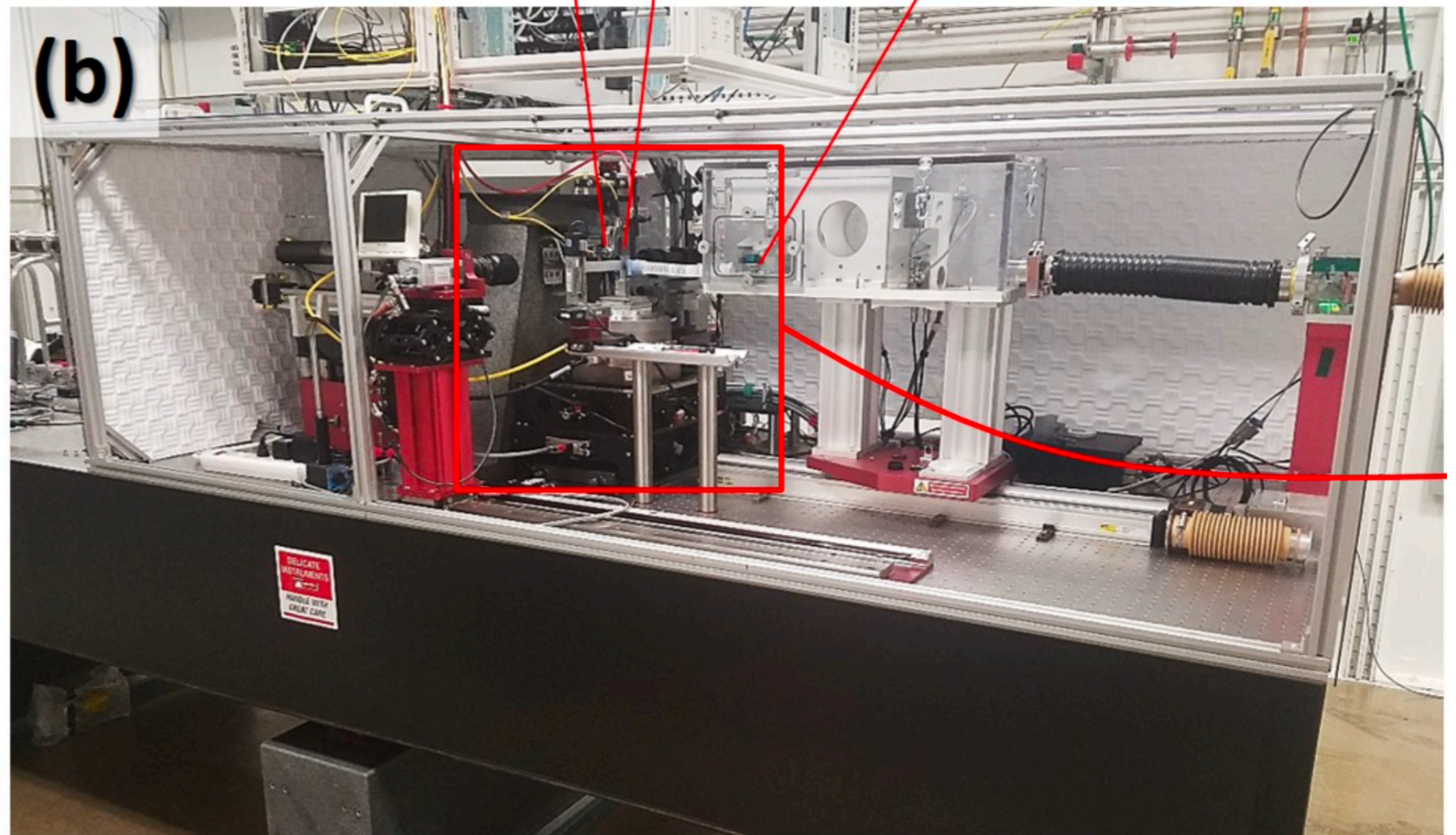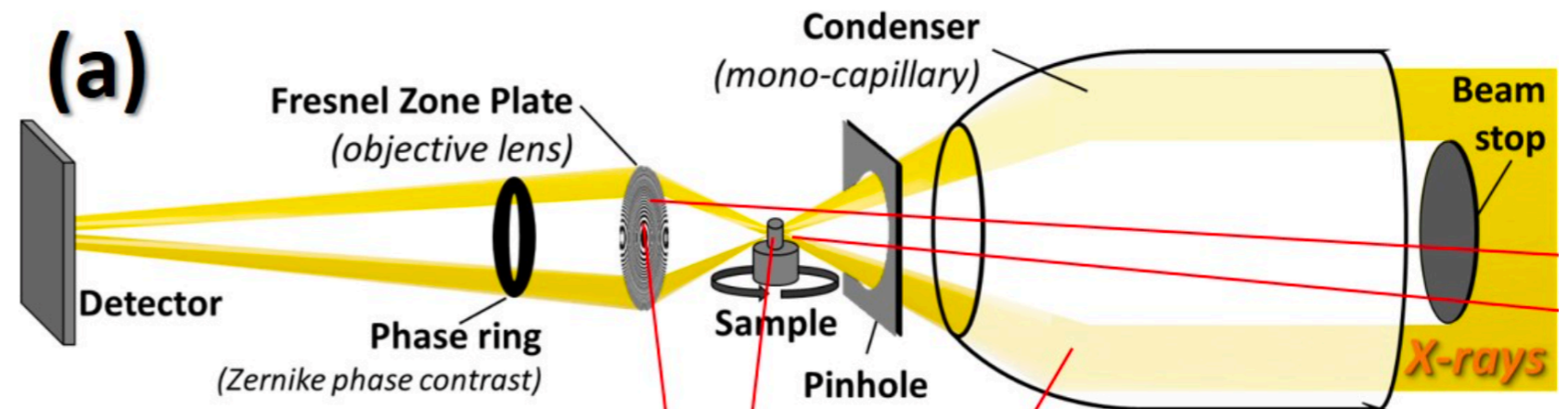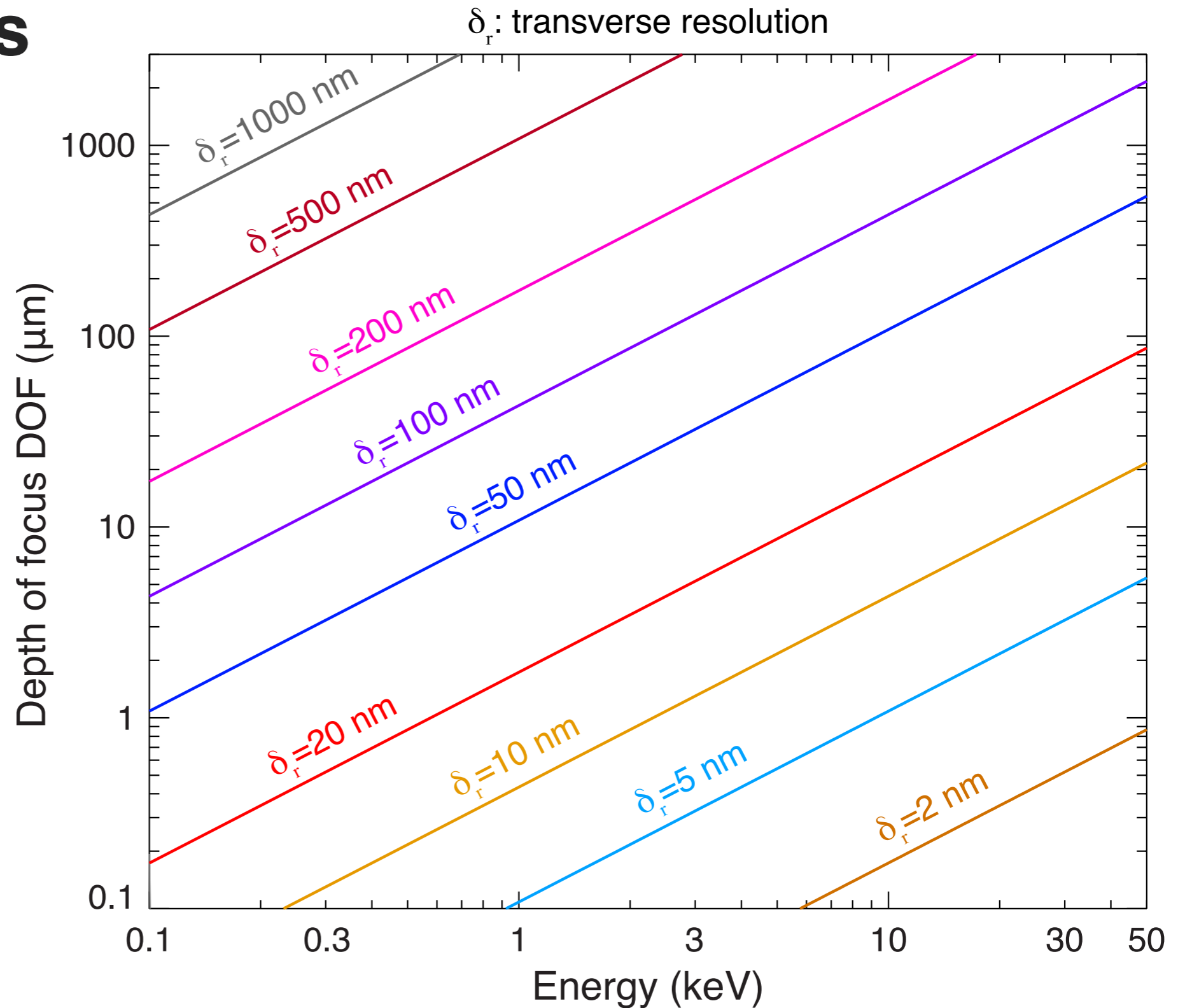
Pure projection images within the Depth of Focus

- Transverse resolution: $\delta_r \Rightarrow \nu = 3.83$

Tomography and sinograms

Illuminating beam

3D object $f(x, y, z)$

2D projection $p(x', z)_\theta$

Object slice

Slice projection $p(x')_{z, \theta}$

$\theta = 0$

Object slice $f(x, y)_z$
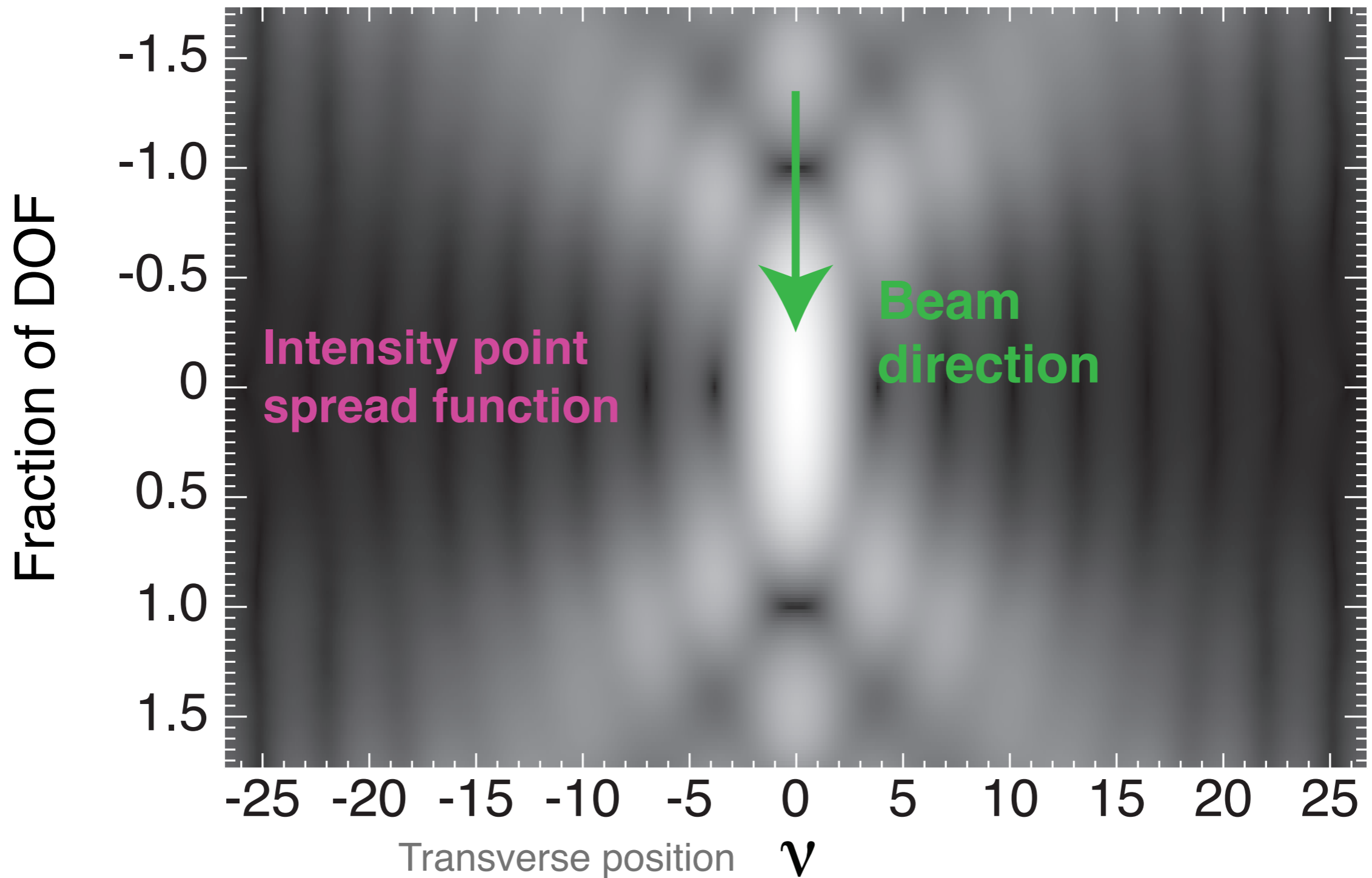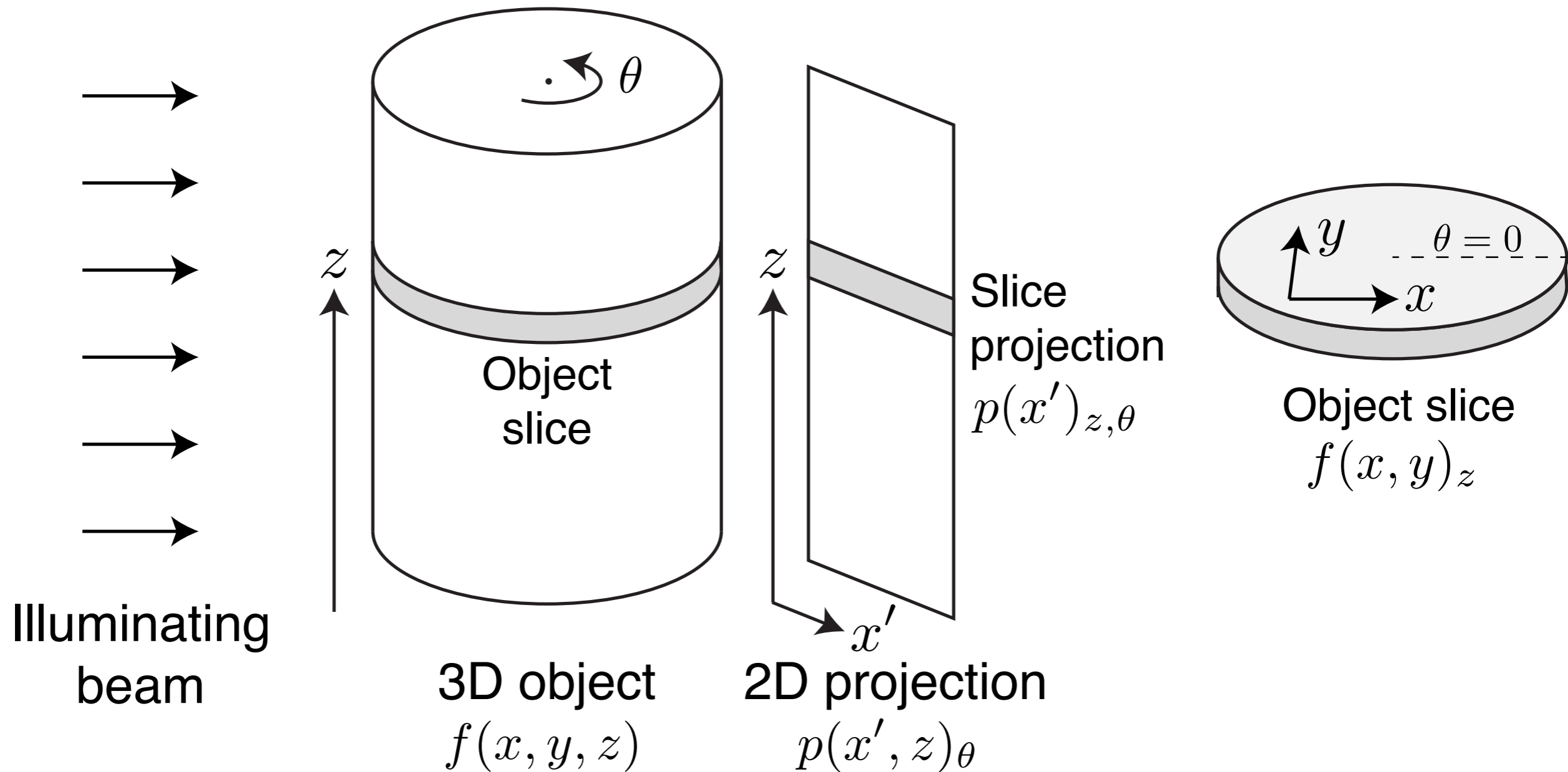
Tomography: the pure projection approximation

- One projection has *no* information along the illumination direction.
- Thus its "thickness" in Fourier space is 1 pixel

Projection image

$160°$

Top view of slice

Illumination

u_y

u_x

Fourier space $\mathcal{F}\{f(x,y)_z\}$
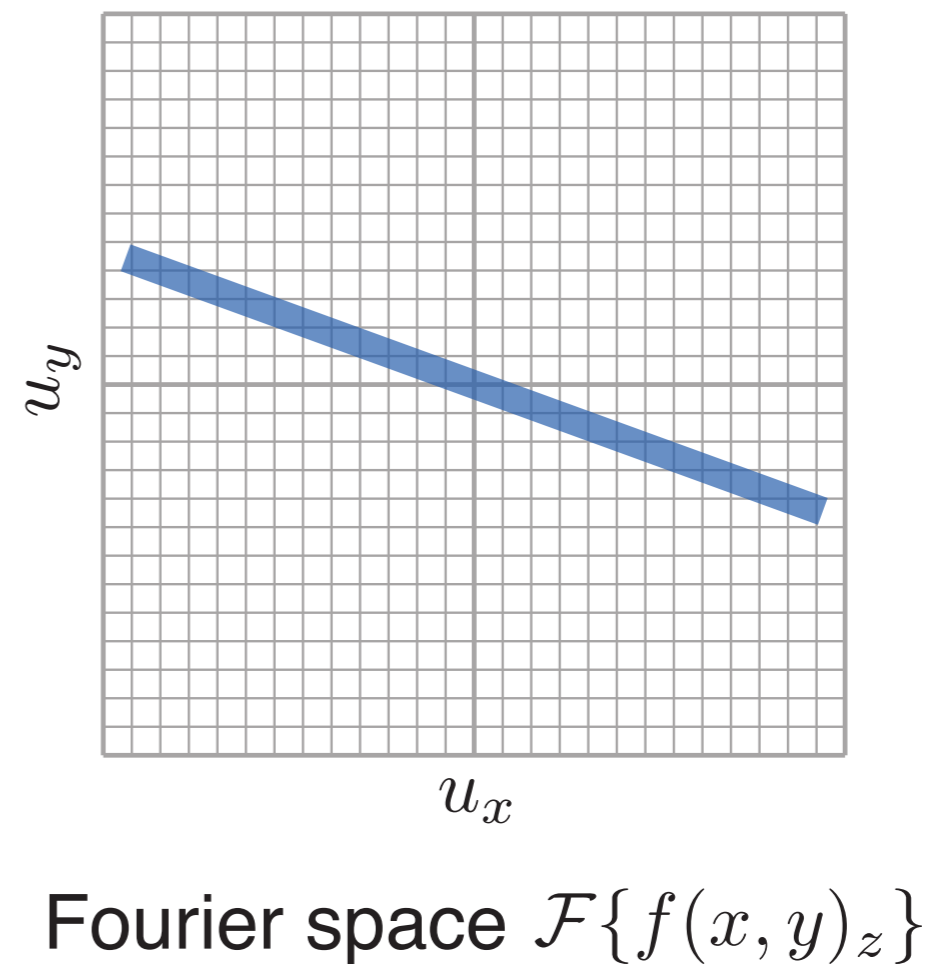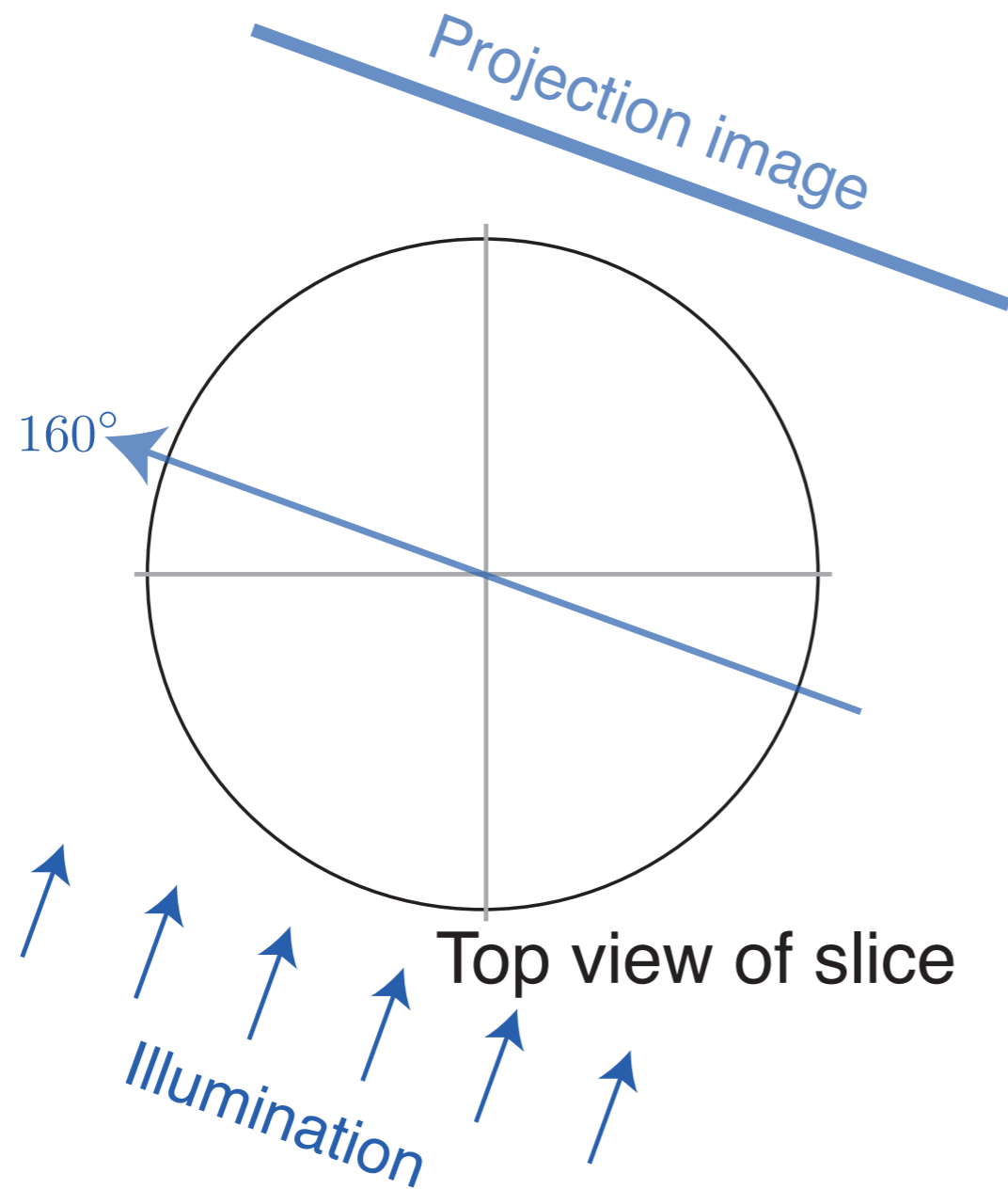
Tomography and sinograms

- Crowther criterion: fill information in to all voxels at the periphery in reciprocal space [Crowther, De Rosier, and Klug, *Proc. Royal Soc. A* **317**, 319 (1970)]

Oblique view of object slice $f(x, y)_z$

$$N_\theta = \pi N_x$$
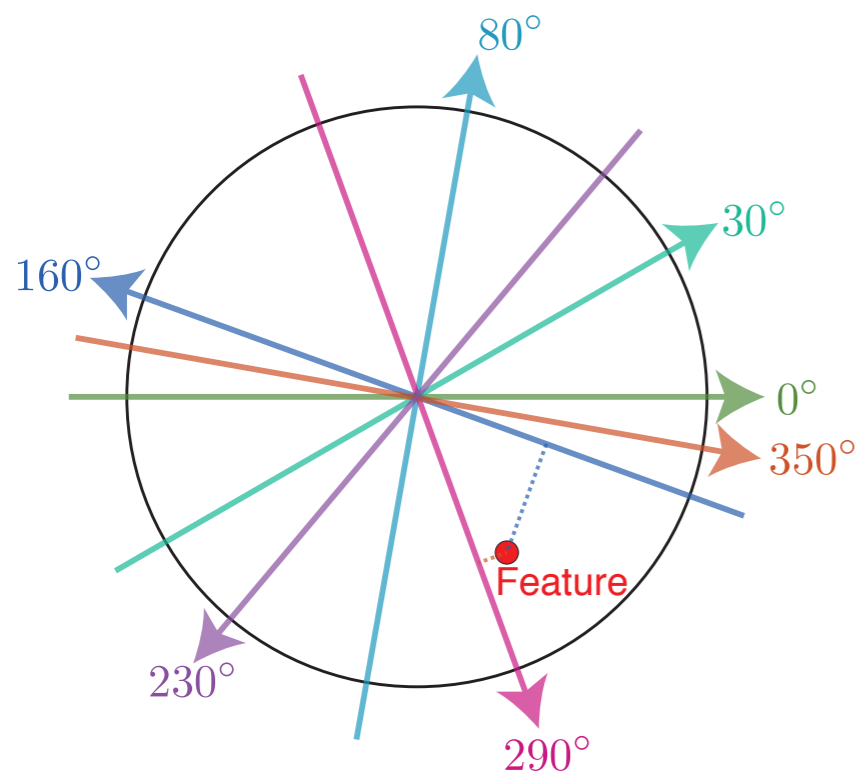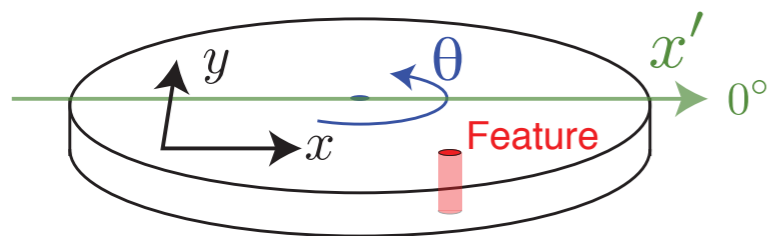
Top view of slice
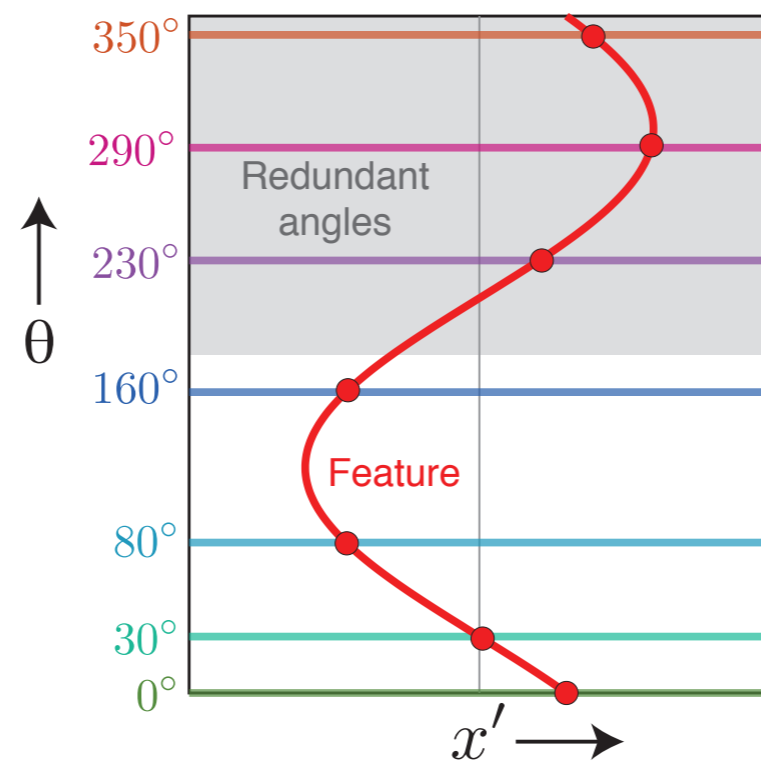
Sinogram
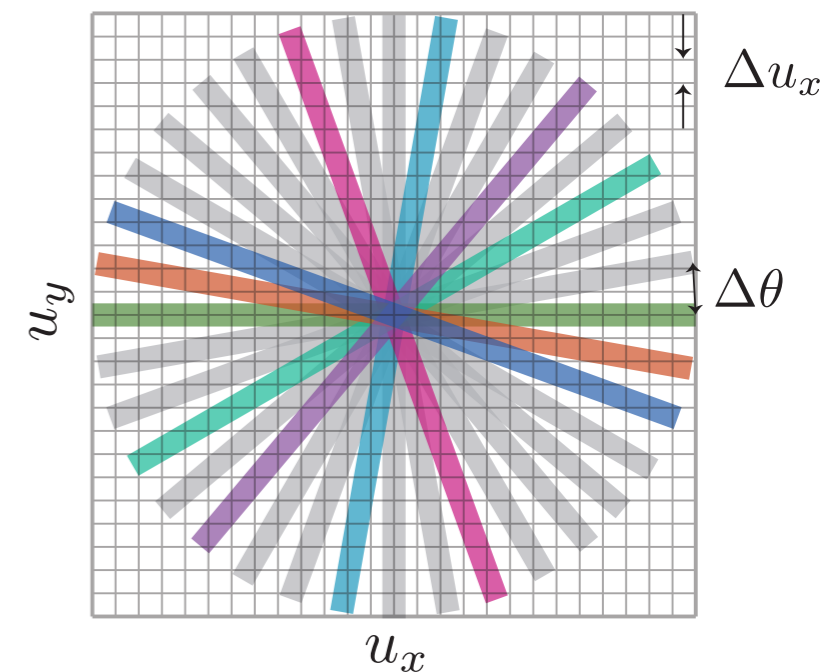
Fourier space $\mathcal{F}\{f(x, y)_z\}$

Zone plate tomography of a zone plate test object
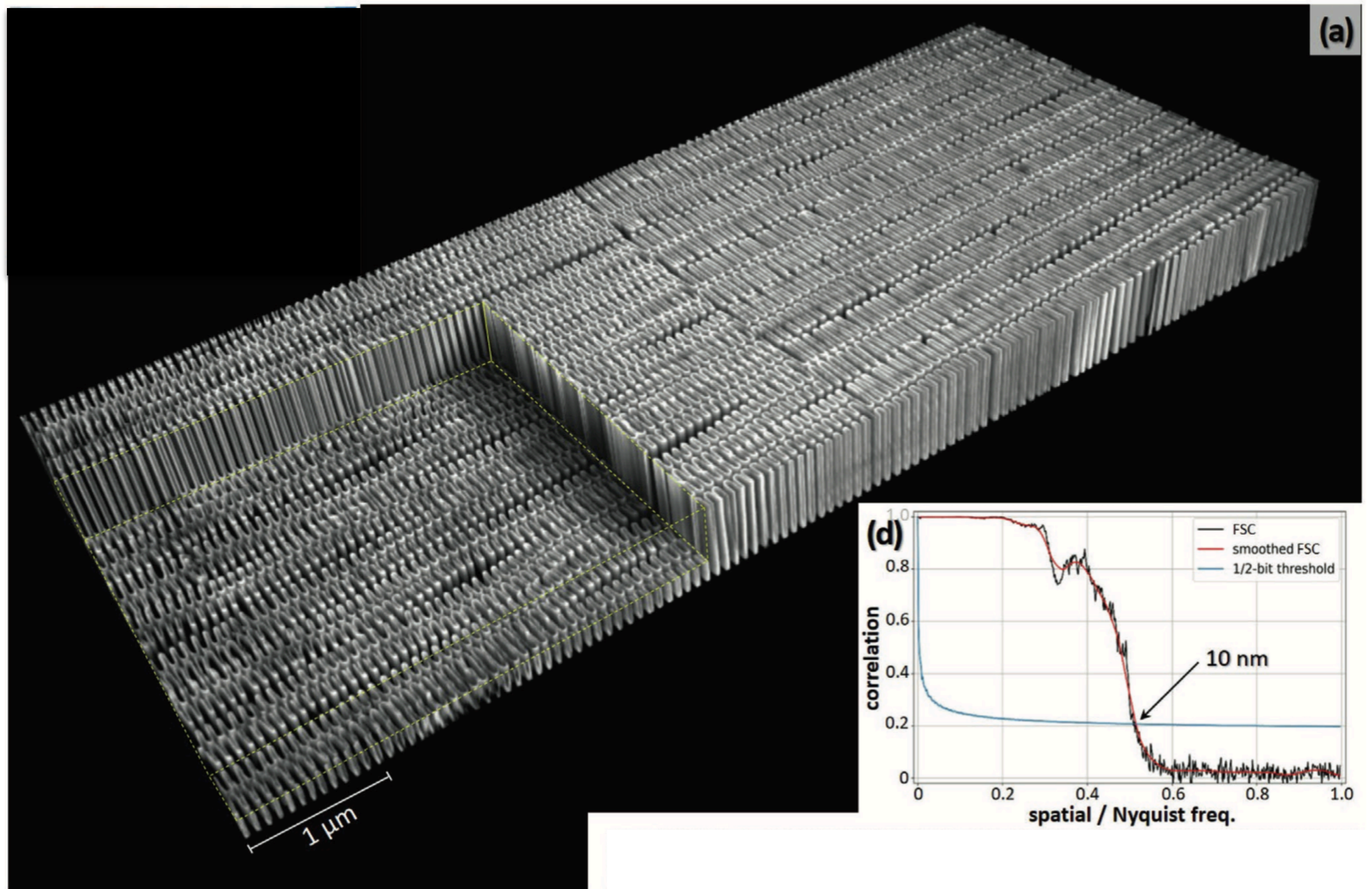
V. De Andrade *et al.*, *Advanced Materials* **33**, 2008653 (2021)

Nanofocusing requires coherent illumination

- Full-width, full-angle phase space of a diffraction limited lens with numerical aperture θ: $(2\theta)\cdot(2\cdot0.61\lambda/\theta)=2.44\lambda$

- Thus need to limit source phase space to $\sim\lambda$ both in x and y

Illumination source

Image: demagnified source, plus aperture diffraction

Controlling spatial coherence

- Spatial filter: pinhole at the focus of a lens. Passes only the spatially coherent fraction of an incident beam.
- X-ray beamlines: image the source to a secondary position with an aperture, for a flux-versus-coherence tradeoff.

OBJECTIVE

PINHOLE

INPUT BEAM PR

SCATTERING FROM DUST PARTICLES

DIRTY SPATIAL PROFILE

CLEAN SPATIAL PROFILE
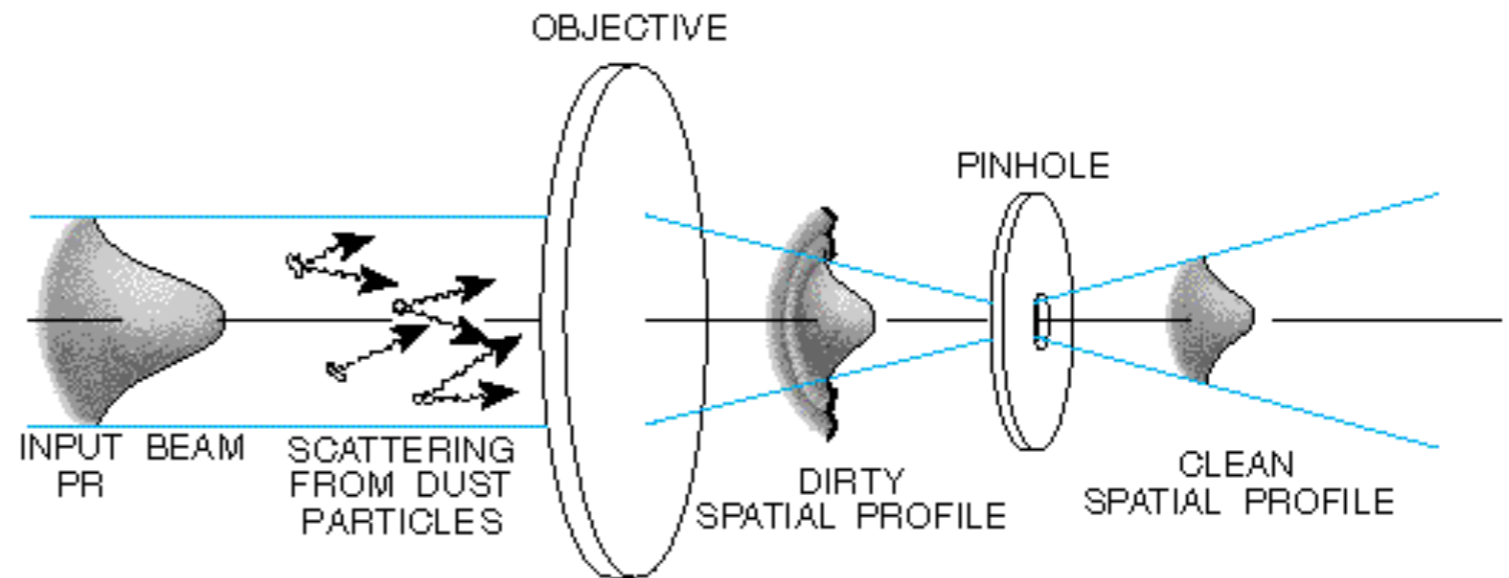
Diagram, photo from Newport catalog

Phase space area and probe focus

How close must p=(source diameter)·(optic's full subtended angle) be to λ? $p \approx 1 \cdot \lambda$ works pretty well!

Normalized to constant source energy

Normalized to constant source photon areal density
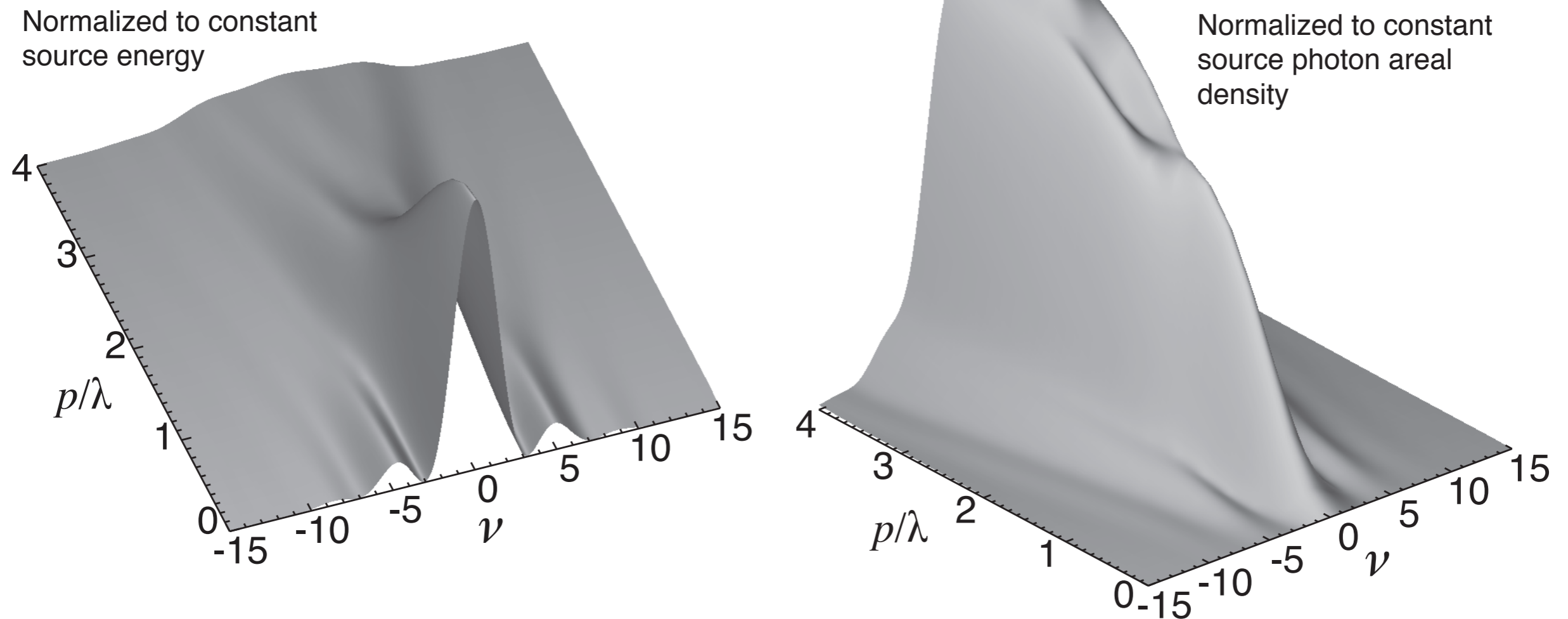
Effect on point spread function PSF (50% central stop)

Jacobsen *et al.*, *Ultramicroscopy* **47**, 55 (1992); Winn *et al.*, *J. Synch. Rad.* **7**, 395 (2000).

How to limit modes?

- Approach 1: distance, with a single nanofocusing optic.
  - Need to demagnify the source size in one step; for a fixed focal length (thus working distance) optic, you need a longer beamline.
  - Example: 40 μm to 20 nm in 200/0.1 meters. Total length: **200 m**.
  - For an optic with fixed diameter (and thus numerical aperture, and resolution), you have no flux-versus-resolution tradeoff.

Multimode source

Other modes

Central coherent mode

Other modes

Nano-focus

L_1

L_2
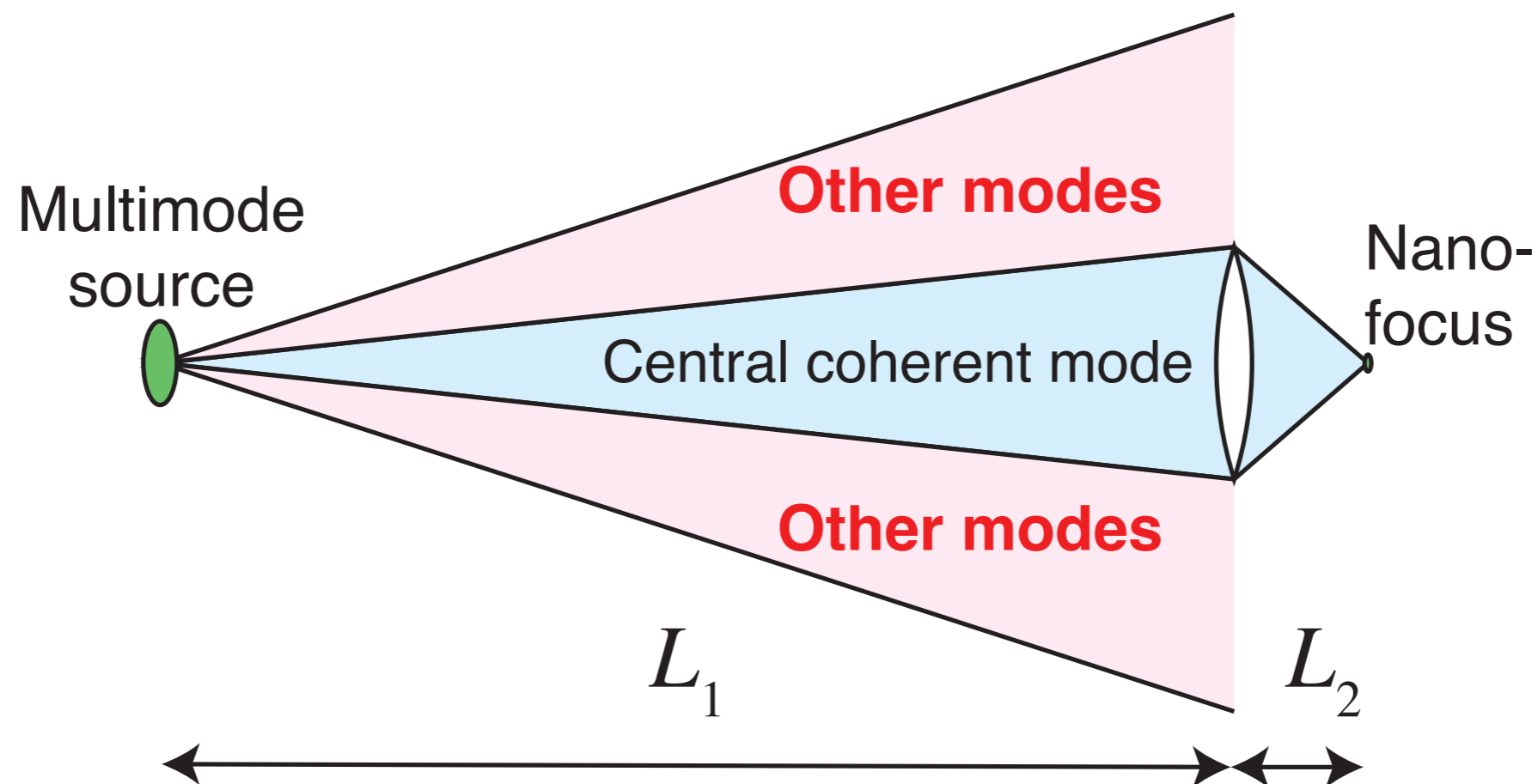
How to limit modes?

- Approach 2: aperture at an intermediate focus.
  - Two-stage demagnification means you can work with a shorter beamline!
  - Example: demagnify source size from 40 μm to 4 μm in 30/3 meters, then 4 μm to 20 nm in 20/0.1 meters. Total length 30+3+20=**53 m**.
  - You can adjust your intermediate aperture and have a flux-versus-resolution tradeoff.

Other modes

Secondary source aperture

Multimode source

Central coherent mode

Nano-focus

Of course, larger phase space in horizontal than vertical...

L_1 L_2 L_3 L_4
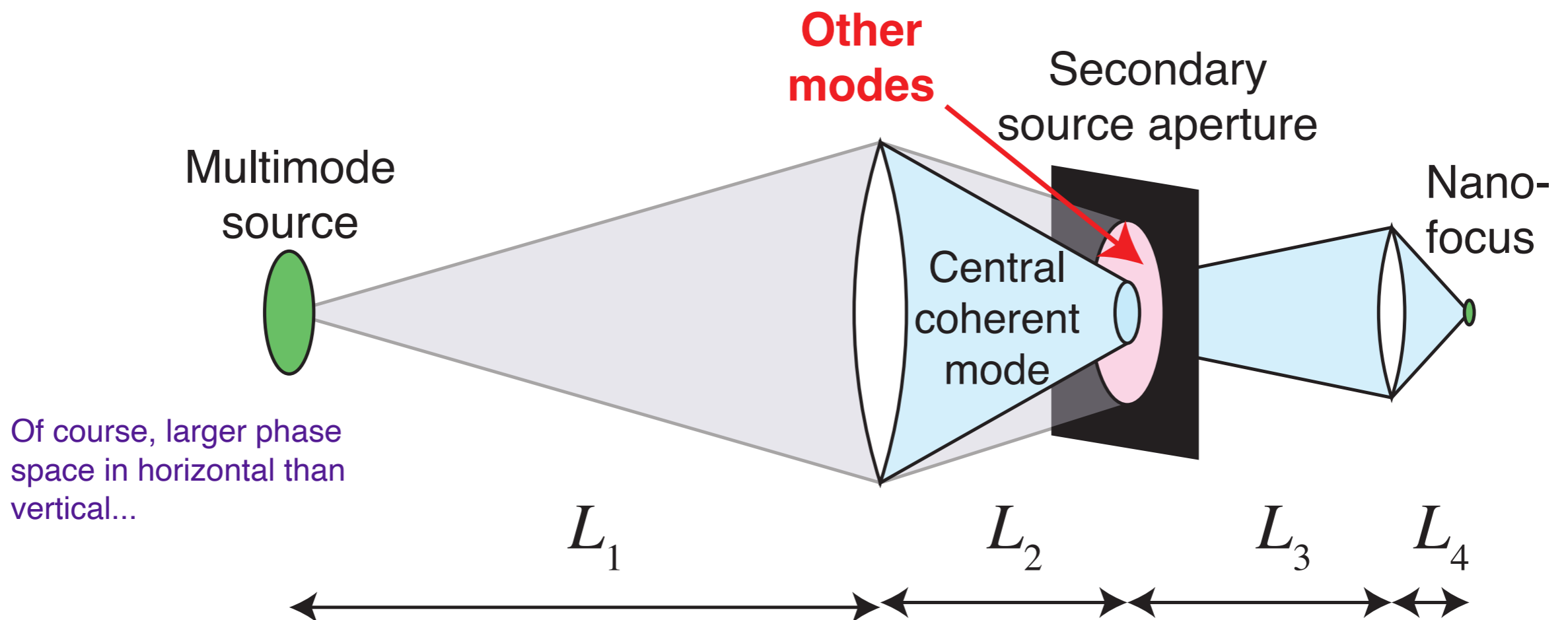
2D imaging with Stony Brook STXMs

2D imaging is moderately useful but...

- Cannot track fluroescently-labeled proteins in living cells
- Resolution is inferior to cryoEM, though do not need to section
- Best utility may lie beyond simple 2D imaging

10 μm
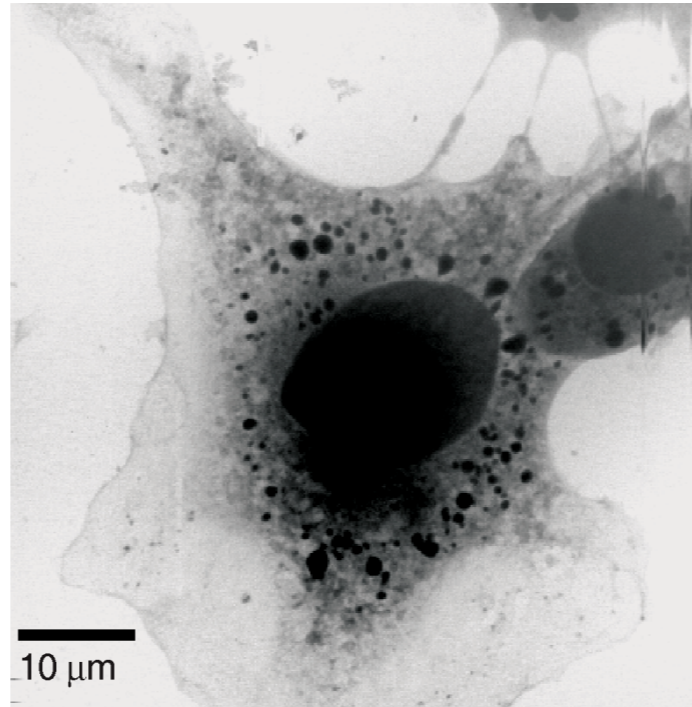
NIL 8 fibroblast (wet, fixed): Oehler *et al.*

Human sperm (unfixed): Wirick, Fleckenstein, Sheynkin *et al.*

2 microns
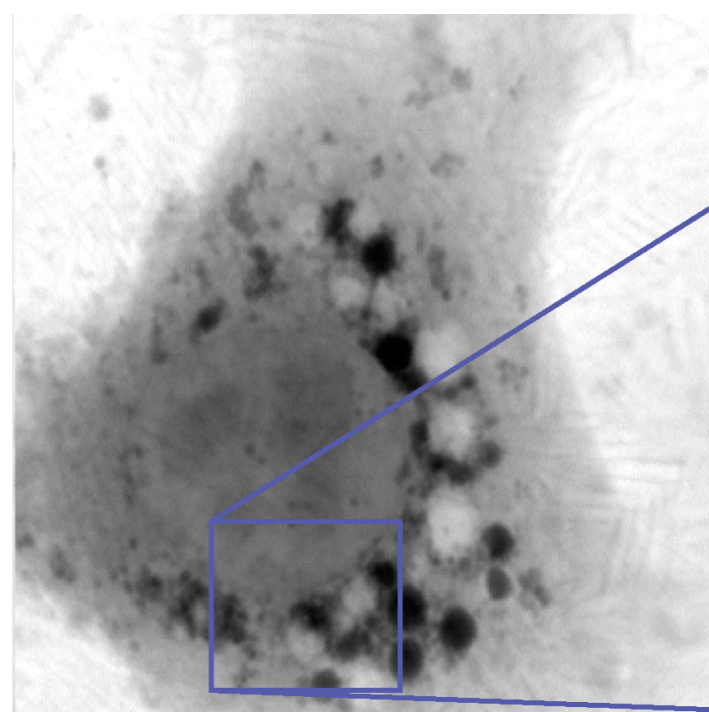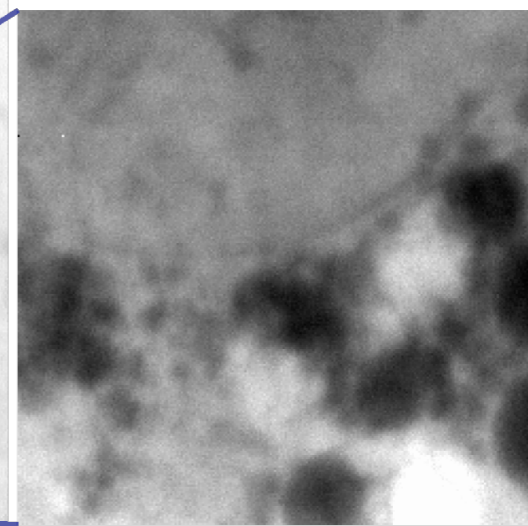
7 μm   2 μm

Fibroblast (frozen hydrated): Maser *et al.*, *J. Micros.* **197**, 68 (2000)

Bohr model and x-ray edges

- Bohr model for atomic number Z (with screening of nuclear charge Z_{screen}), and principal quantum number n (with quantum defect δ_ℓ):

$$E = E_0 \frac{(Z - Z_{\mathrm{screen}})^2}{(n - \delta_\ell)^2}$$

- E_0=13.6 eV

- $Z_{\mathrm{screen}} \simeq 1$ for n=1

- Quantum defect is usually small (like δ_ℓ<1)

- K edges: transition from n=2 to n=1

- L edges: transition from n=3 to n=2

Absorption edges

Lambert-Beer law: linear absorption coefficient μ

$$I = I_0 e^{-\mu(E) \cdot t} = I_0 e^{-D(E)}$$

This coefficient makes a jump at specific elemental absorption edges!

This example: 0.1 μm protein in water
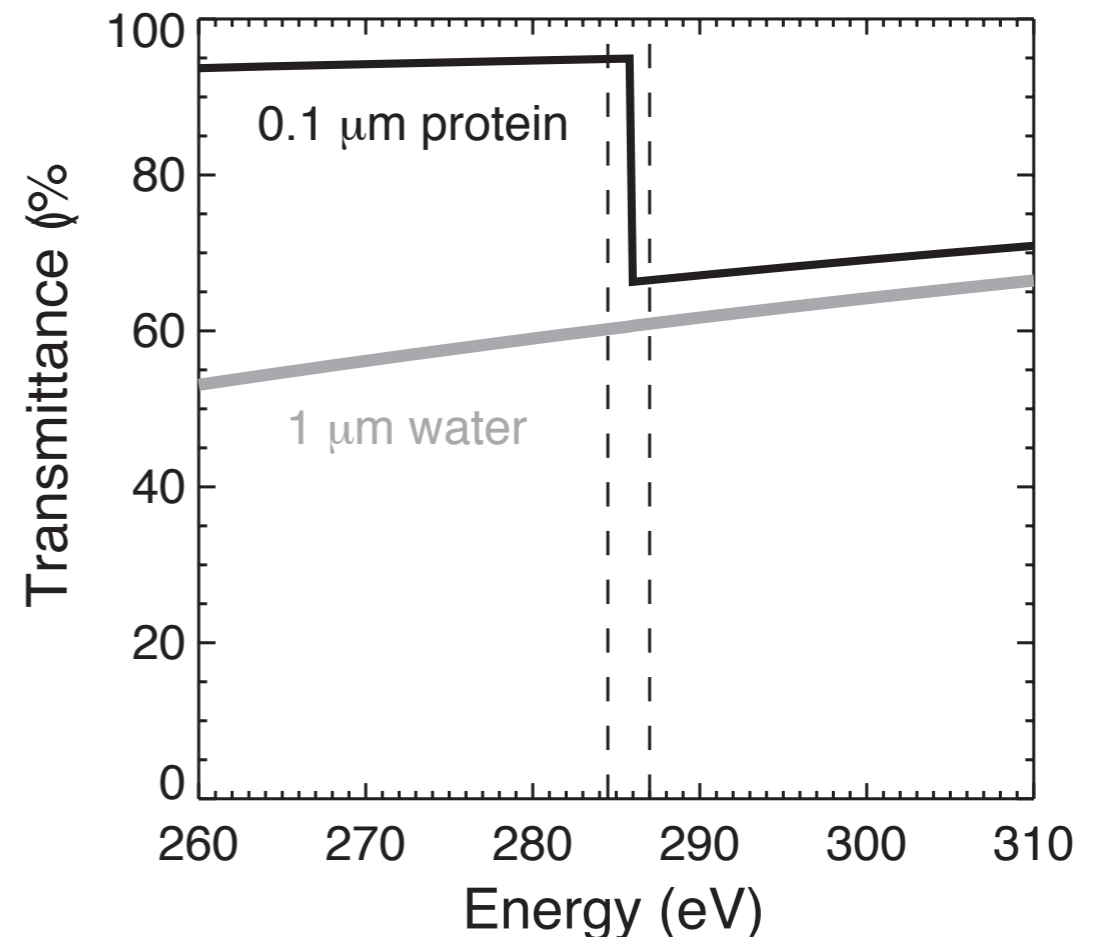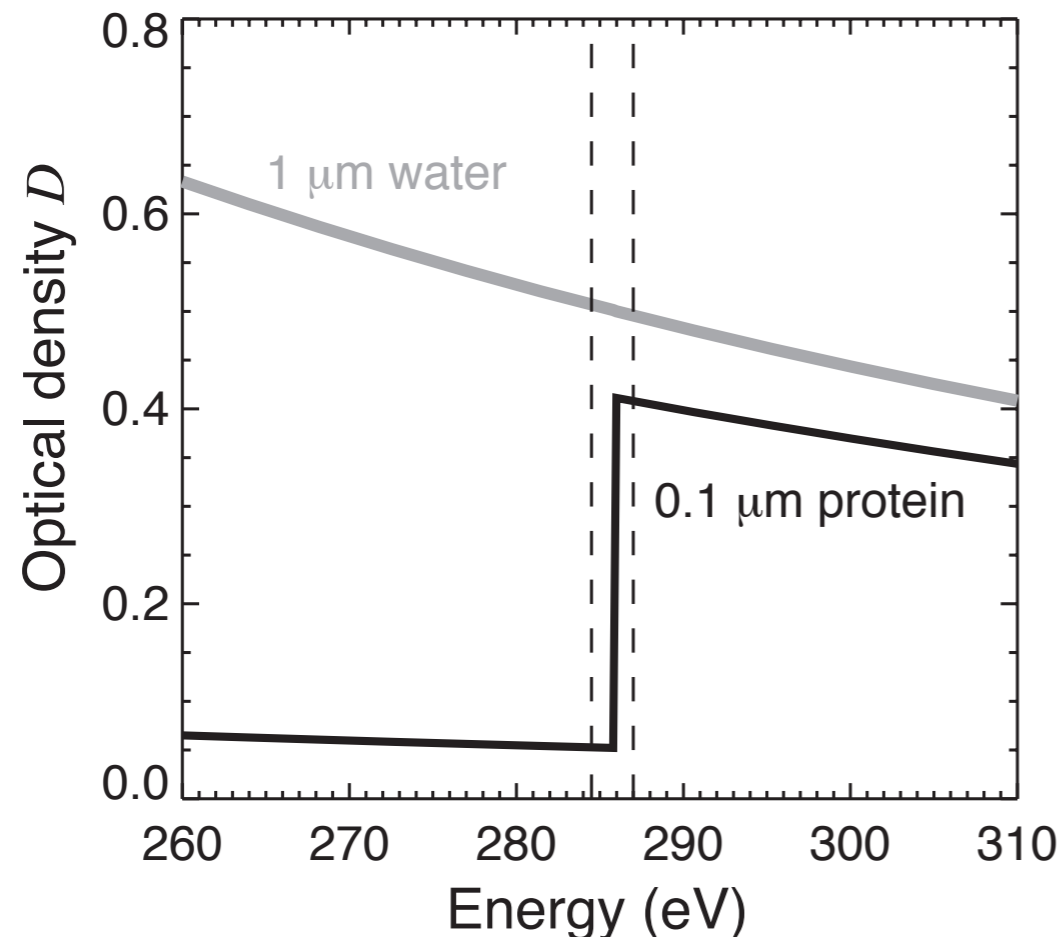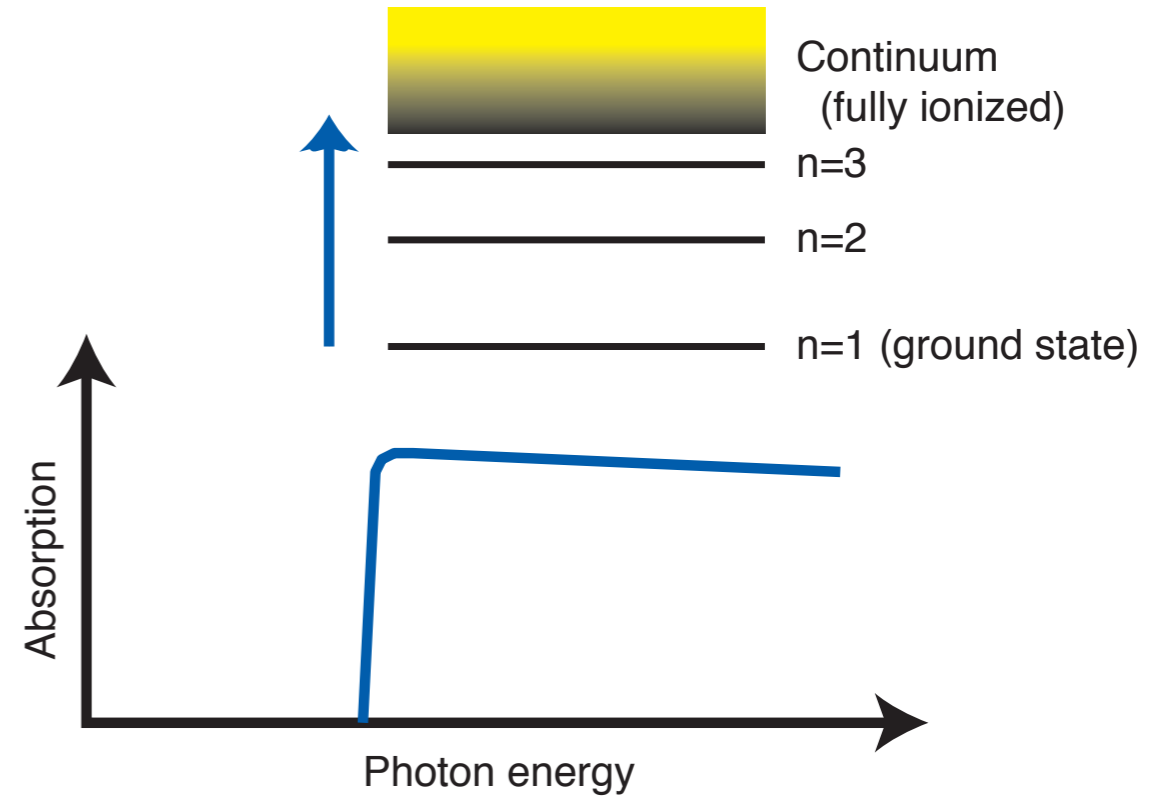
Chemical energies in eV

- Chemistry: C-H bond is 104 kcal/mol or 435 kJoules/mol:

$$\left(435 \frac{\text{kJ}}{\text{mol}}\right) \cdot \left(\frac{10^3 \text{ J}}{\text{kJ}}\right) \cdot \left(\frac{1 \text{ eV}}{1.602 \times 10^{-19} \text{ J}}\right) \cdot \left(\frac{1}{6.02 \times 10^{23} \text{ molecules/mol}}\right)$$

  or E=4.5 eV/molecule.

- Photon wavelength associated with 4.5 eV is

$$E = \frac{hc}{\lambda} = \frac{1240 \text{ eV} \cdot \text{nm}}{\lambda}$$

  or λ=275 nm.

- More broadly, chemical bonds involve 300-900 kJ/mol, or 3-9 eV/molecule, or 130-400 nm light.

Near-edge absorption fine structure (NEXAFS) or X-ray absorption near-edge structure (XANES)
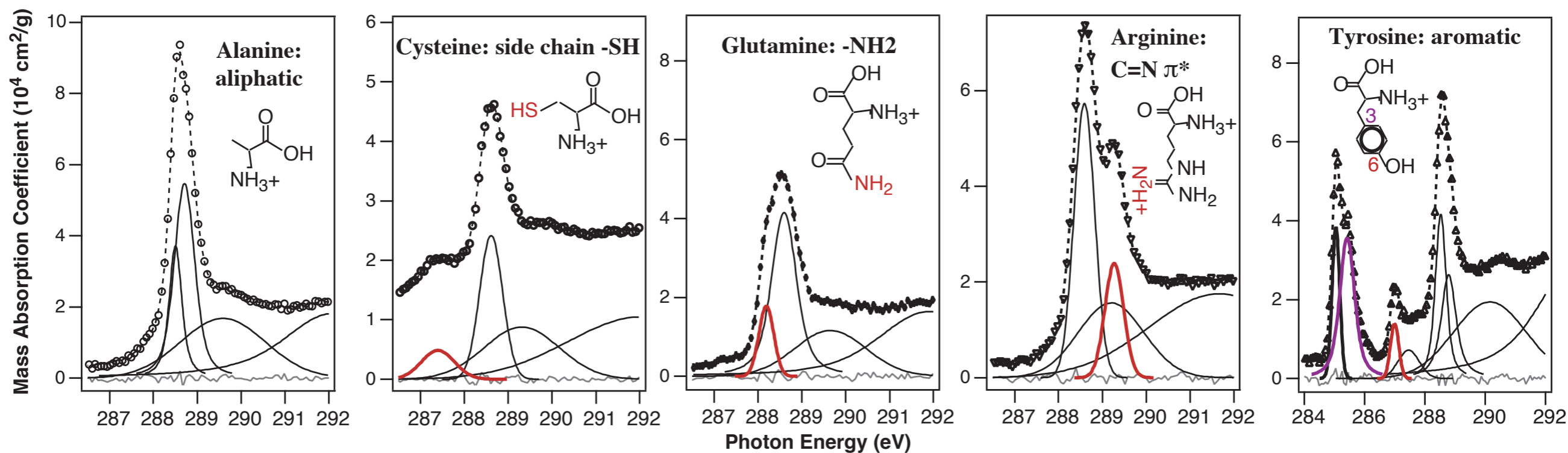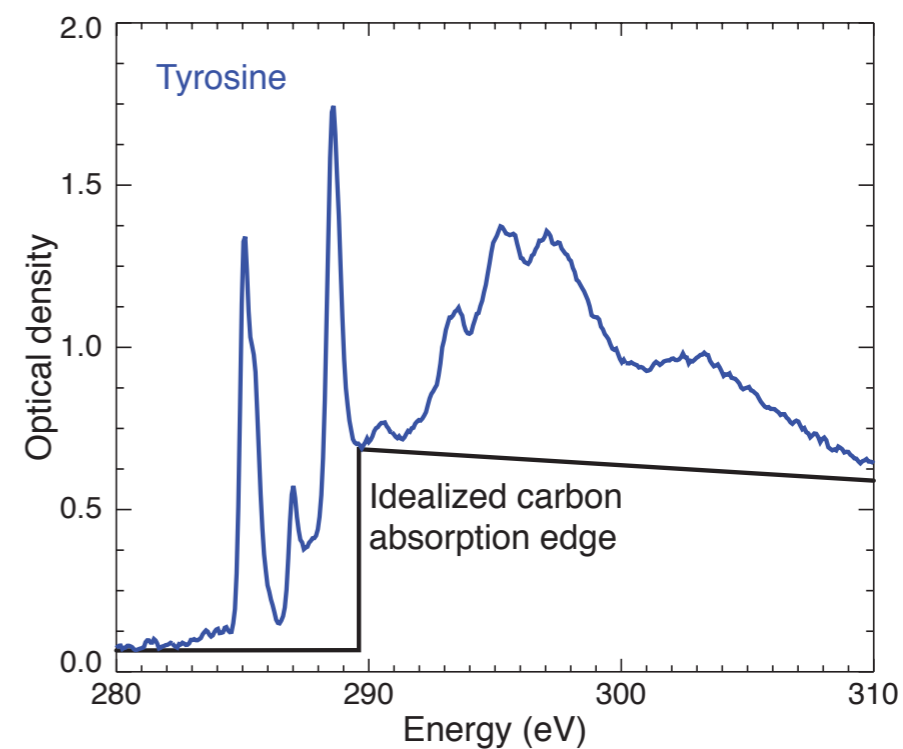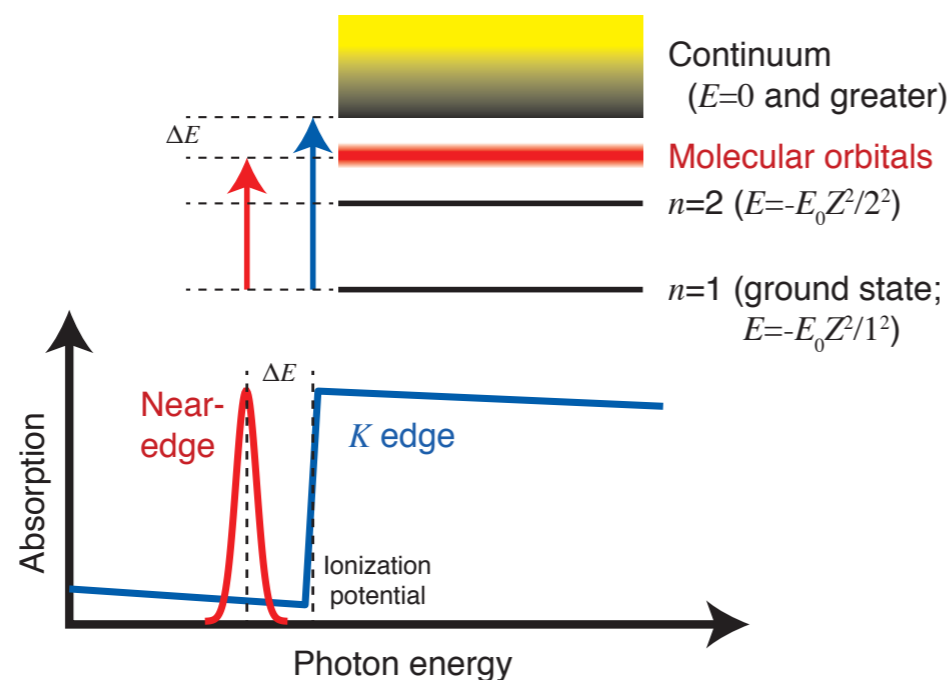
Amino acids example: K. Kaznacheyev *et al.*, *J. Phys. Chem.* **A 106**, 3153 (2002)

X-ray microscopy of colloids

- U. Neuhäusler (Stony Brook/Göttingen), S. Abend (Kiel), G. Lagaly (Kiel), C. Jacobsen (Stony Brook), *Colloid and Polymer Science* **277**, 719 (1999).

- Emulsion: water, oil droplets, clay, and layered double hydroxides (LDH).

- "Caged" part of oil droplet remains fixed; "uncaged" part can disperse.
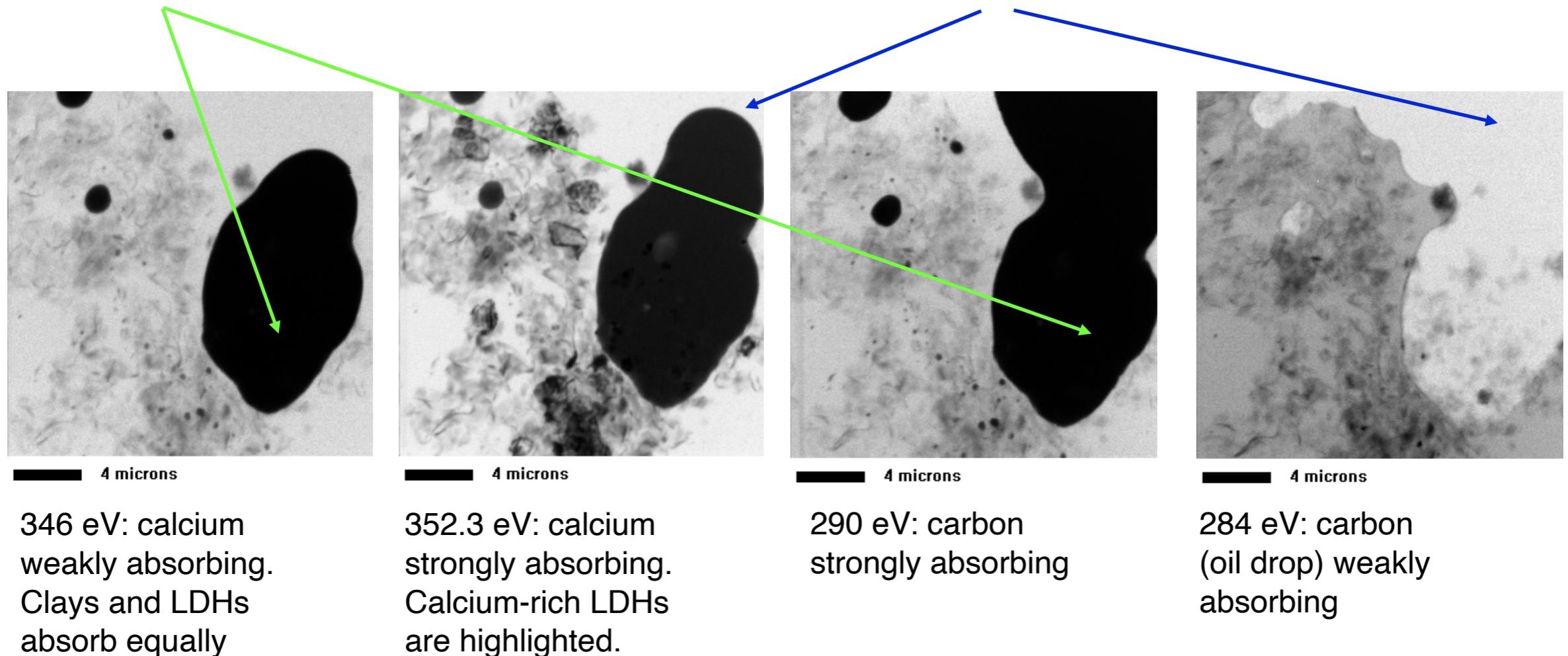
346 eV: calcium weakly absorbing. Clays and LDHs absorb equally

352.3 eV: calcium strongly absorbing. Calcium-rich LDHs are highlighted.

290 eV: carbon strongly absorbing

284 eV: carbon (oil drop) weakly absorbing

Optimized analysis

PAPER

View Article Online
View Journal

Non-negative matrix analysis for effective feature extraction in X-ray spectromicroscopy

Rachel Mak,[a] Mirna Lerotic,[b] Holger Fleckenstein,[c] Stefan Vogt,[d] Stefan M. Wild,[e] Sven Leyffer,[e] Yefim Sheynkin[f] and Chris Jacobsen*[dag]
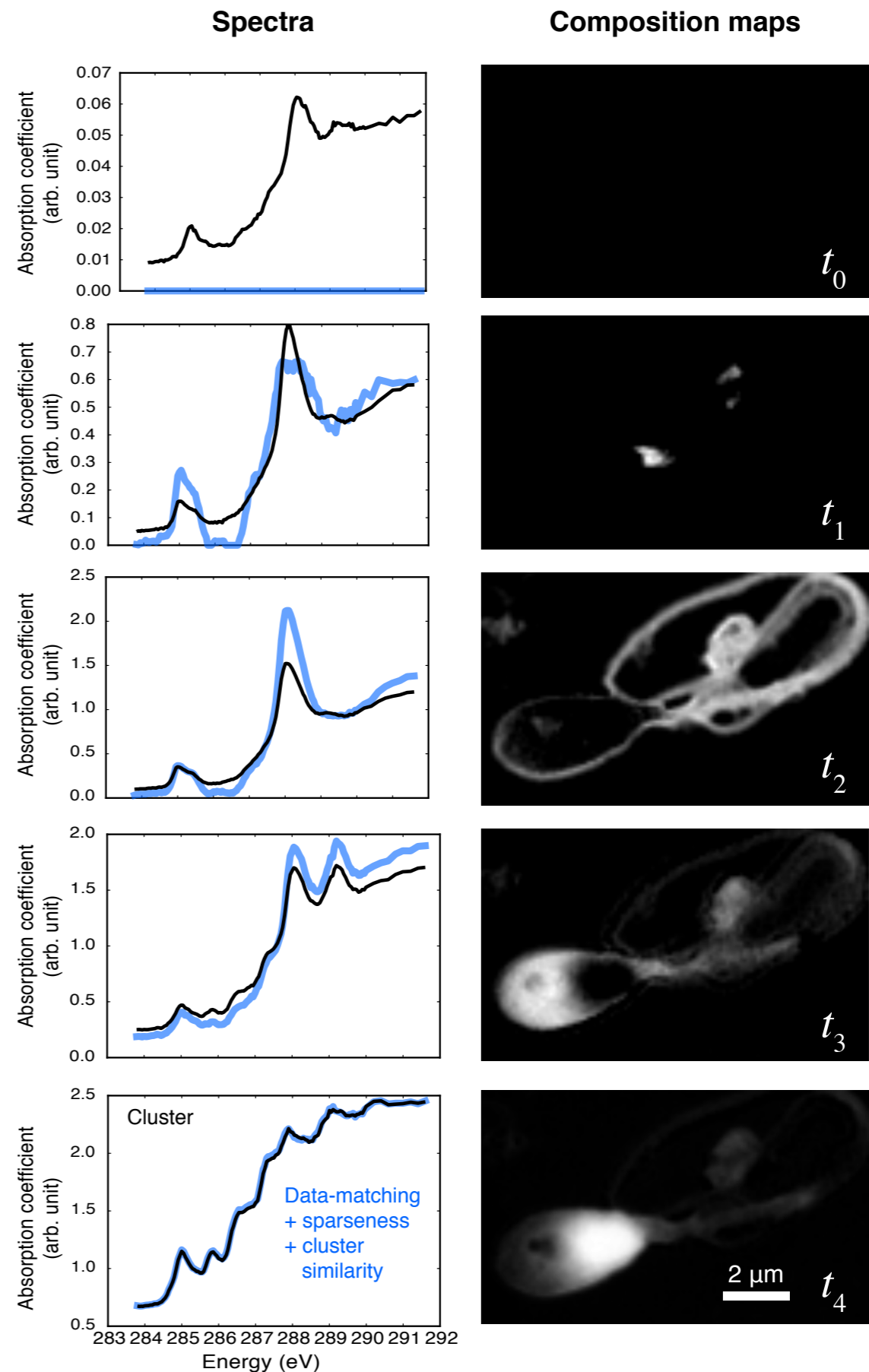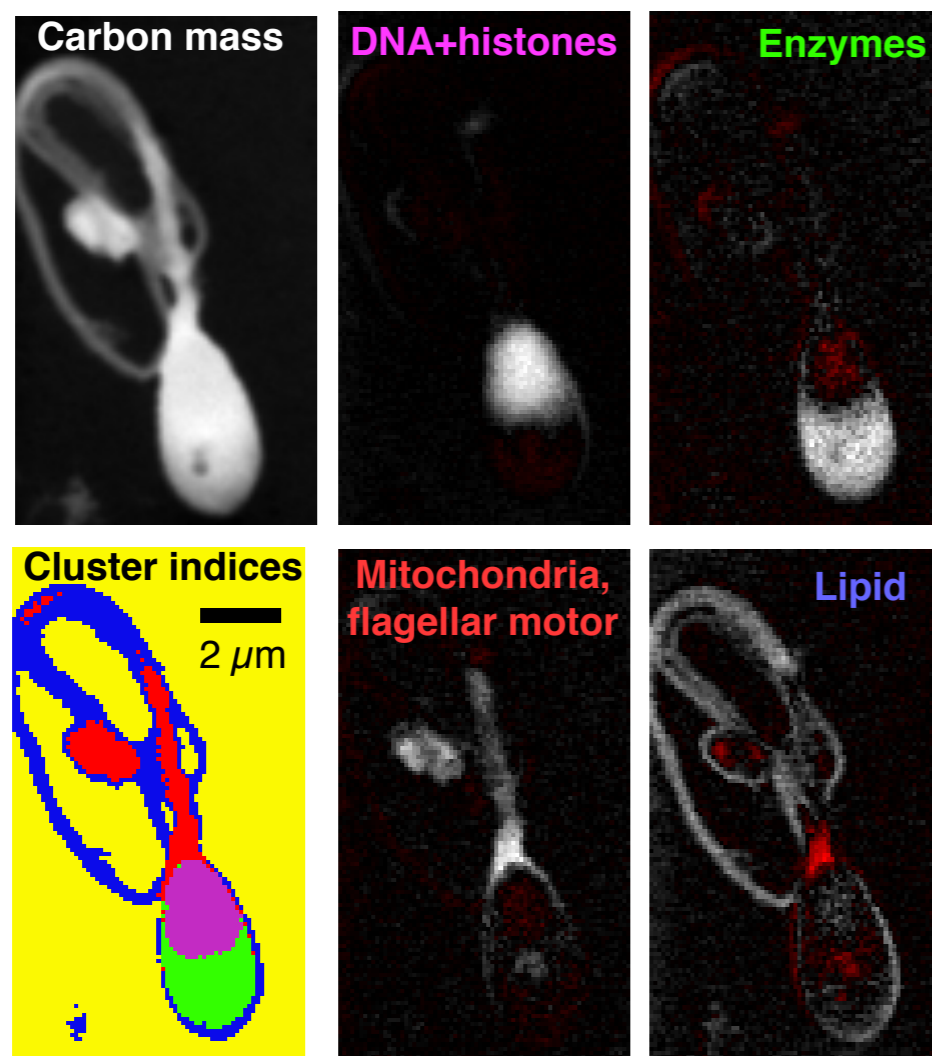
Silverman Hall
Northwestern University

X-ray fluorescence microscopy

- Energy dispersive detectors: 3.65 eV per electron-hole pair separation in Si.

- 10 keV photon produces 2740 electrons. Fluctuations: $(2740)^{1/2}=52$, so uncertainty is $(52/2740)*10,000$ eV=190 eV.

- Detector at 90°: minimize elastic scattering.

Undulator

Monochromator

Zone plate objective

Order Sorting Aperture

Sample, raster scanned

XRF Detect.

Pixelated area detector
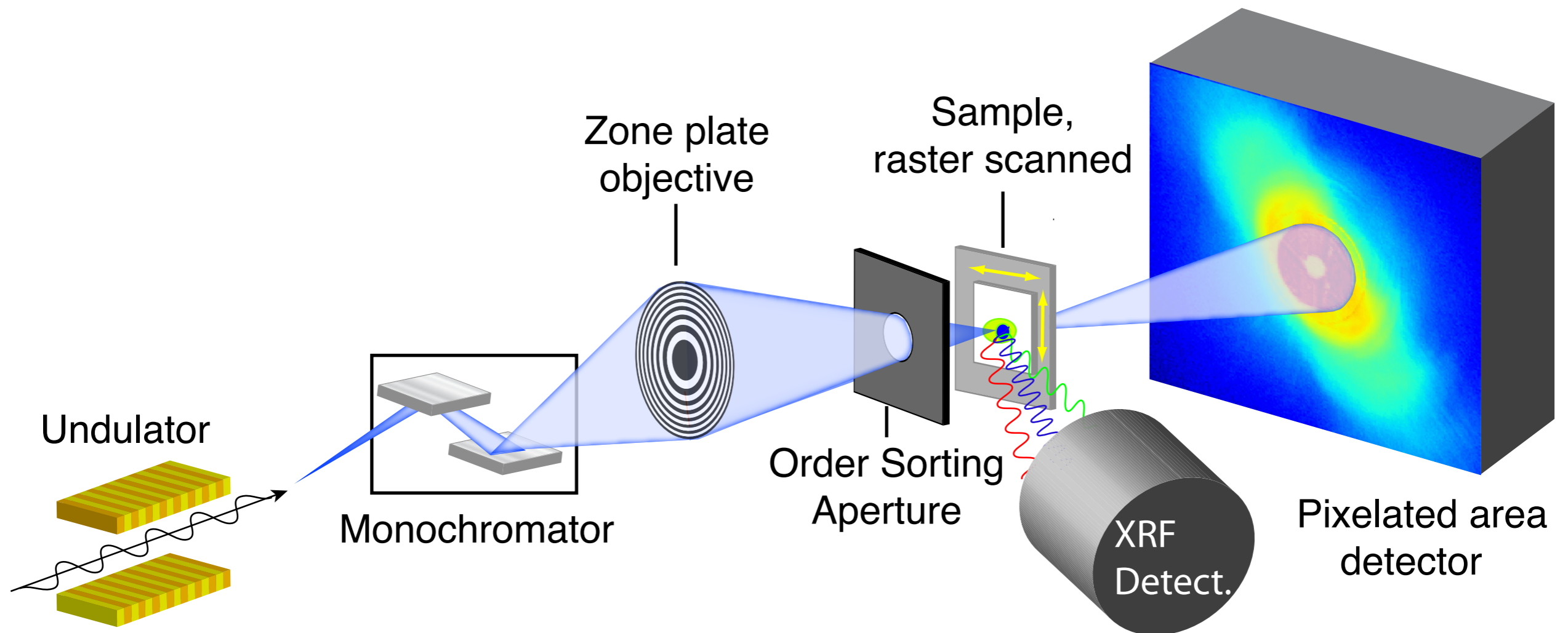
Fluorescence yield

Fluorescence yield ω=fraction of time you get a fluorescent photon rather than an Auger electron
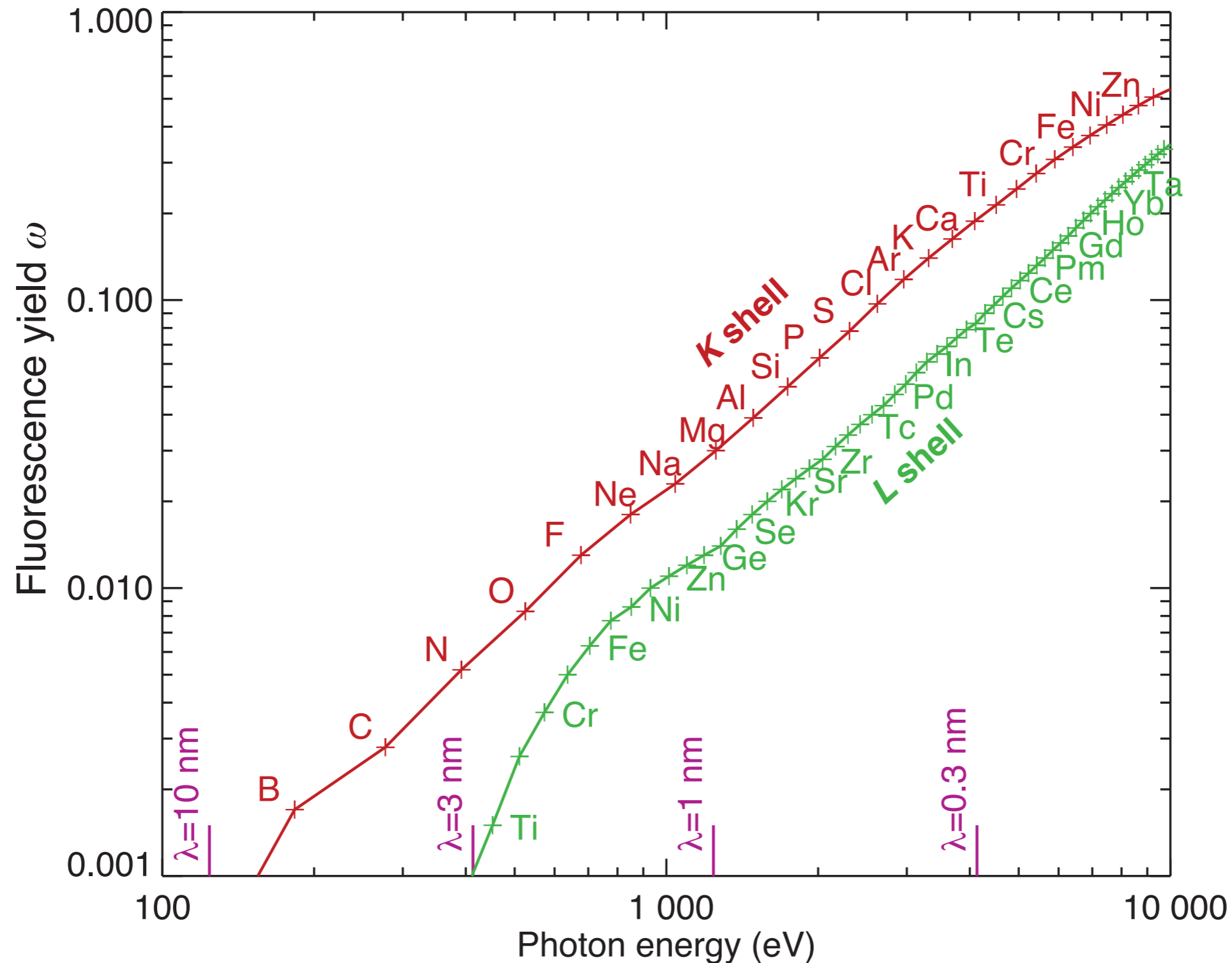
Exciting x-ray fluorescence

X rays and protons produce a dramatically lower continuum background, increasing sensitivity (but proton microprobes induce much more damage)

Electrons: linear scale

X rays: log scale
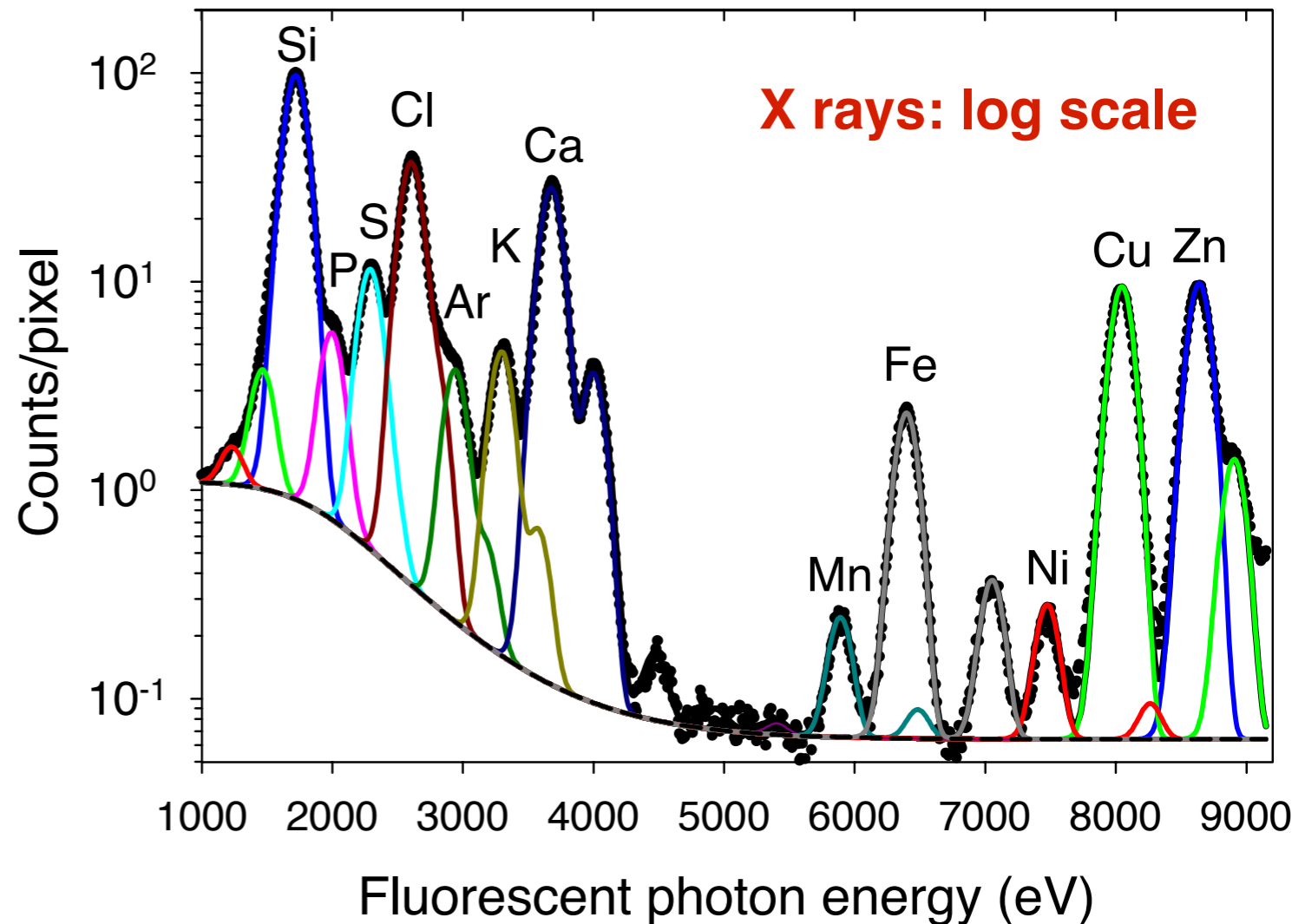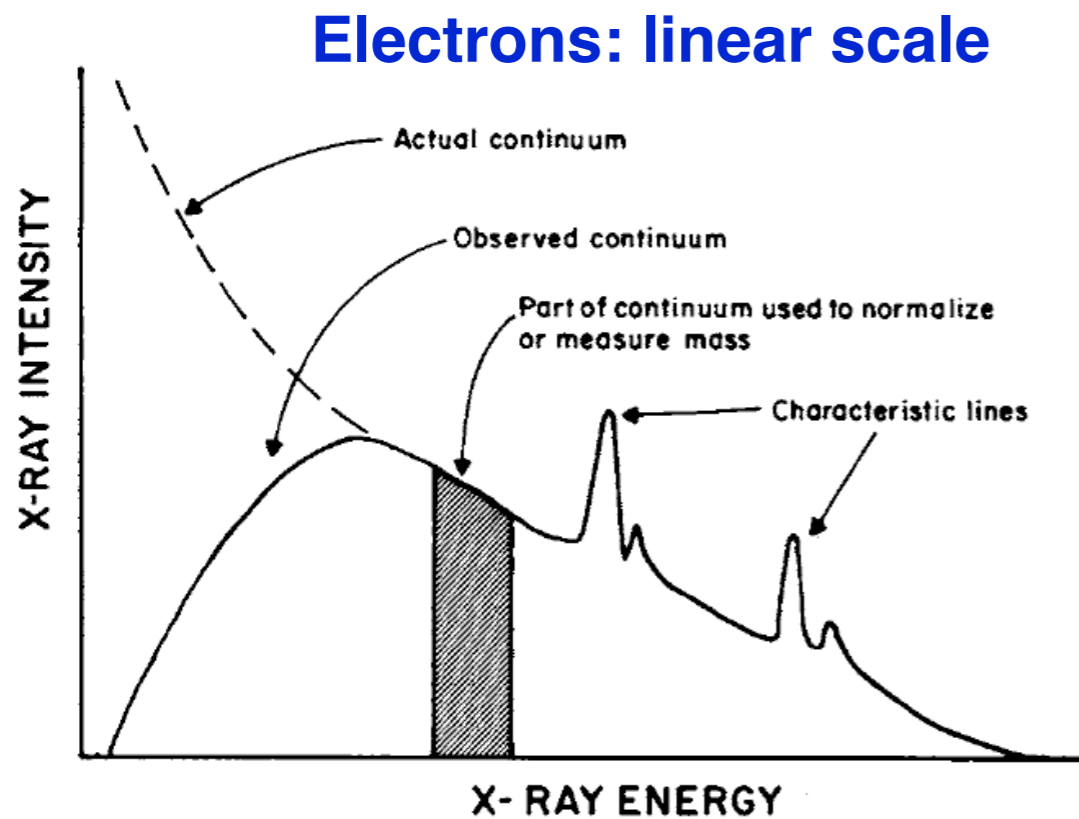
LeFurgey and Ingram, *Environmental Health Perspectives* **84**, 57 (1990)

Twining *et al.*, *Anal. Chem.* **75**, 3806 (2003). Analysis approach: Vogt, Maser, and Jacobsen, *J. Phys. IV* **104**, 617 (2003).

Example x-ray spectrum and fit
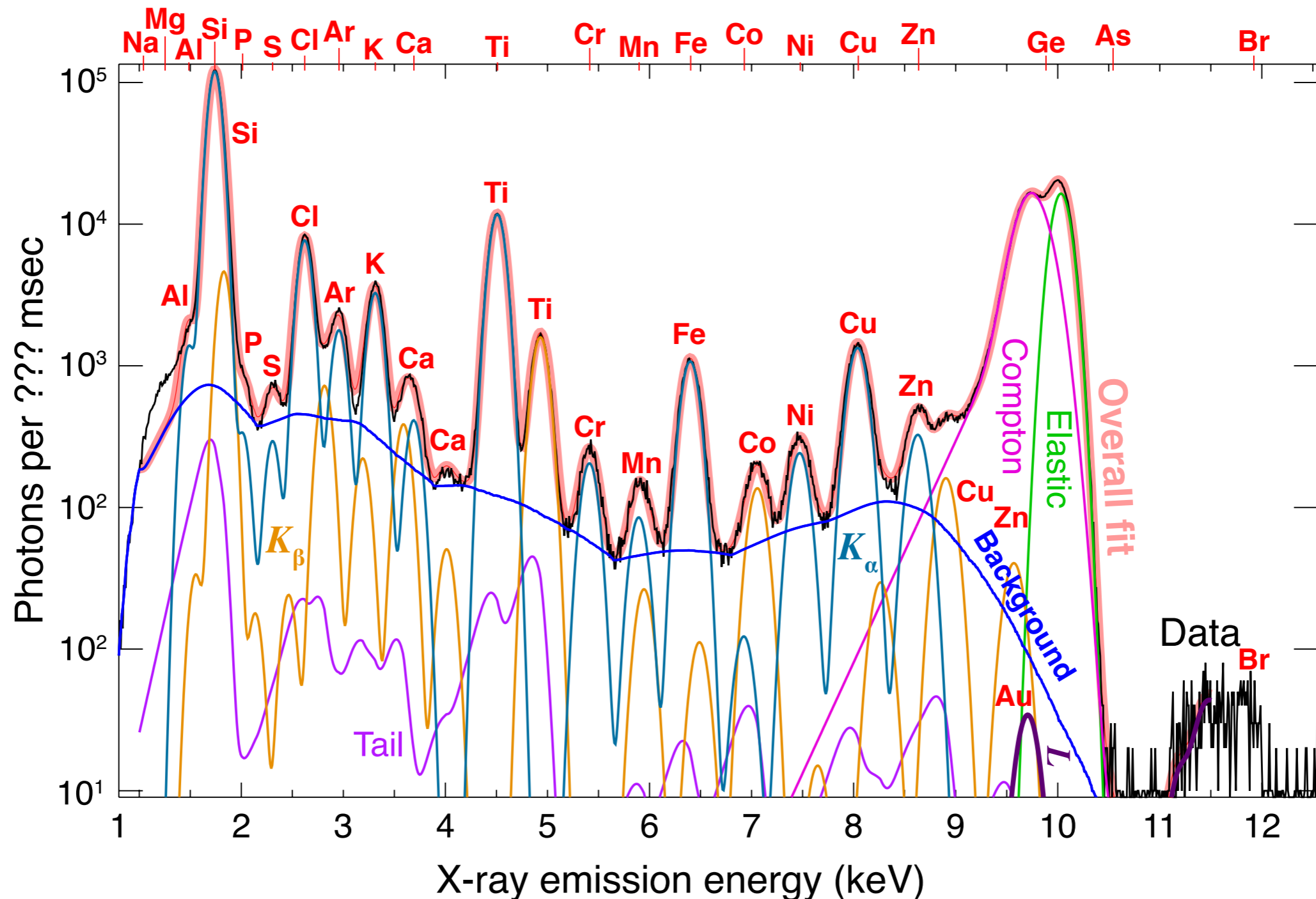
Spectrum: Olga Antipova, APS. Fit: S. Vogt, *J. Phys. IV France* **104**, 635 (2003). See also Ryan and Jamieson, *Nucl. Inst. Meth. B* **77**, 203 (1993); and Solé *et al.*, *Spectrochimica Acta B* **62**, 63 (2007).

Electron probes in thick specimens
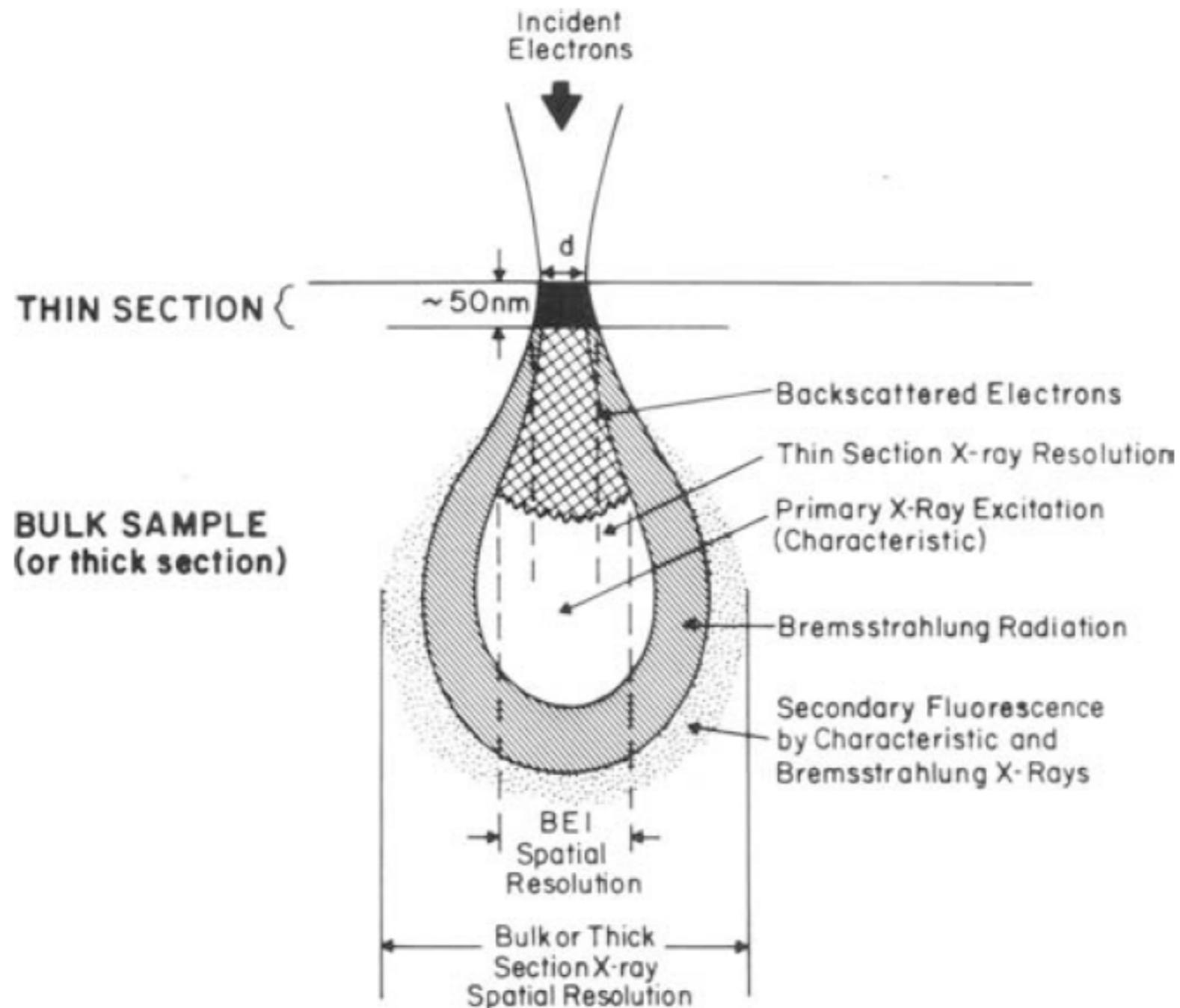
Electron beams broaden in thick specimens due to sidescattering; x-ray beams do not. LeFurgey and Ingram, *Environmental Health Perspectives* **84**, 57 (1990).
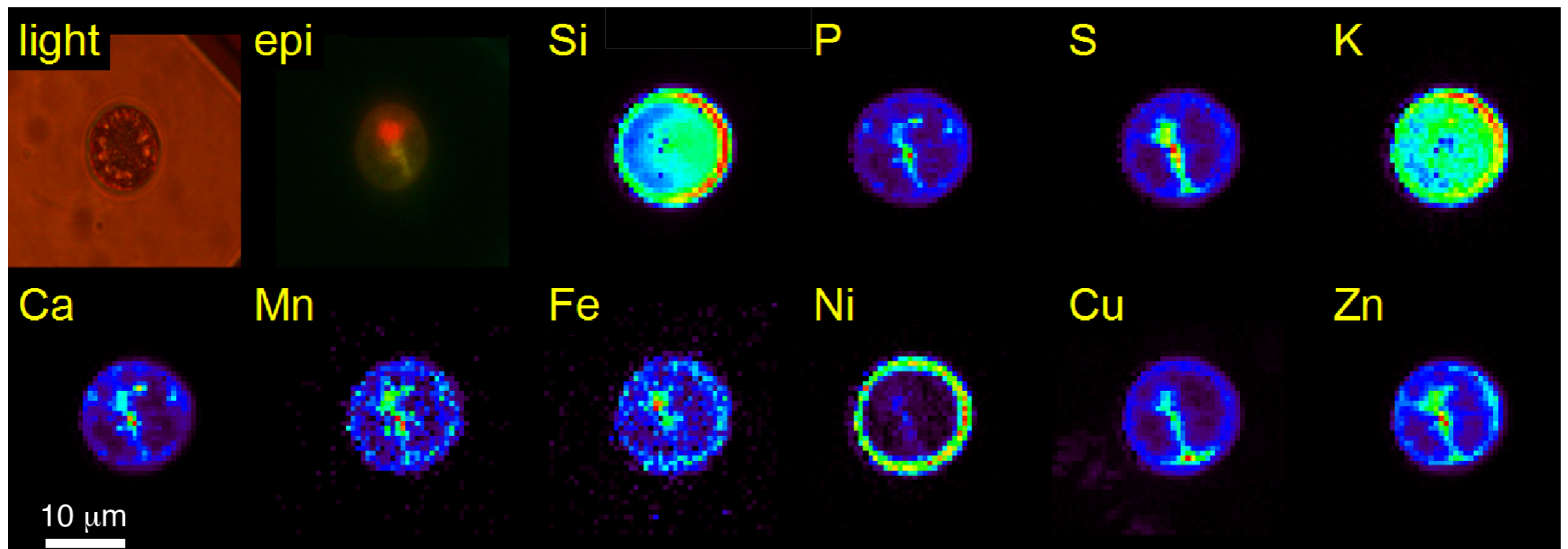
Global carbon cycle
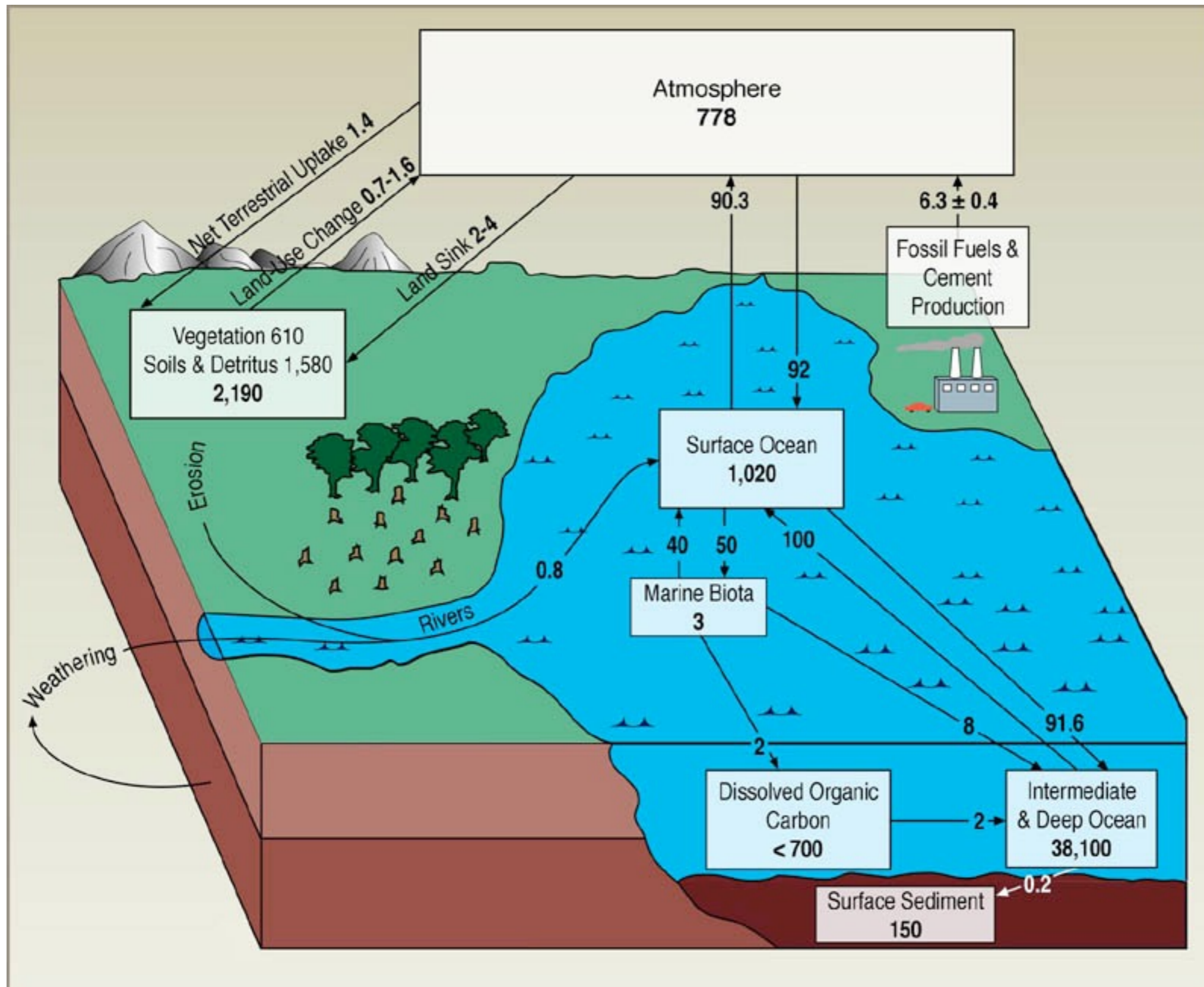
petagrams, petagrams/year (climatescience.gov)

Iron and carbon in the ocean

- Seed Southern Pacific with bioavailable iron to increase CO_2 uptake?
- Requires understanding of iron and carbon uptake in phytoplankton; combine fluorescence with phase contrast.

light epi Si P S K

Ca Mn Fe Ni Cu Zn

10 µm

B. Twining, S. Baines, N. Fisher, J. Maser, S. Vogt, C. Jacobsen, A. Tovar-Sanchez, and S.Sañudo-Wilhelmy, *Anal.. Chem.* **75**, 3806 (2003)

Cruising the Southern Pacific

Quantitative 3D fluorescence of a diatom
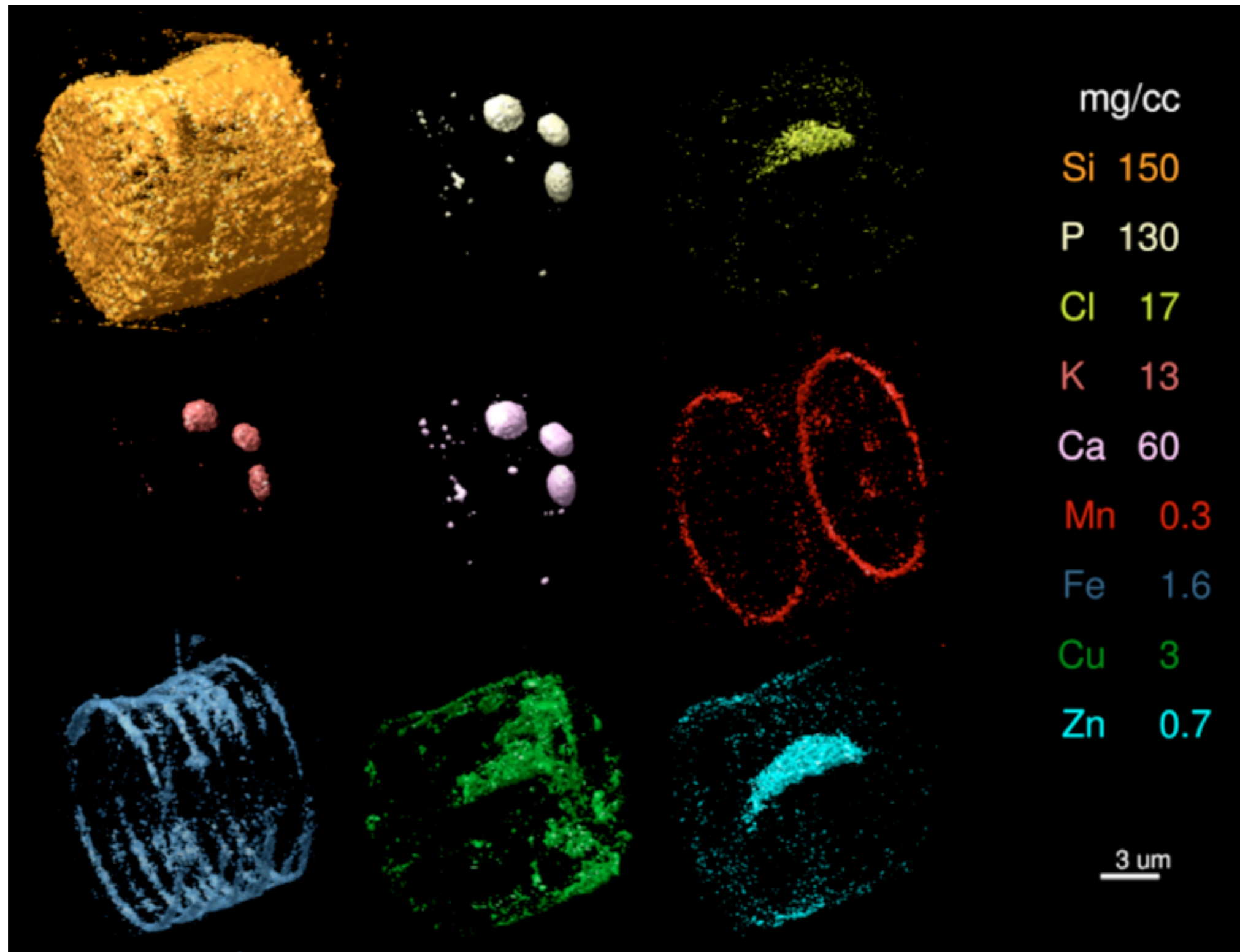
M. de Jonge, C. Holzner, S. Baines, B. Twining, K. Ignatyev, J. Diaz, D. Howard, A. Miceli, I. McNulty, C. Jacobsen, S. Vogt, *Proc. Nat. Acad. Sci.* **107**, 15676 (2010)

Fluorescence tomography
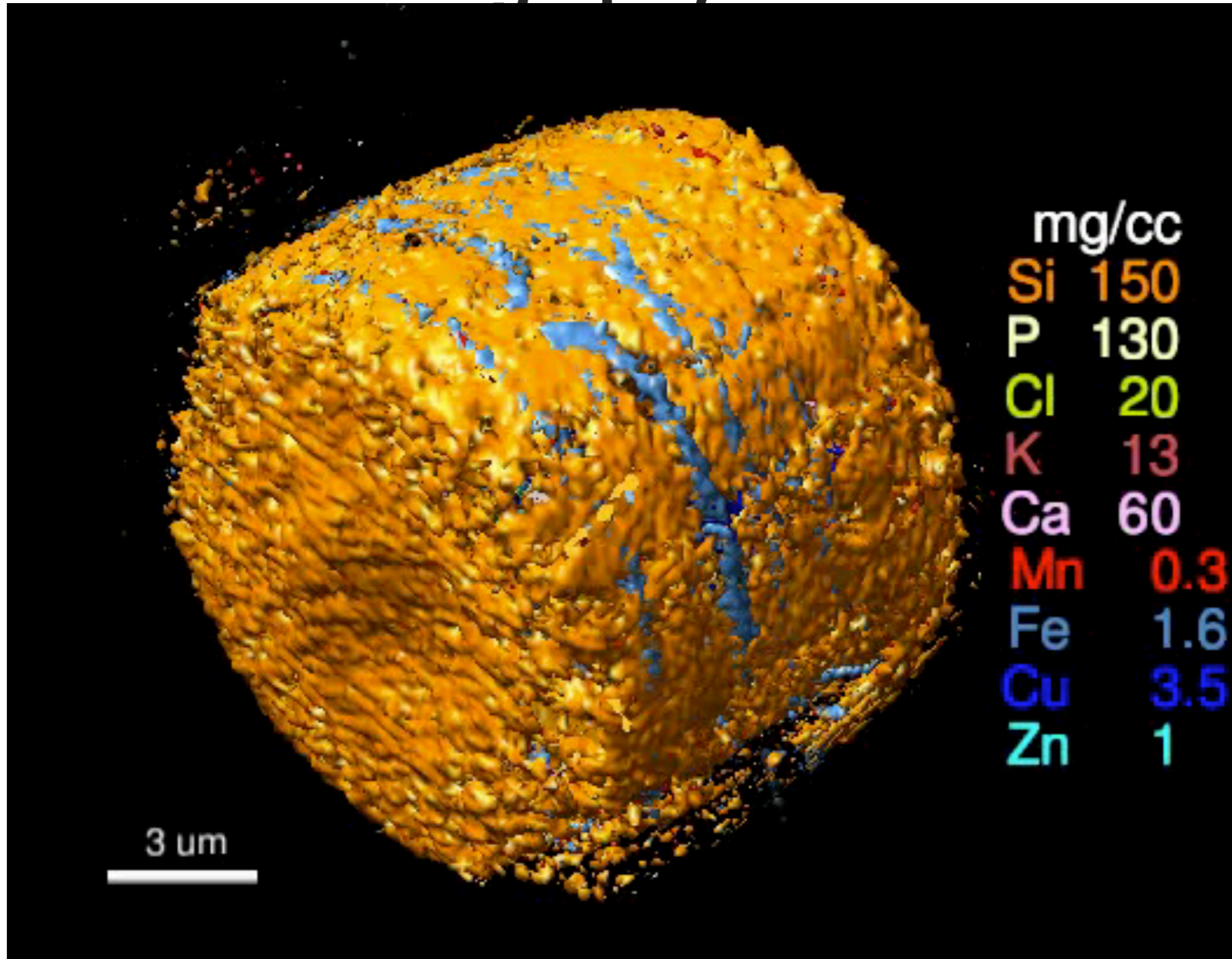
de Jonge *et al.*, *Proc. Nat. Acad. Sci.* **107**, 15676 (2010).

X-ray fluorescence microscopy

- Energy dispersive detectors: 3.65 eV per electron-hole pair separation in Si.

- 10 keV photon produces 2740 electrons. Fluctuations: $(2740)^{1/2}=52$, so uncertainty is $(52/2740)*10,000$ eV=190 eV.

- Detector at 90°: minimize elastic scattering.

Undulator

Monochromator

Zone plate objective

Order Sorting Aperture

Sample, raster scanned

XRF Detect.

Pixelated area detector
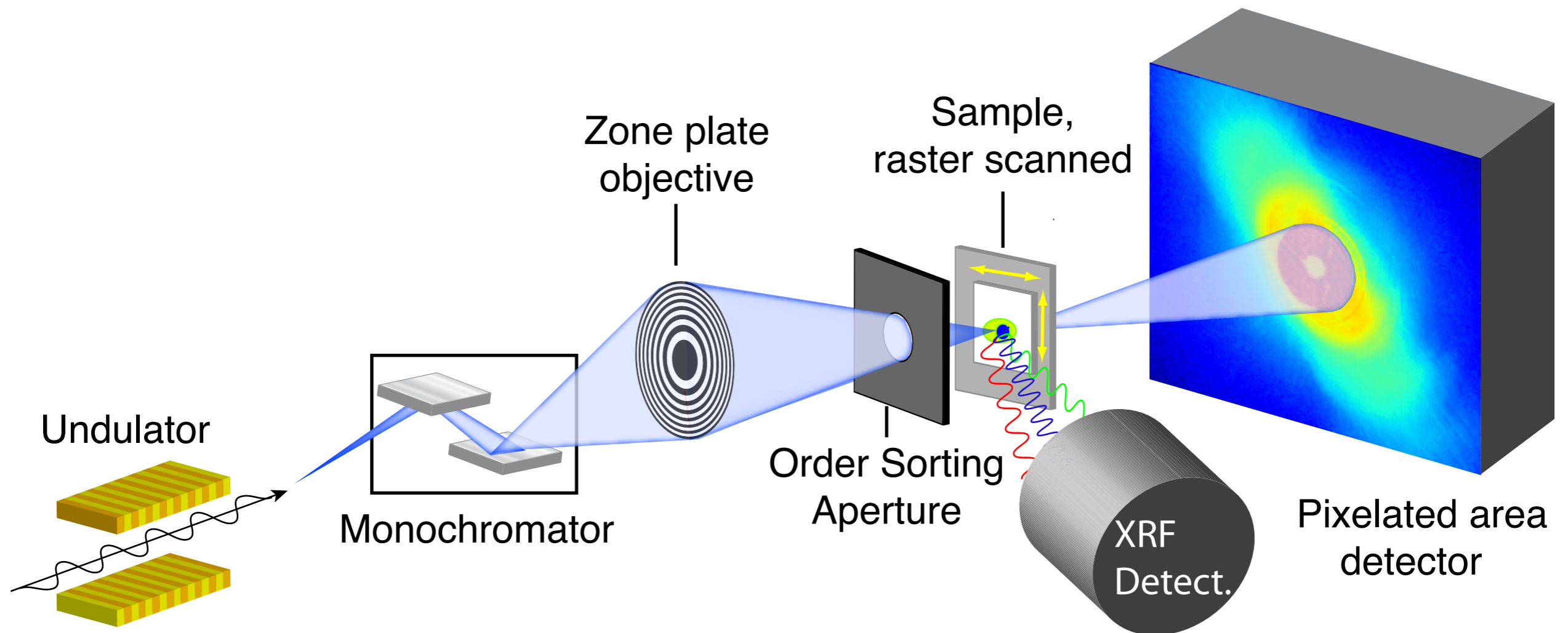
Combined x-ray ptychography and fluorescence

- *Chlamydomonas reinhardtii*, frozen in <0.1 msec from the living state, imaged whole under cryogenic conditions.

- 80 nm resolution in fluorescence, 18 nm resolution in ptychography

- Deng, Vine, Chen, Jin, Nashed, Peterka, Vogt, and Jacobsen, *Scientific Reports* **7**, 445 (2017)
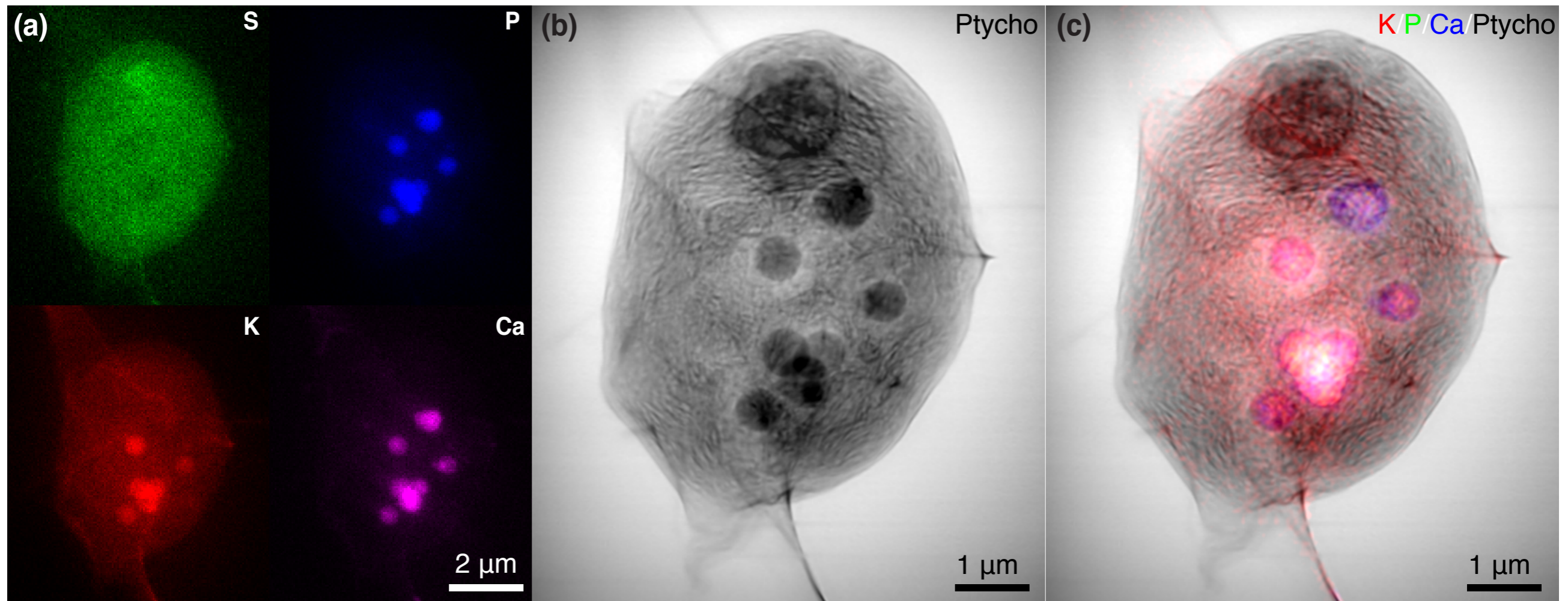
Frozen hydrated alga in 3D

- Deng, Lo, Gallagher-Jones, Chen, Pryor Jr., Jin, Hong, Nashed, Vogt, Miao, and Jacobsen, *Science Advances* **4**, eaau4548 (2018)

- 3D resolution of about 100 nm

Removing/re-adding in turn:
Cl
S
K
P
Ca
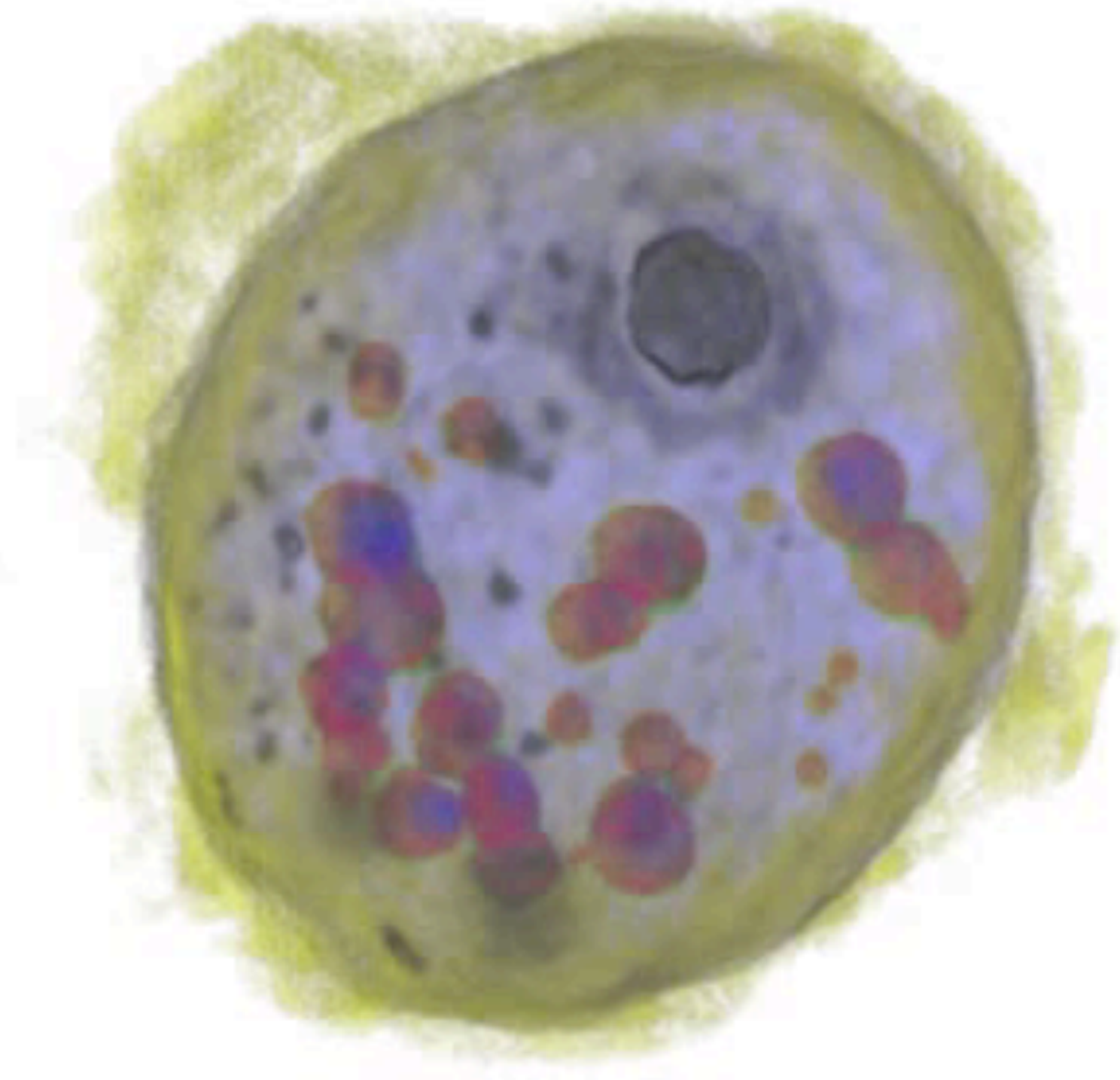
Depth of focus

- Numerical aperture: semi-angle of lens θ

- Transverse resolution δ_r is

$$\delta_r = 0.61 \frac{\lambda}{\theta}$$

- Depth of focus DOF is

$$\text{DOF} = 2\frac{\lambda}{\theta^2}$$
$$= 5.4 \frac{\delta_r^2}{\lambda}$$

δ_r: transverse resolution

Depth of focus DOF (µm) vs Energy (keV), with lines for δ_r=1000 nm, δ_r=500 nm, δ_r=200 nm, δ_r=100 nm, δ_r=50 nm, δ_r=20 nm, δ_r=10 nm, δ_r=5 nm, δ_r=2 nm
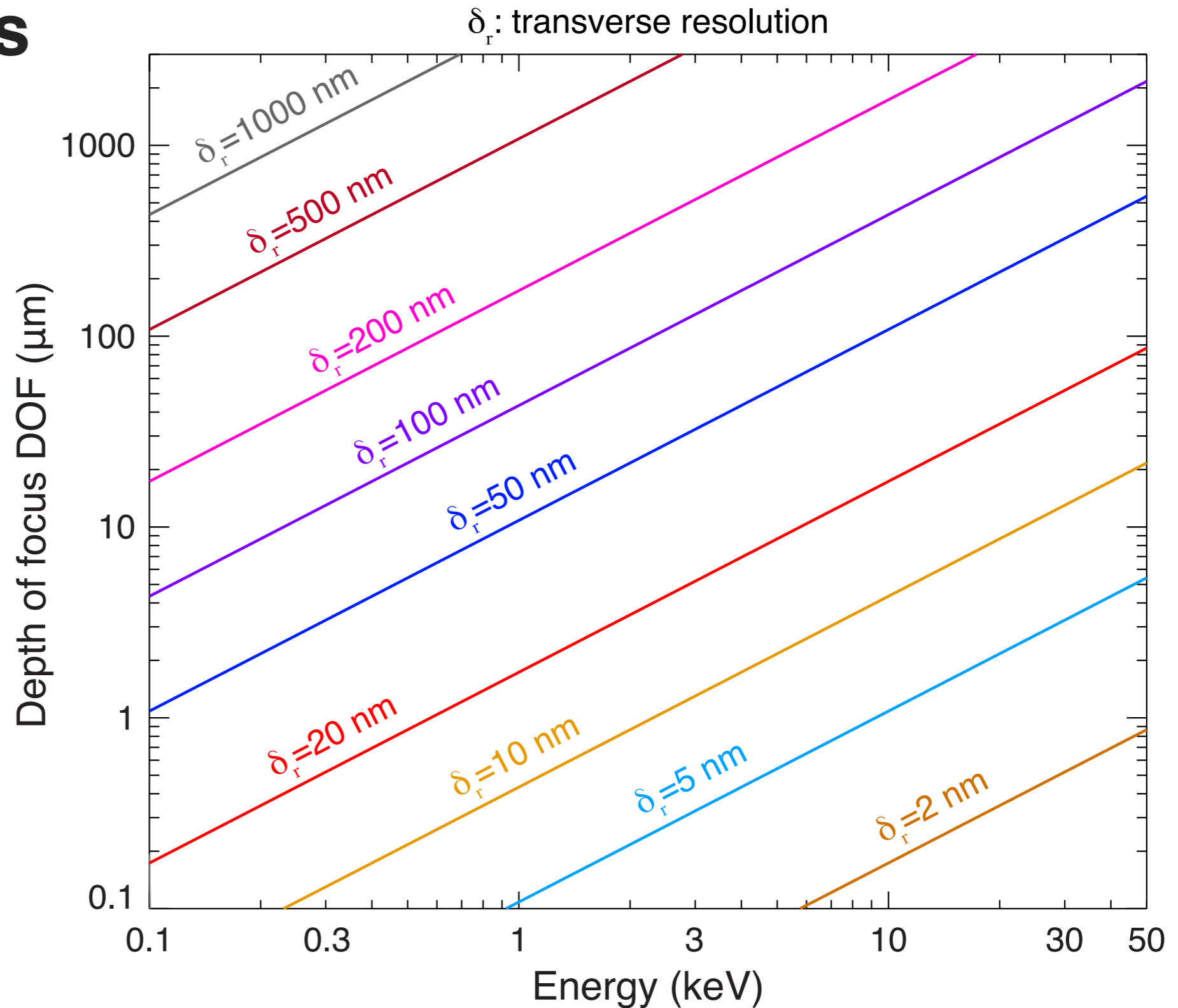
The multislice method

- Multislice method: Cowley and Moodie, *Proceedings of the Physical Society of London B* **70**, 486 (1957); *Acta Crystallographica* **10**, 609 (1957).

- Visible light: beam propagation method. Van Roey *et al.*, *JOSA* **71**, 803 (1981).

- Accounts for multiple scattering effects.

- It even reproduces mirror reflectivity and waveguide effects in x-ray optics! Li and Jacobsen, *Optics Express* **25**, 1831 (2017).
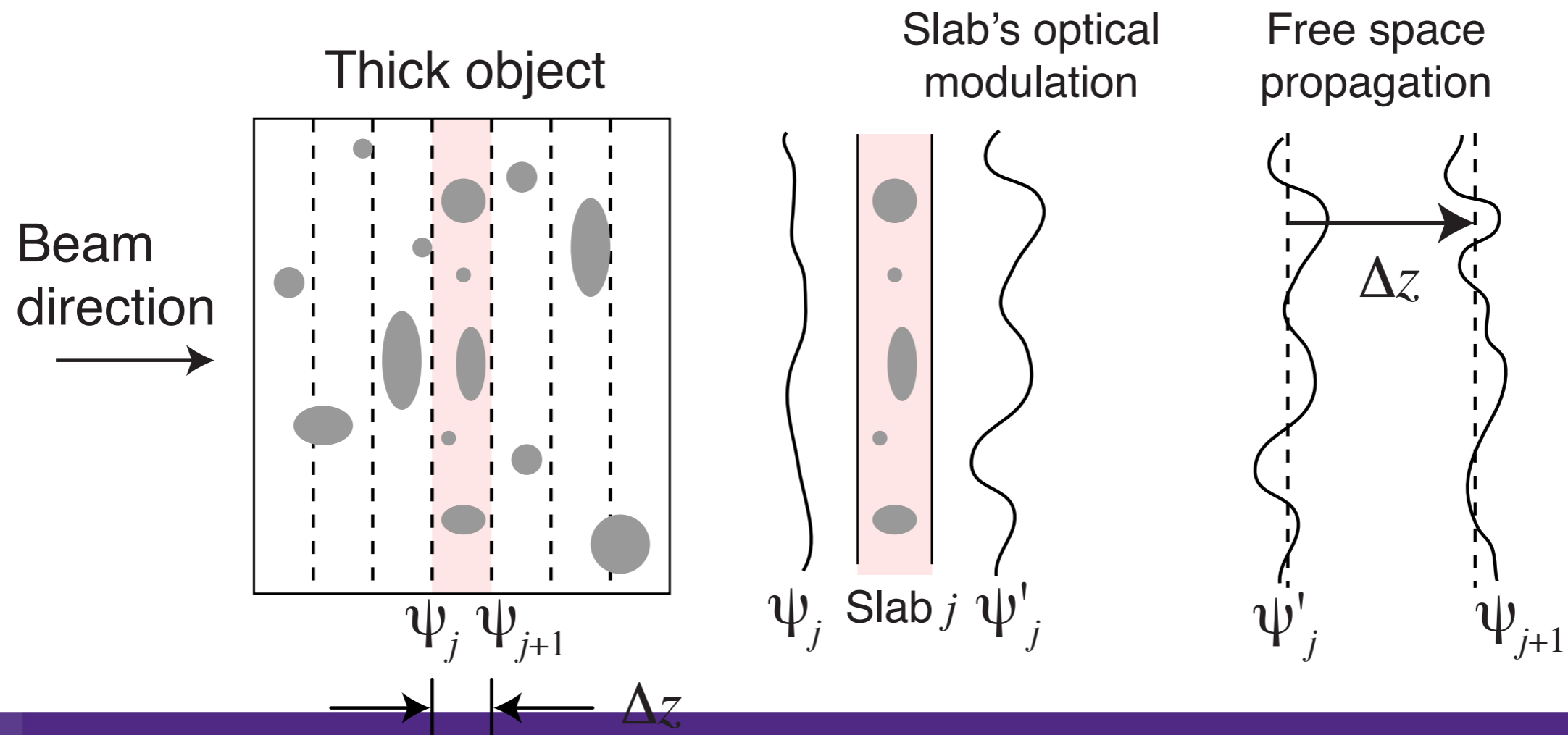
Beyond the depth of focus, and Kierkegaard

- Søren Kierkegaard (1813-1855): "life must be lived forwards, but it is best understood backwards"

- Wavefield through a simulated cell: Thibault, Elser, Jacobsen, Shapiro, and Sayre, *Acta Cryst. A* **62**, 248 (2006).

(a) *(b)* *(c)*

(intensity scaled up)
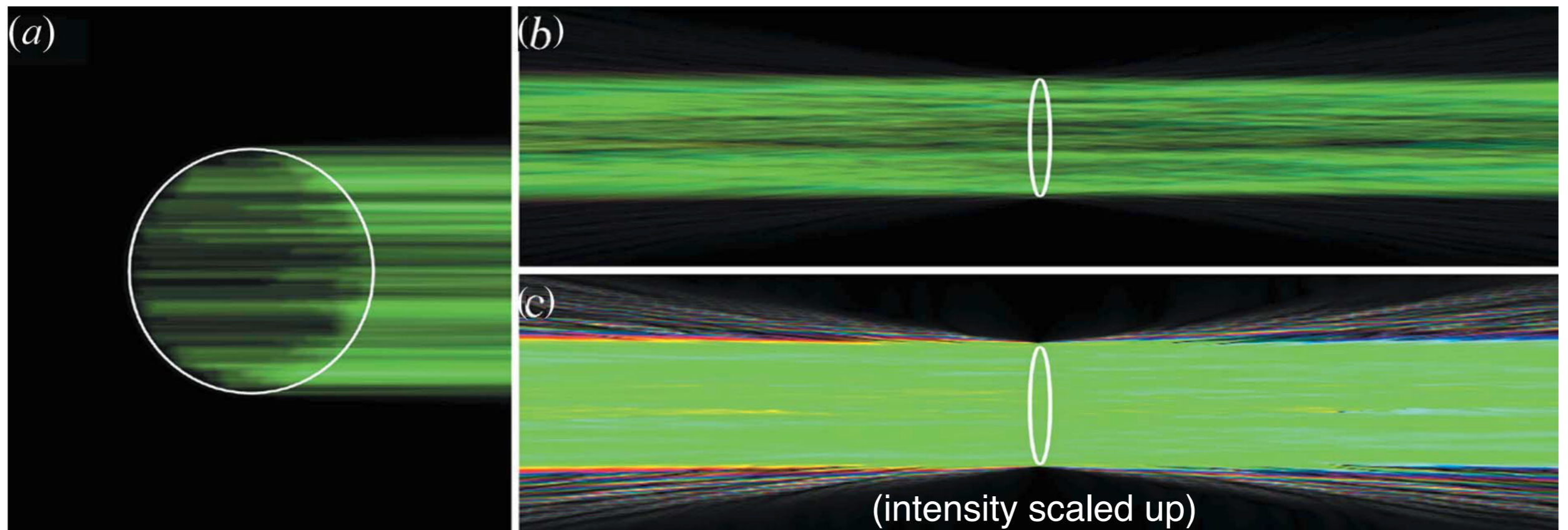
Forward multislice propagation of a wave through a simulated cell

Backward propagation of the correctly-phased far-field wavefield

Numerical optimization of cost functions

- If you know the forward model (multislice), you can define a cost function:

$$C = |I_{\mathrm{measured}} - I_{\mathrm{predicted}}| + \lambda_n R_n$$

- From a present guess of the object, calculate $I_{\mathrm{predicted}}$. Adjust guess based on derivatives (gradient descent), including regularizers R. Iterate.

- No need for phase unwrapping.

Automatic differentiation for beyond depth-of-focus

- M. Du, Y. Nashed, S. Kandel, D. Gürsoy, and C. Jacobsen, "Three dimensions, two microscopes, one code: automatic differentiation for x-ray nanotomography beyond the depth of focus limit," *Science Advances* **6**, eaay3700 (2020).

- With automatic differentiation, one can easily change the experimental approach and use a slight modification of the same computer code to reconstruct the object.
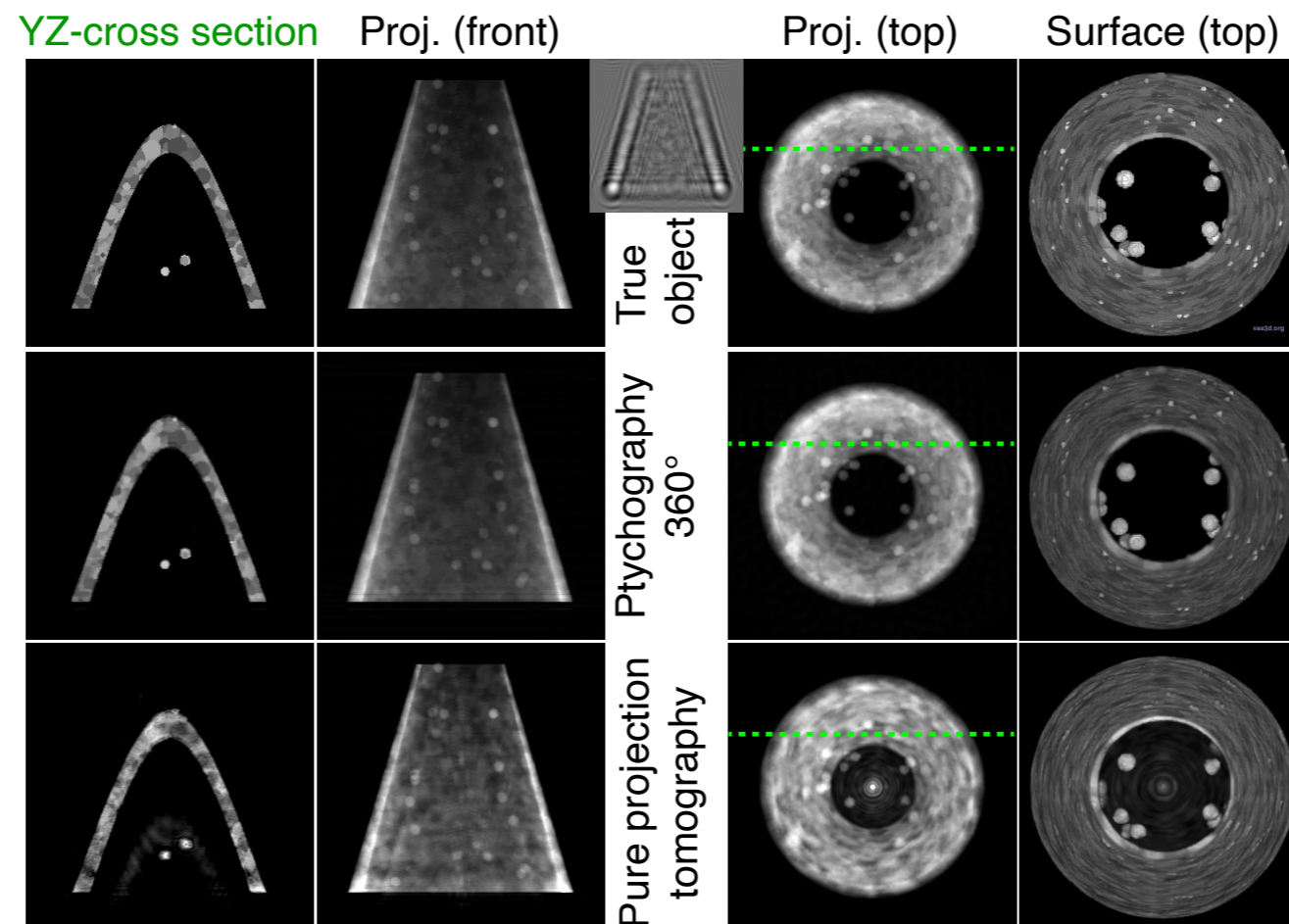
Poisson and Gaussian statistics

- Poisson distribution: if the average value over many, many tests is $\bar{n}$, what's the probability P of seeing n on one particular test?

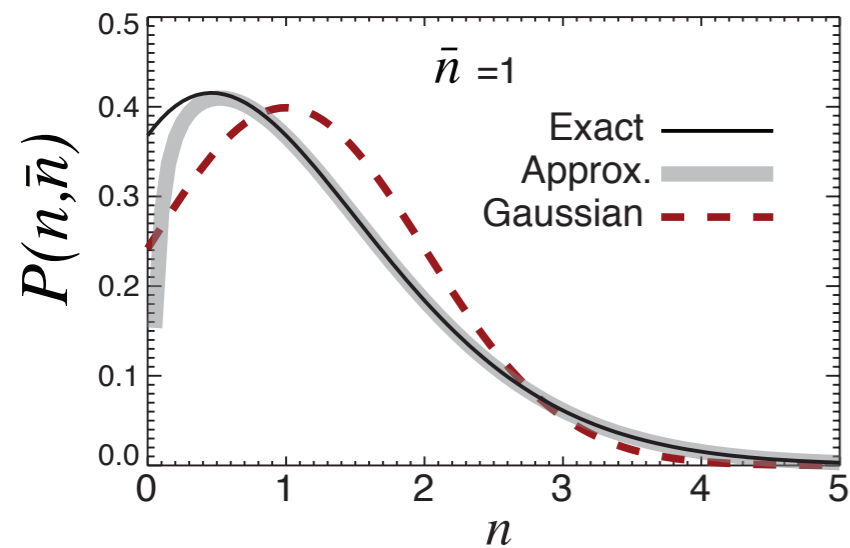$$P(n, \bar{n}) = \frac{\bar{n}^n}{n!} \exp(-\bar{n})$$

- Gaussian distribution: same meaning for $\bar{n}$, n, and P, but valid only for large $\bar{n}$:

$$P(n, \bar{n}) = \frac{1}{\sqrt{2\pi\bar{n}}} \exp\left[-\frac{(n - \bar{n})^2}{2\bar{n}}\right]$$

"Bell curve"

Comparing Poisson (exact) and Gaussian

- The Gaussian approximation works well for even very small values of $\bar{n}$
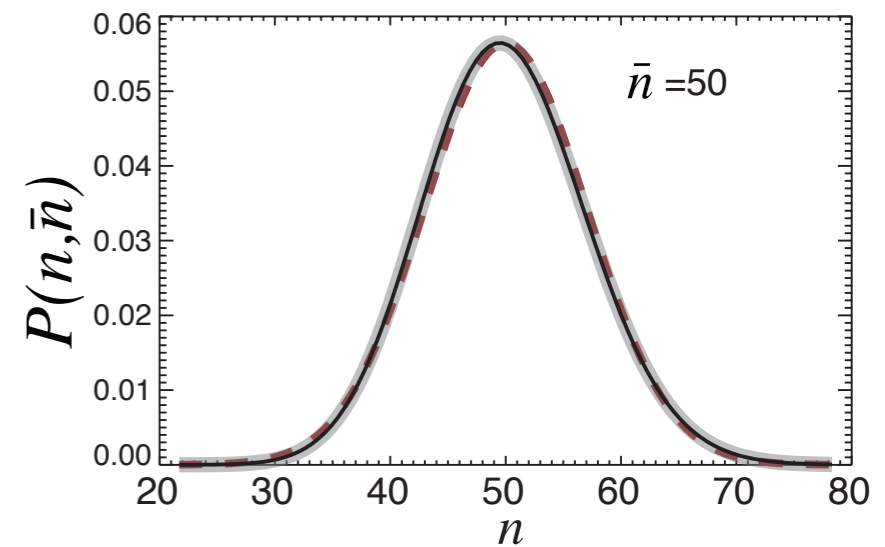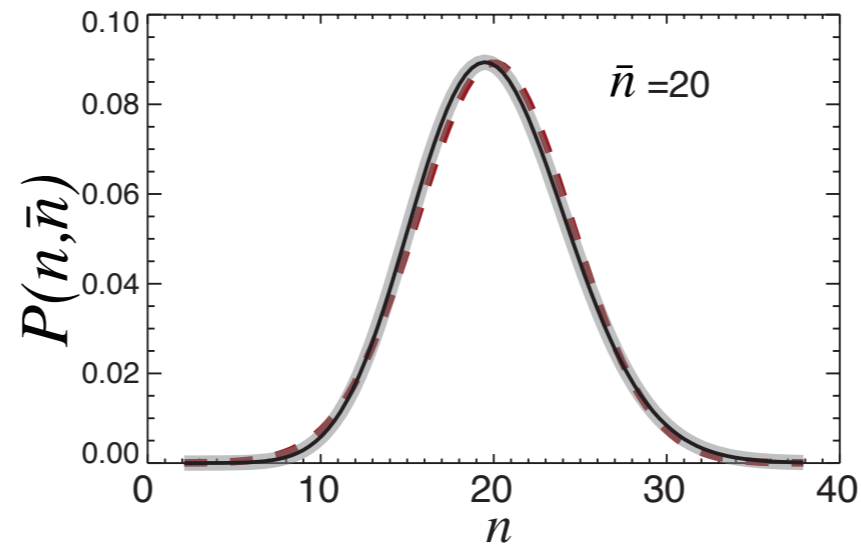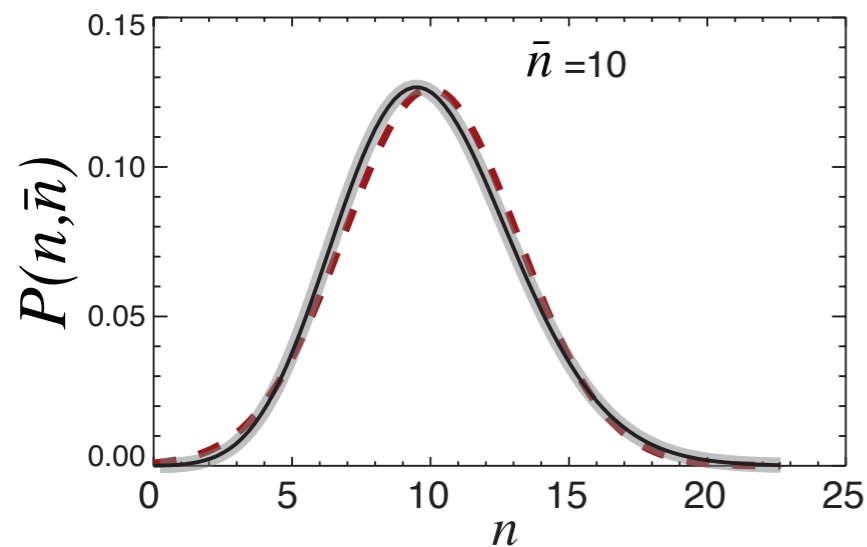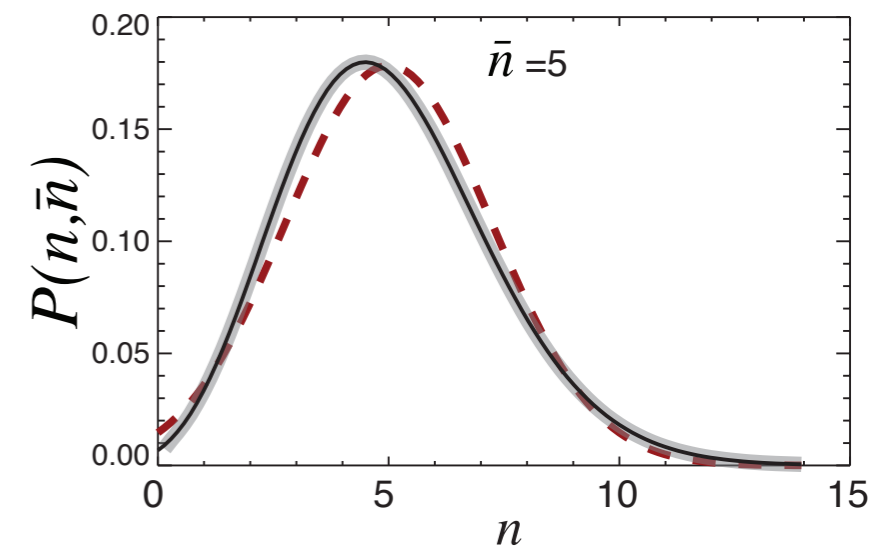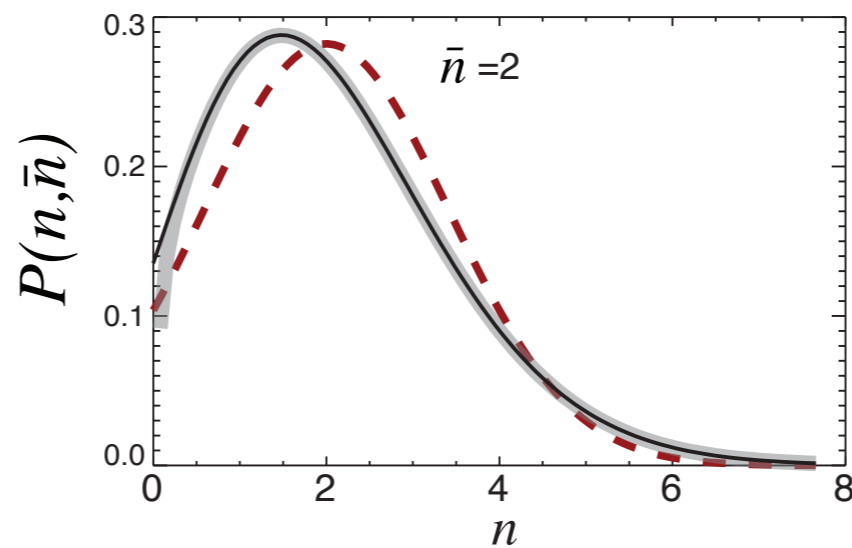
Signal to noise and required number of photons

- Simple statistics on $\bar{n}$ incident photons:

$$\mathrm{SNR} = \frac{\mathrm{Signal}}{\mathrm{Noise}} = \frac{\bar{n}|I_f - I_b|}{\sqrt{(\sqrt{\bar{n}}I_f)^2 + (\sqrt{\bar{n}}I_b)^2}} = \sqrt{\bar{n}}\frac{|I_f - I_b|}{\sqrt{I_f + I_b}} = \sqrt{\bar{n}}\Theta$$

where Θ=contrast parameter, I_f=intensity of feature, I_b=intensity of background. Also account for absorption in overlaying layers.
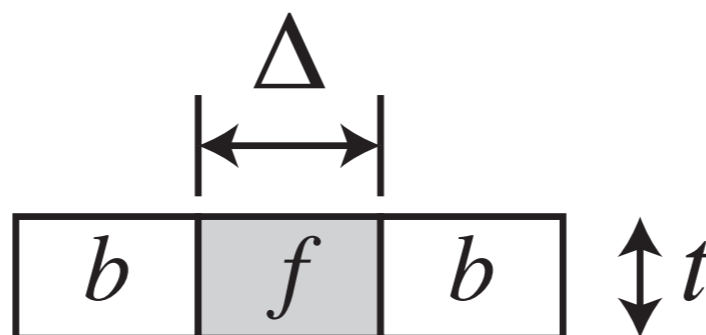
- Thus required number of incident photons $\bar{n}$ is

$$\bar{n} = \frac{\mathrm{SNR}^2}{\Theta^2}$$

- See e.g., Glaeser, *J. Ultrastruct. Res.* **36**, 466 (1971); Sayre *et al.*, *Ultramicroscopy* **2**, 337 (1977); Sayre *et al.*, *Science* **196**, 1339 (1977)

What about imaging in 3D?

- Rainer Hegerl and Walter Hoppe, *Zeitschrift für Naturforschung* **31**(a), 1717 (1976):

> A three-dimensional reconstruction requires the same integral dose as a conventional two-dimensional micrograph provided that the level of significance and the resolution are identical. The necessary dose D for one of the K projections in a reconstruction series is, therefore, the integral dose divided by K.
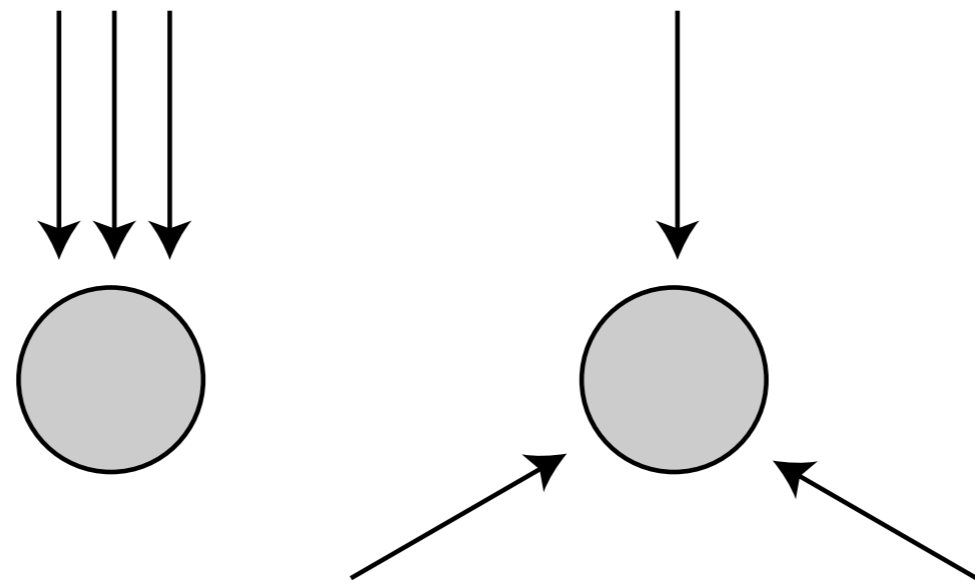
- Originally controversial; now embedded in practice of single particle electron microscopy, medical x-ray tomography.

Calculating dose

- SI units for ionizing radiation: 1 Gray=1 J/kg=100 rad

- Lambert-Beer law with inverse absorption length µ(=1.3 mm for protein at 8.98 keV):

$$I = I_0 e^{-\mu x} \qquad \text{with} \qquad \mu = 2\frac{\rho N_A}{A} r_e \lambda f_2$$

- Energy per thickness with inverse absorption length µ:

$$\frac{dE}{dx} = h\nu \, \frac{dI}{dx} = h\nu \, \mu \, I_0 e^{-\mu \cdot 0} = I_0 \, h\nu \, \mu$$

- Energy per mass (note: I0 is effectively n̄):

$$\frac{dE}{dm} = \frac{dE}{dx}\frac{1}{\text{Area} \cdot \rho} = h\nu \, \mu \, I_0 \frac{1}{\text{Area} \cdot \rho} = h\nu \, \frac{I_0 \mu}{\text{Area} \cdot \rho}$$

Dose numbers

- G factor: number of bonds broken per 100 eV. G~5 for many organic molecules (room temp.)

- Quick estimate to break 1 bond per atom:

$$\frac{(20 \text{ eV/atom}) \cdot (N_A \text{ atoms/mol}) \cdot (1.6 \times 10^{-19} \text{ J/eV})}{(12 \text{ g/mol}) \cdot (10^{-3} \text{ kg/g})} = 1.6 \times 10^8 \text{ Gray}$$

- Representative dose in crystallography:

$$\frac{10^{14} \text{ photons}}{(50 \ \mu\text{m})^2} \frac{(8979 \text{ eV/photon}) \cdot (1.6 \times 10^{-19} \text{ J/ev})}{(1300 \ \mu\text{m}) \cdot (1.35 \text{ g/cm}^3) \cdot (10^{-4} \text{ cm}/\mu\text{m})^3 \cdot (10^{-3} \text{ kg/g})} = 3.3 \times 10^7 \text{ Gray}$$

- "Henderson limit" [Henderson, *Q. Rev. Biophys.* **28**, 171 (1995)]: 2×10^7 Gray is when diffraction spots fade.

- X-ray microscopy: doses of 10^6-10^8 Gray are common, depending on resolution

Dose versus resolution for transmission x-ray imaging

• Calculation of radiation dose using best of phase, absorption contrast and 100% efficient imaging
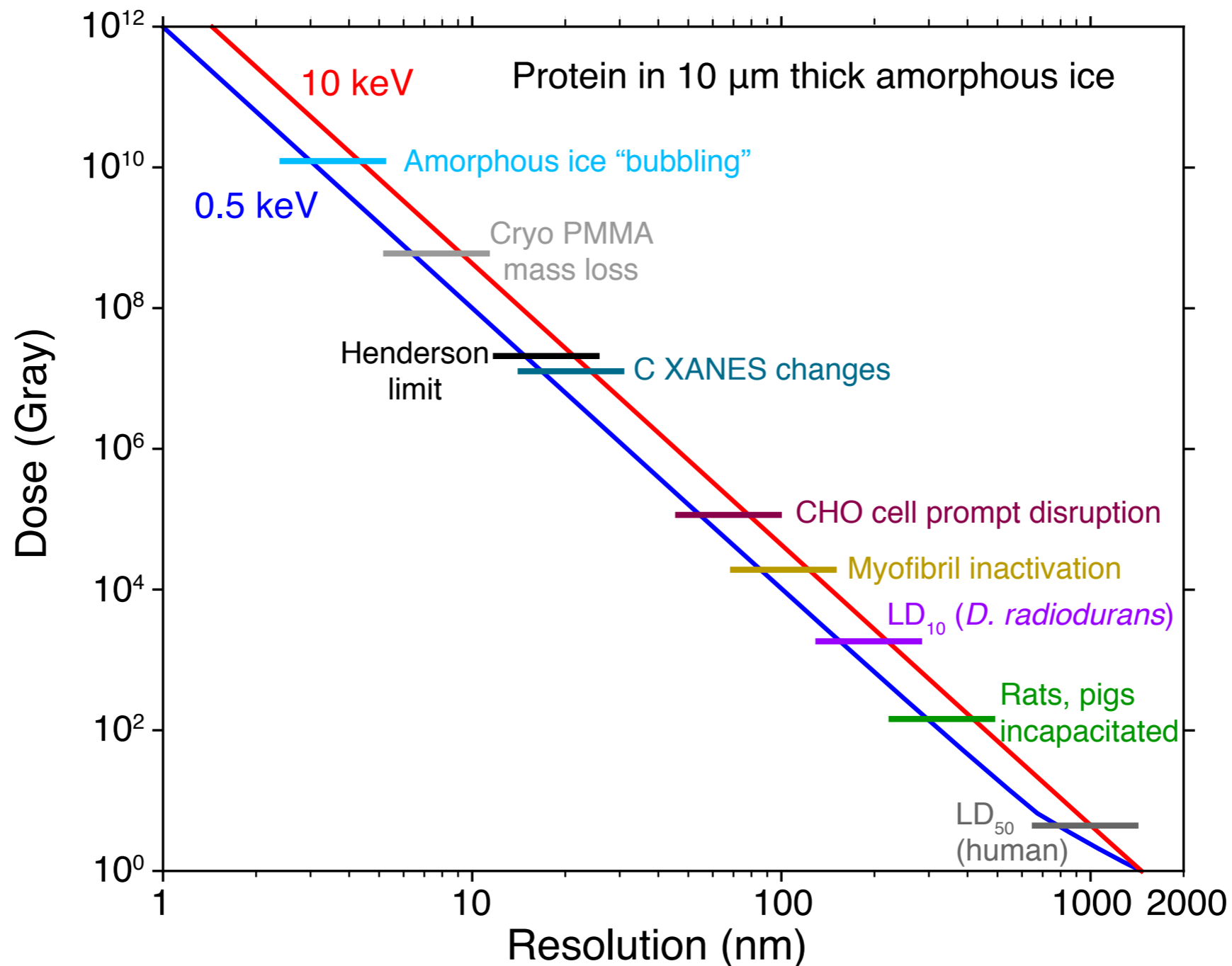
Du and Jacobsen, *Ultramicroscopy* **184**, 293-309 (2018).

X-ray and electron microscopy are complementary

10 nm resolution phase contrast imaging of protein in ice

10 keV "hard" X rays

500 eV "soft" X rays

(no energy filter)

(energy filter)

300 keV electrons
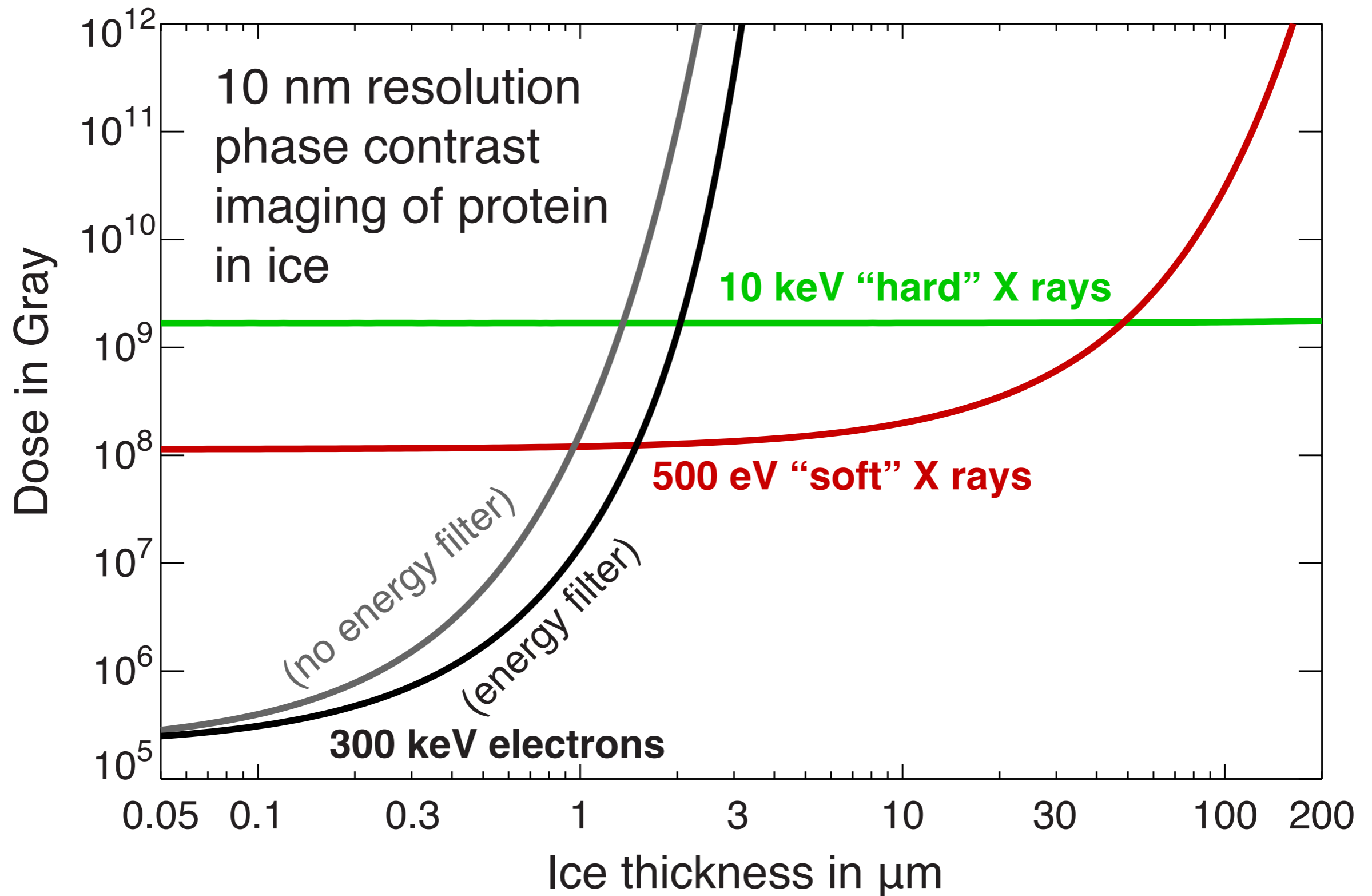
Ming Du and Chris Jacobsen, *Ultramicroscopy* **184**, 293-309 (2018). doi:10.1016/j.ultramic.2017.10.003

X-ray microscopy of initially living cells

- Radiation dose in high resolution x-ray, electron microscopy is ~10^6-10^8 Gray

- 5 Gray (really 5 Sievert) kills people!

- Chinese hamster ovarian (CHO) fibroblasts in culture medium with periodic reflow.

- "Red for dead" fluorescent dyes used to confirm viability over hours with no x-ray exposure.

- Imaged in a soft x-ray scanning transmission microscope (NSLS X1A)
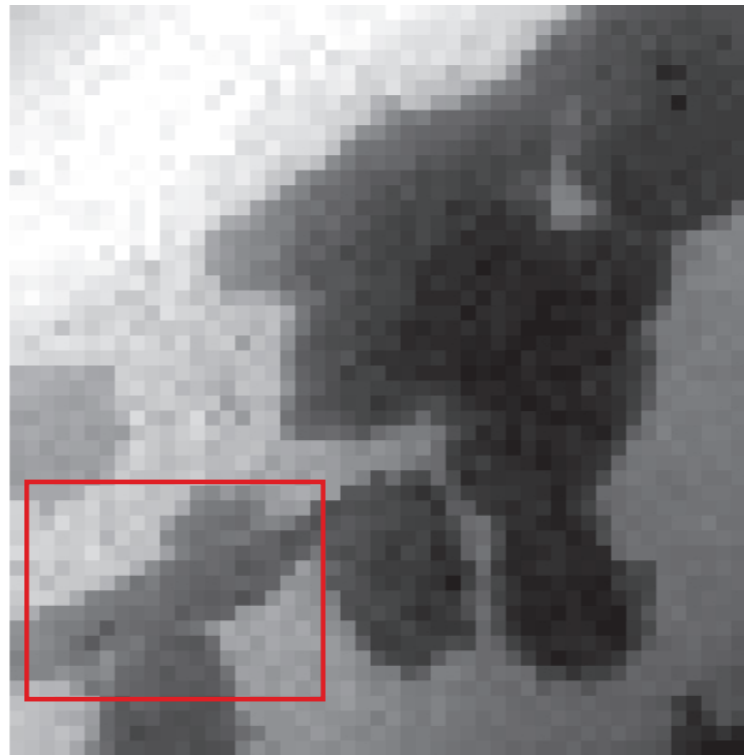
Experiment by V. Oehler, J. Fu, S. Williams, and C. Jacobsen, Stony Brook using specimen holder developed by Jerry Pine and John Gilbert, CalTech. In Kirz, Jacobsen, and Howells, *Quarterly Reviews of Biophysics* **28**, 33 (1995).

▬ 10 μm
6.0×10^2 Gray, ET=2 minutes

1 Gray=1 Joule/kg absorbed
1 Sievert=1 Gray•RBE (relative biological effectiveness of radiation type)
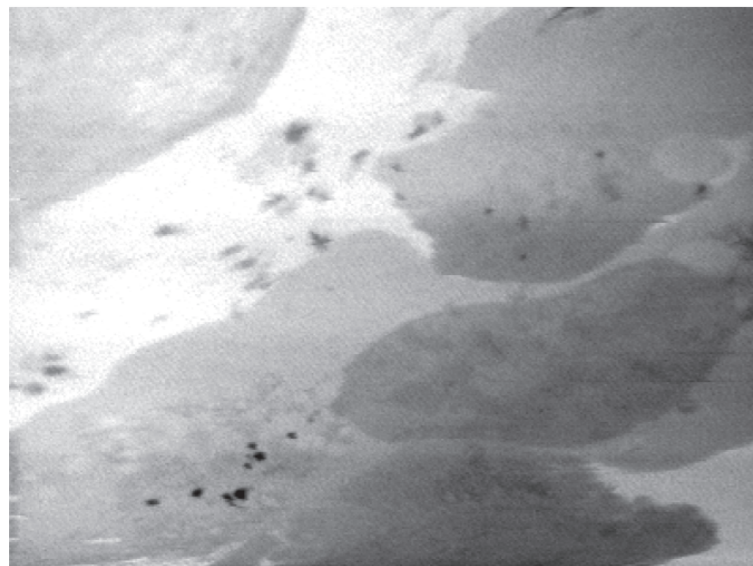
▬ 5 μm
1.2×10^5 Gray, ET=9.5 min
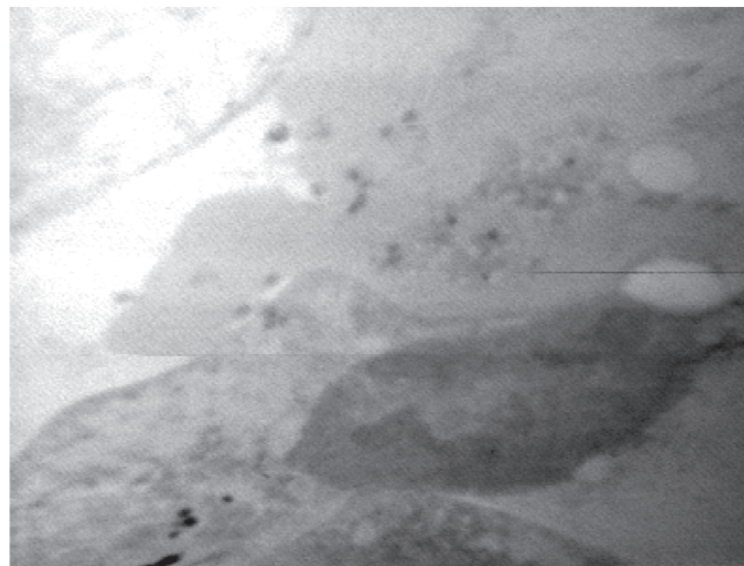
▬ 5 μm
2.4×10^5 Gray, ET=17 min
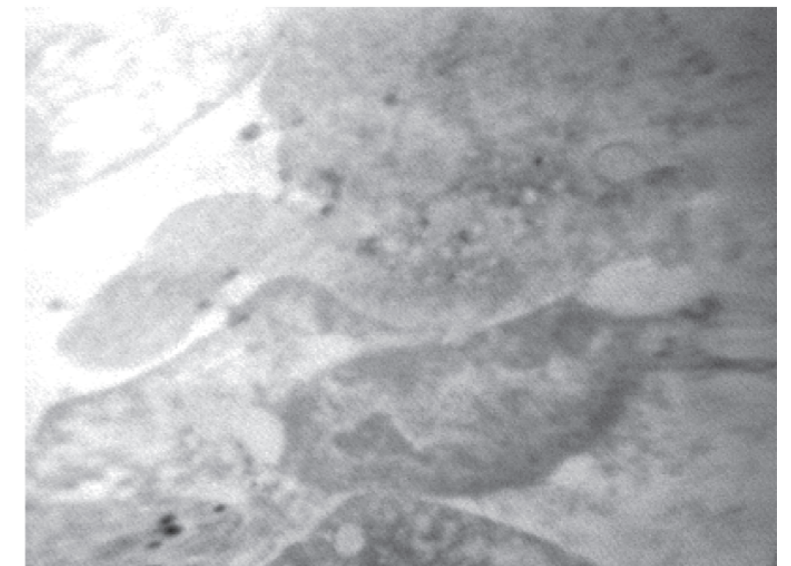
▬ 5 μm
3.7×10^5 Gray, ET=24.5 min

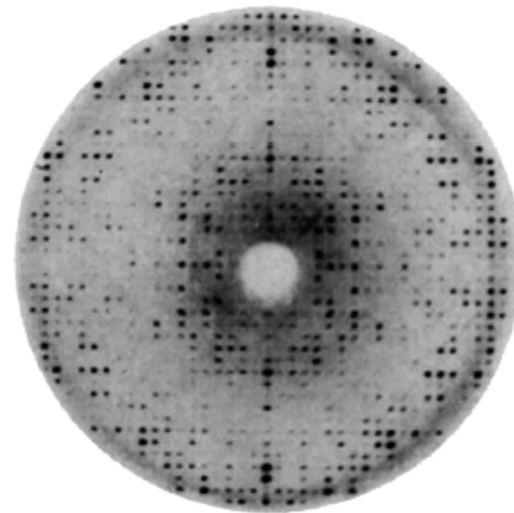# Wet, fixed samples: one image is OK

- Chromosomes are among the most sensitive specimens.
- *V. faba* chromosomes fixed in 2% glutaraldehyde. S. Williams *et al.*, *J. Microscopy* **170**, 155 (1993)
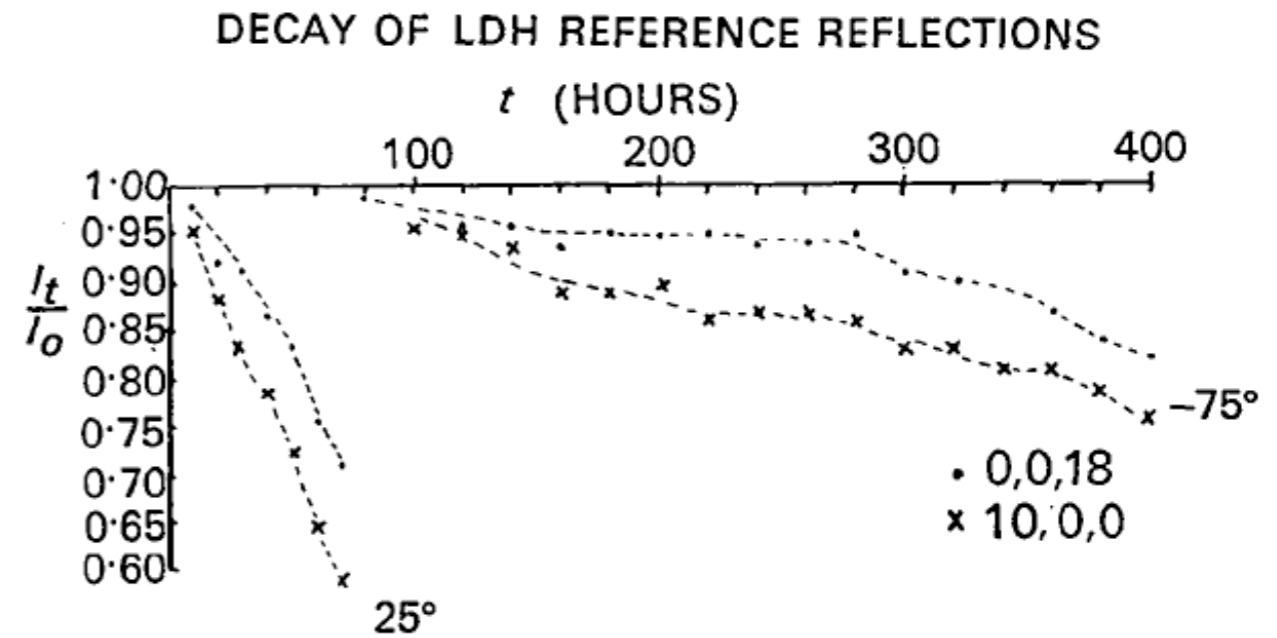- Repeated imaging of one chromosome shows mass loss, shrinkage

Mutiple images: previous dose in Gray

0 $3.5 \cdot 10^5$ $1.4 \cdot 10^6$ $2.4 \cdot 10^6$

5 μm
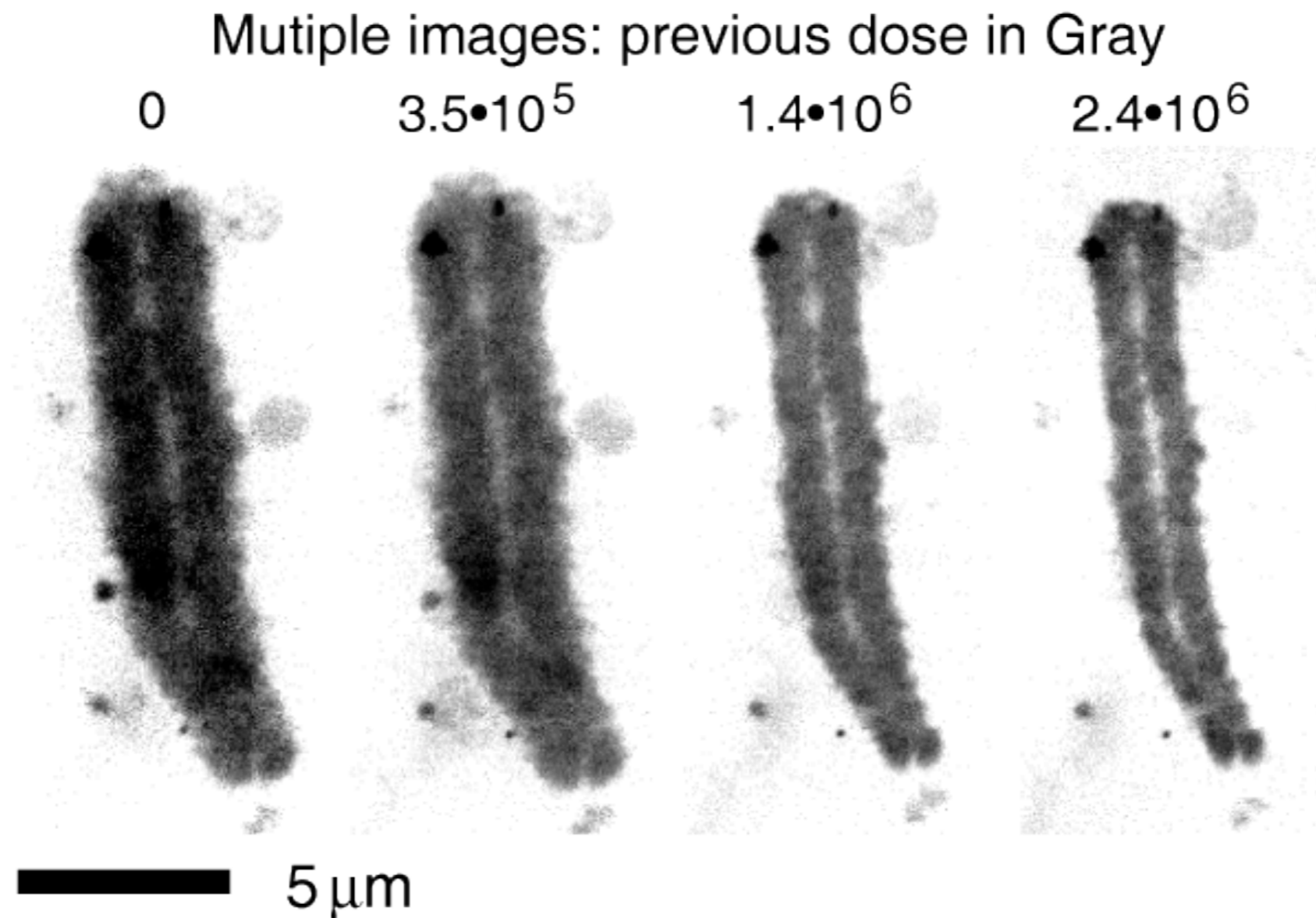
Cryo crystallography

25°C

-75°C

DECAY OF LDH REFERENCE REFLECTIONS

t (HOURS)

$\frac{I_t}{I_0}$

• 0,0,18
× 10,0,0

−75°

25°
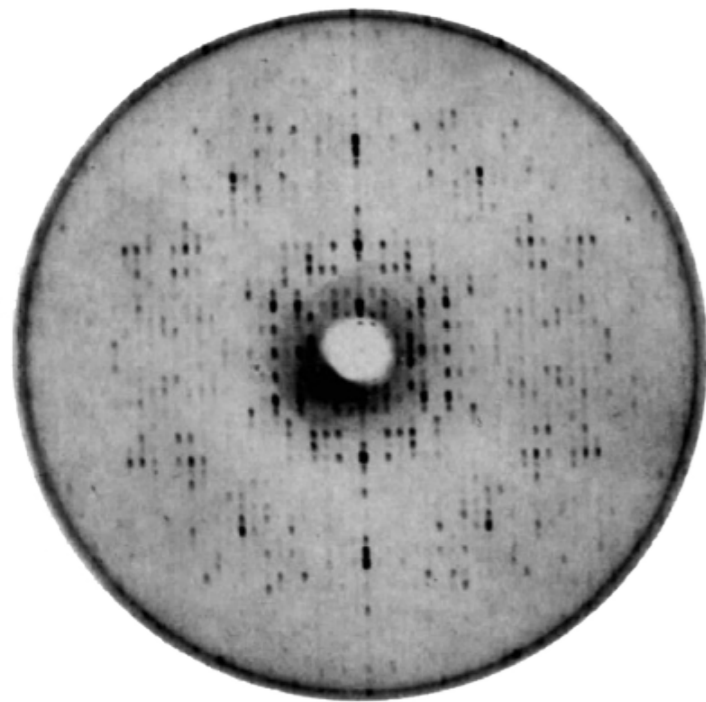
Fig. 5. The ratio I_t/I_0 for two reference reflections plotted as a function of exposure time for a typical native and frozen crystal. I_t represents the intensity at time t. Results for 0,0,18 and 10,0,0 are shown with dots and crosses respectively.
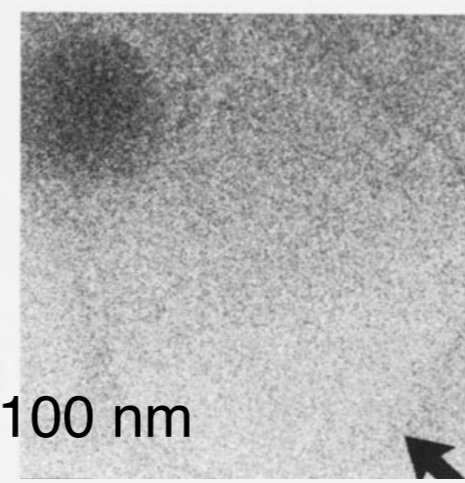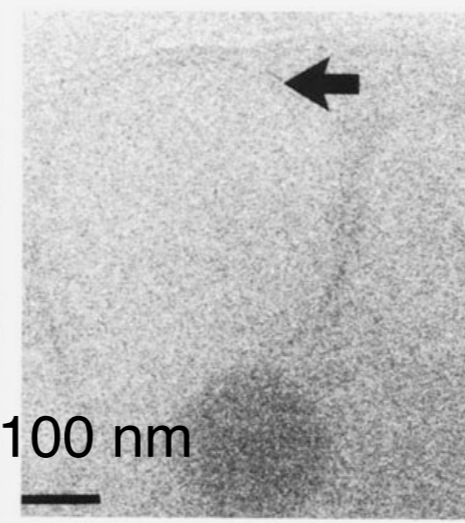
Crystallographic Studies on Lactate Dehydrogenase at -75°C

BY DAVID J. HAAS* AND MICHAEL G. ROSSMANN

Crystals of lactate dehydrogenase (LDH) were frozen by equilibration in a sucrose–ammonium sulfate solution, and then dipping into liquid nitrogen. The rate of radiation damage for frozen crystals was tenfold less than for crystals at room temperature. The physical properties of frozen crystals are discussed. Analysis of 3·5 Å data collected at −75°C for native LDH and two heavy atom derivatives showed that these derivatives retained their isomorphism in the frozen state.

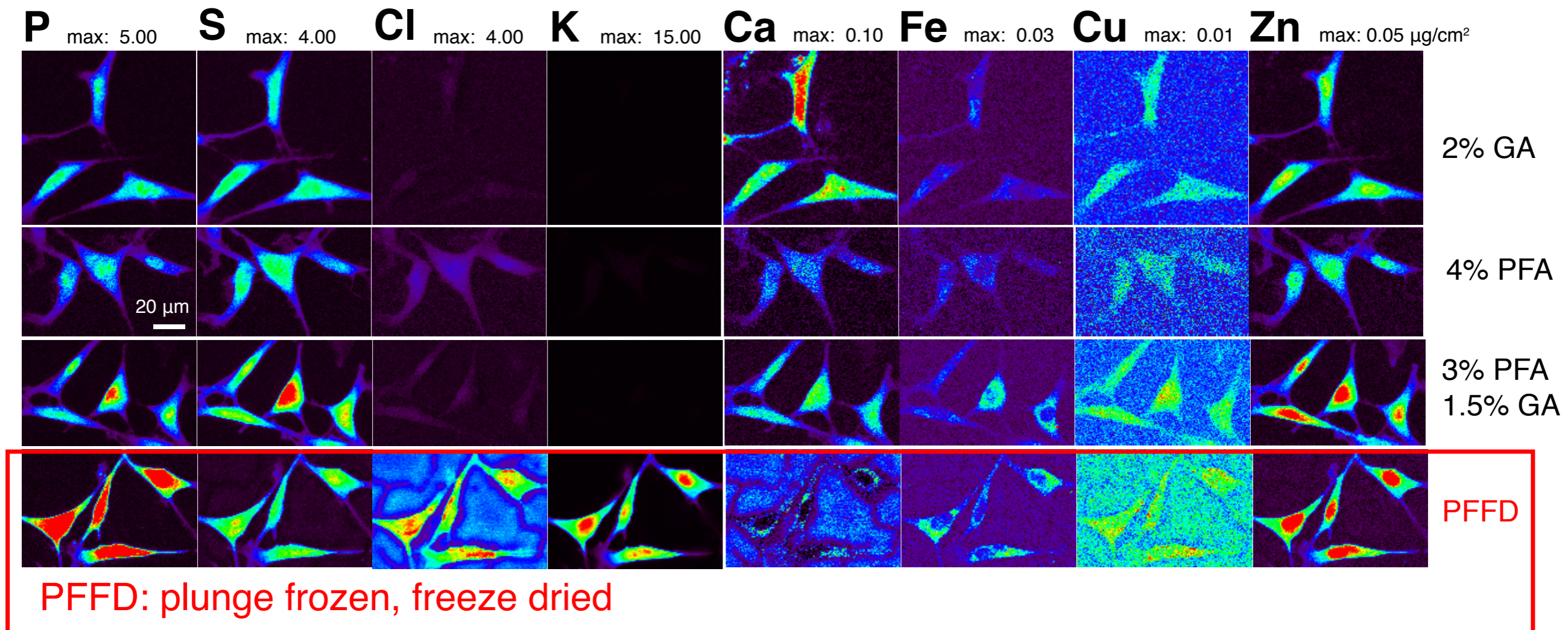See also Low, Chen, Berger, Singman, and Pletcher, *PNAS* **56**, 1746 (1966)

A

100 nm
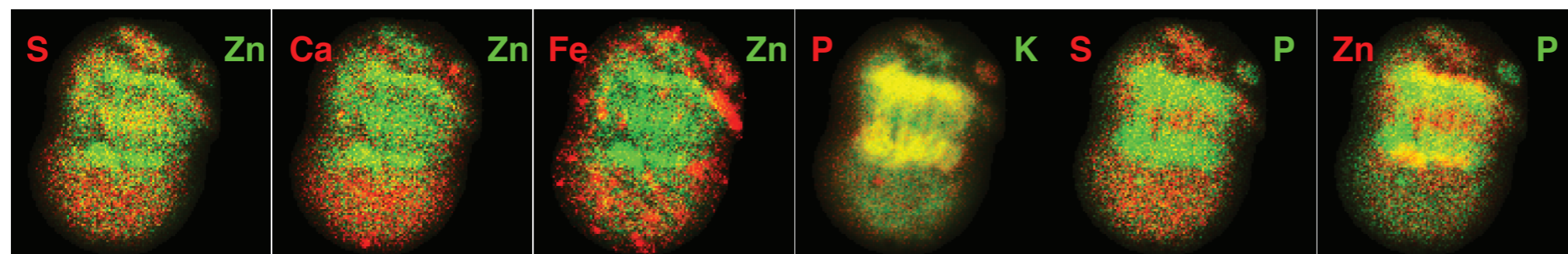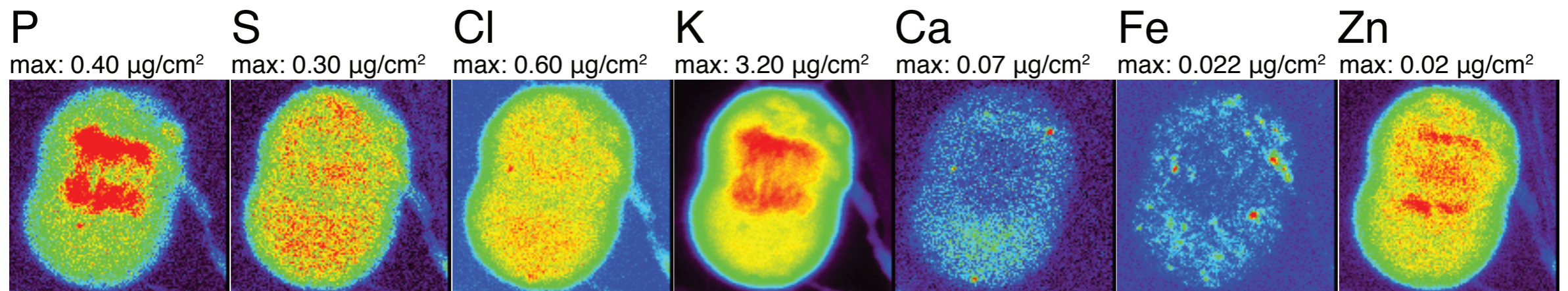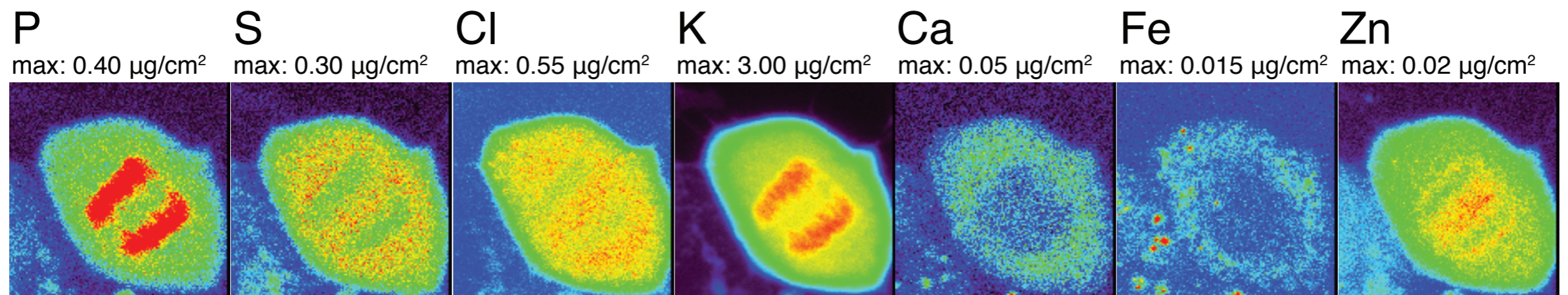
100 nm
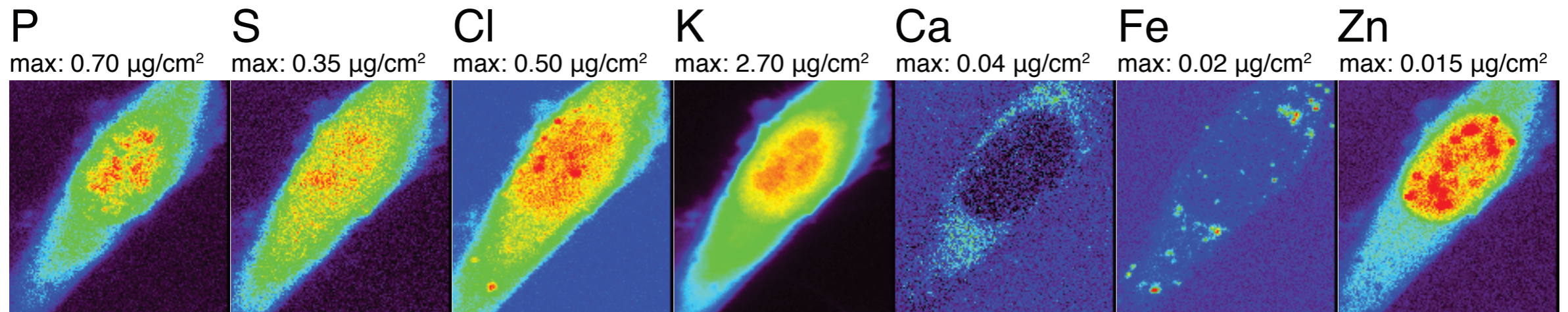
1 μm

B

1 μm

500 nm

Frozen hydrated

- Human blood platelets
- 1 MeV transmission electron microscope (JEOL-1000)
- O'Toole, Wray, Kremer, and McIntosh, *J. Struct. Bio.* **110**, 55 (1993)
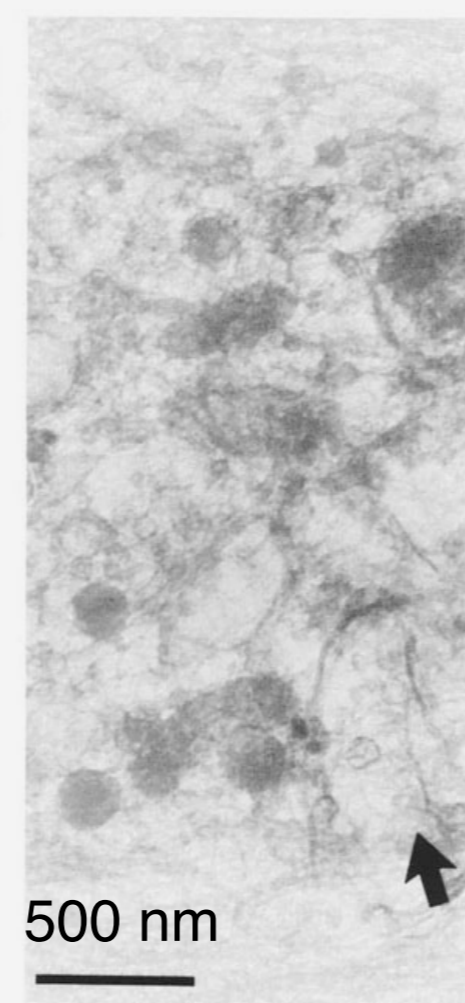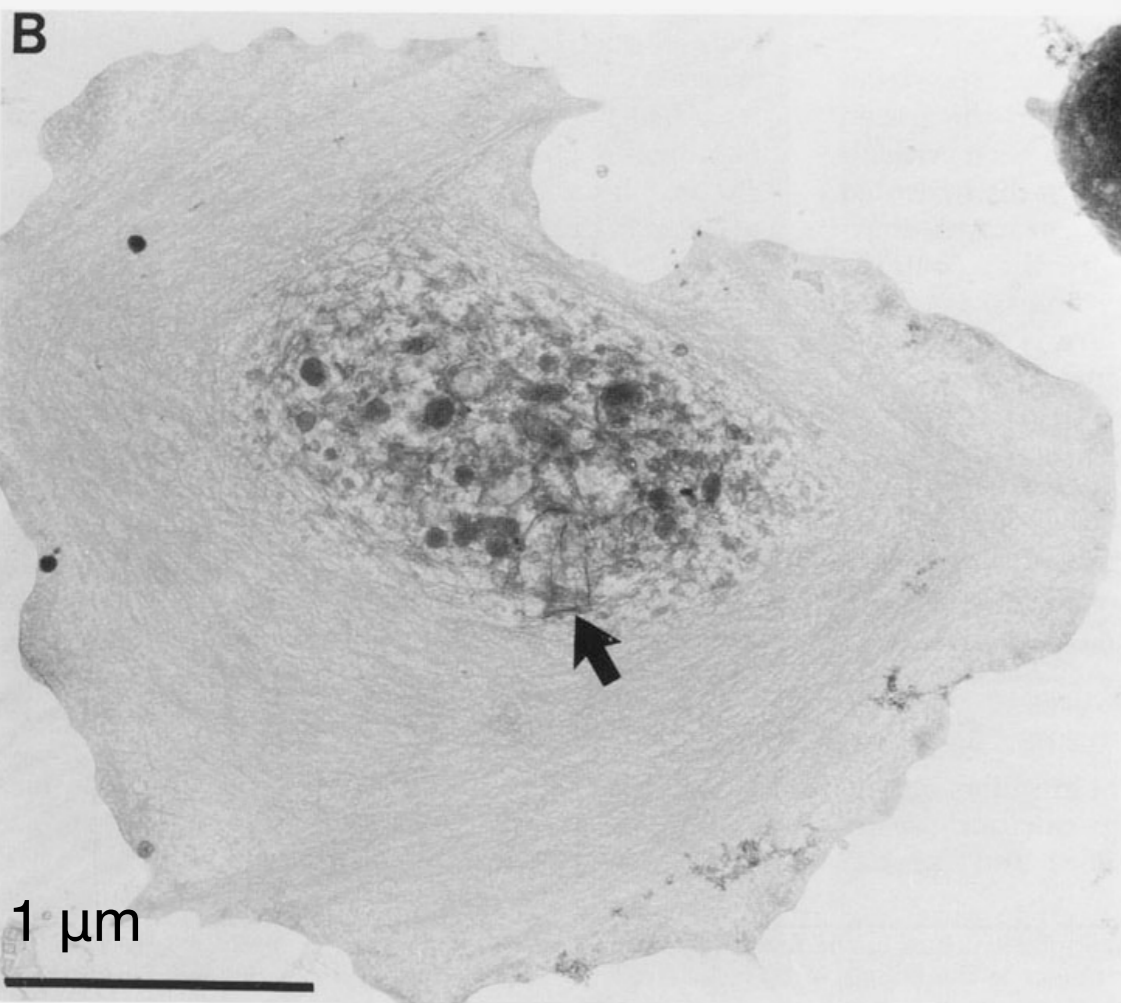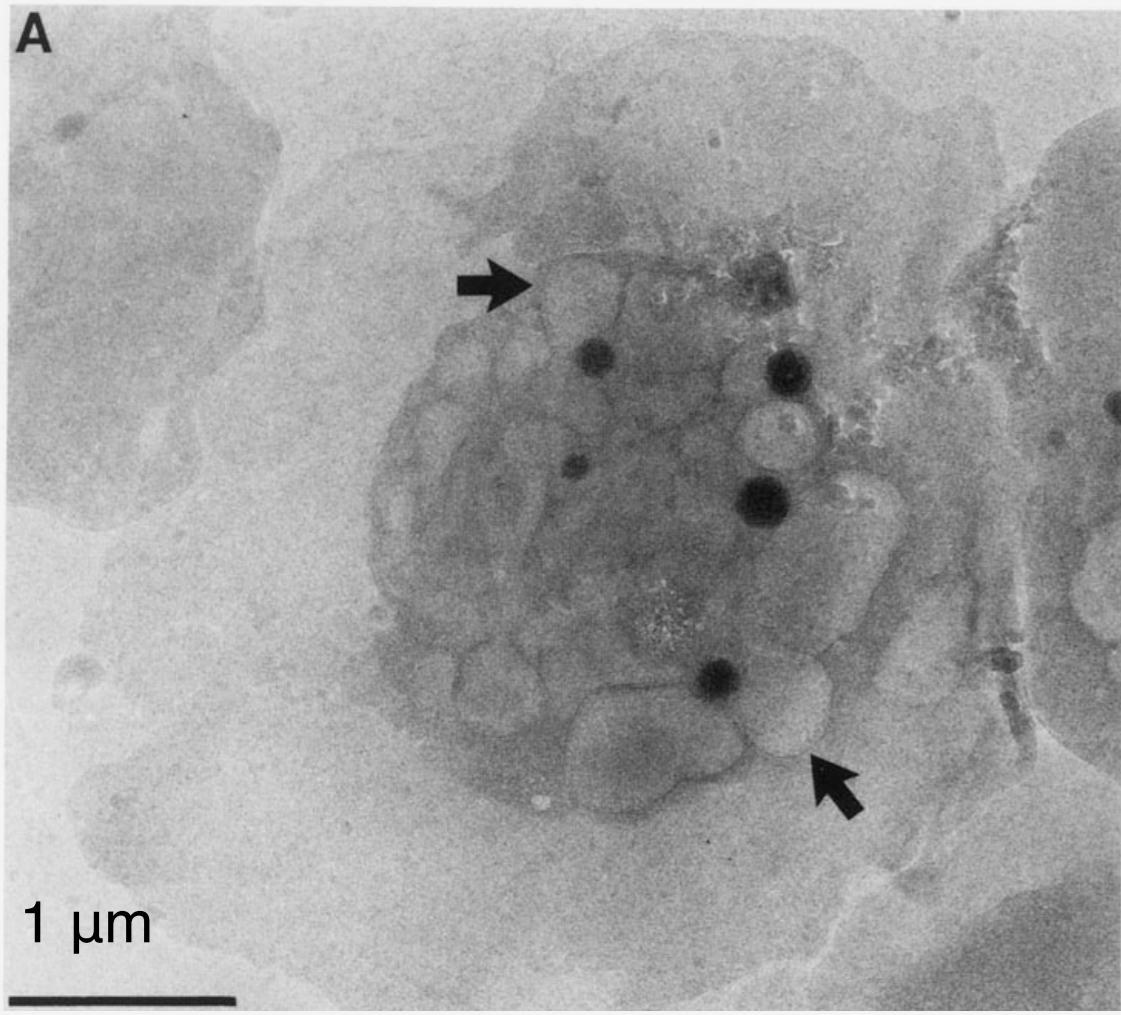
2% glutaraldehyde fix
1% OsO$_4$ postfix
critical-point dry

Cryo preservation keeps chemistry intact

- Jin, Paunesku, Lai, Gleber, Chen, Finney, Vine, Vogt, Woloschak, and Jacobsen, *J. Microscopy* **265**, 81 (2017).

- See also Perrin, Carmona, Roudeau, and Ortega, *J. Analyt. Atom. Spectr.* **30**, 2525 (2015).

Metals in cell division

P max: 0.70 µg/cm²	S max: 0.35 µg/cm²	Cl max: 0.50 µg/cm²	K max: 2.70 µg/cm²	Ca max: 0.04 µg/cm²	Fe max: 0.02 µg/cm²	Zn max: 0.015 µg/cm²
P max: 0.40 µg/cm²	S max: 0.30 µg/cm²	Cl max: 0.55 µg/cm²	K max: 3.00 µg/cm²	Ca max: 0.05 µg/cm²	Fe max: 0.015 µg/cm²	Zn max: 0.02 µg/cm²
P max: 0.40 µg/cm²	S max: 0.30 µg/cm²	Cl max: 0.60 µg/cm²	K max: 3.20 µg/cm²	Ca max: 0.07 µg/cm²	Fe max: 0.022 µg/cm²	Zn max: 0.02 µg/cm²

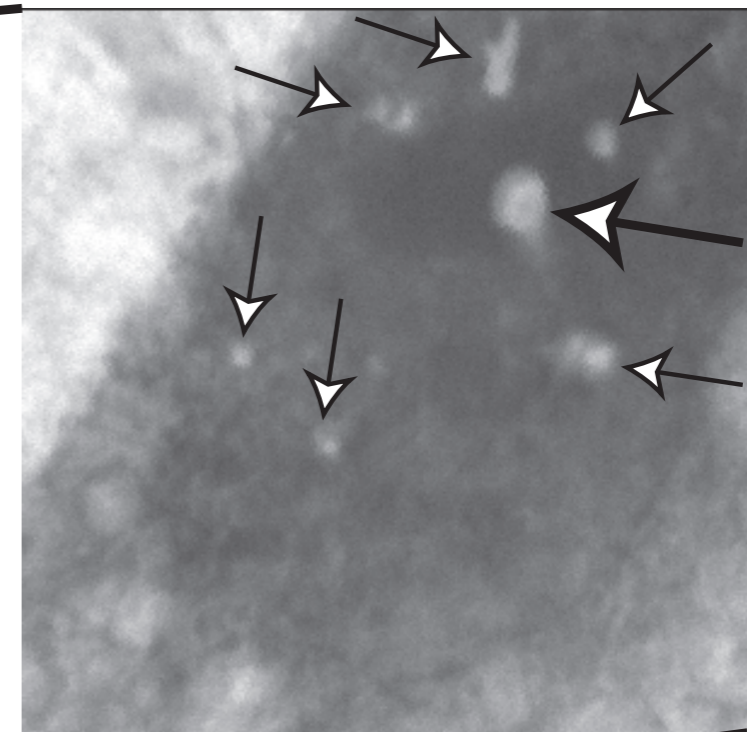S Zn   Ca Zn   Fe Zn   P K   S P   Zn P

Qiaoling Jin, Everett Vacek,
Si Chen, Barry Lai,
Tom O'Halloran, Chris Jacobsen

Radiation damage resistance in cryo microscopy

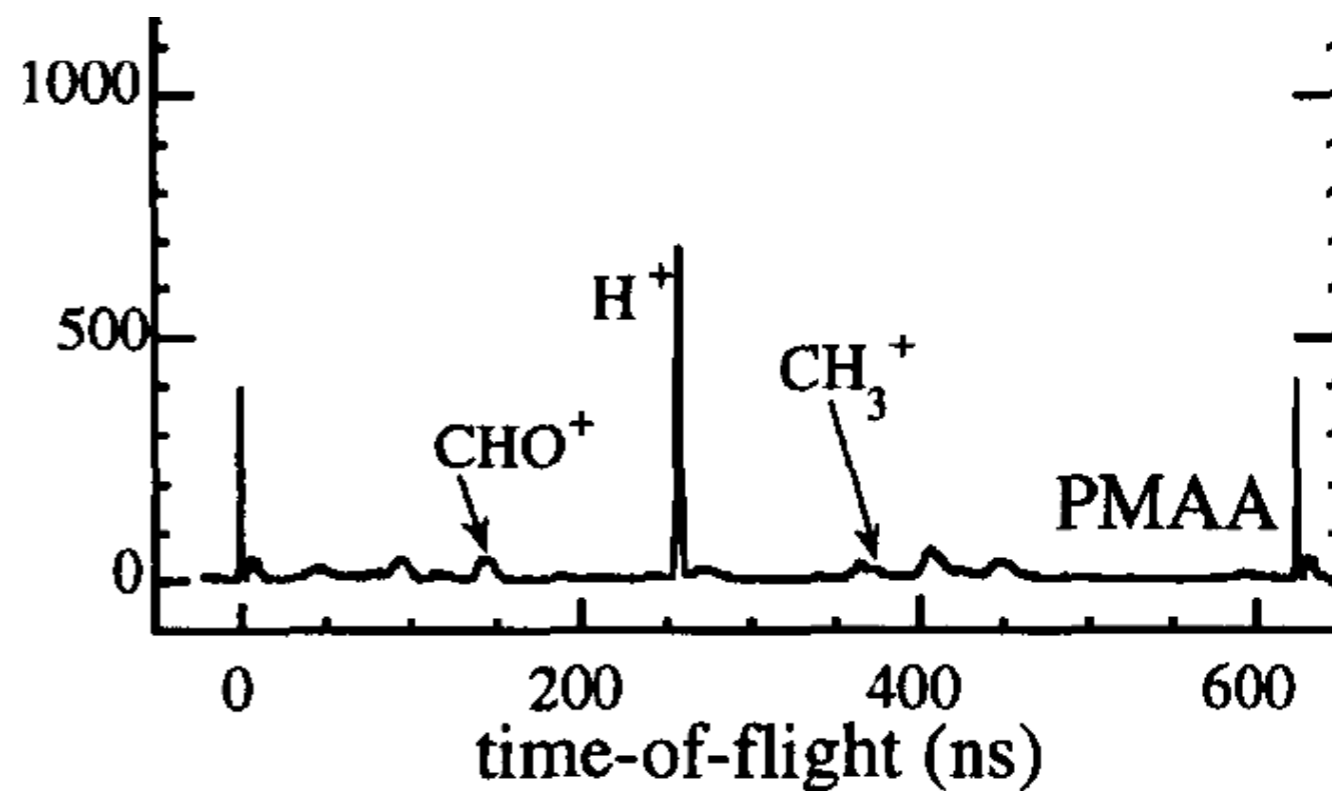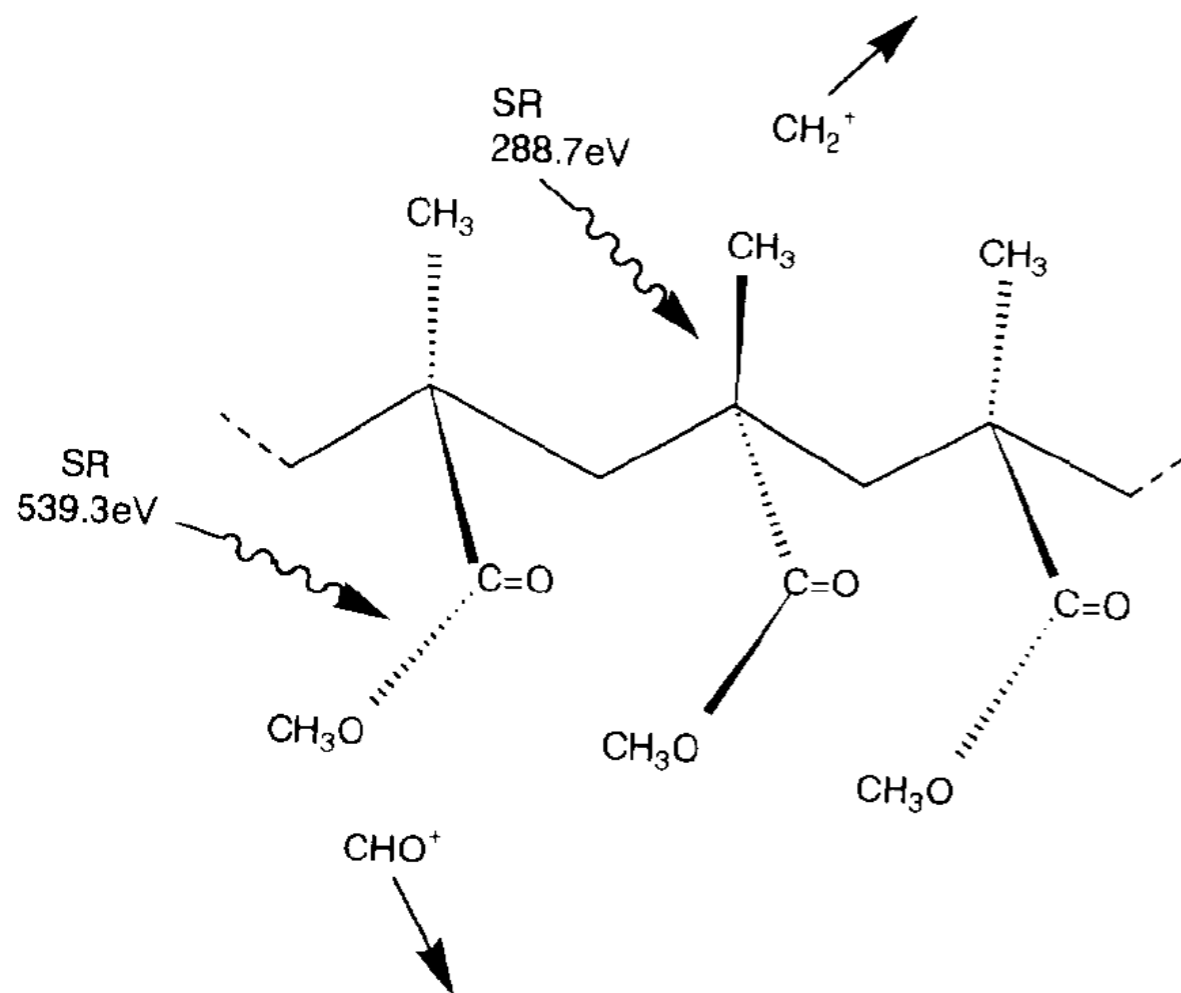Frozen hydrated fibroblast image after exposing
several regions to ~10^{10} Gray
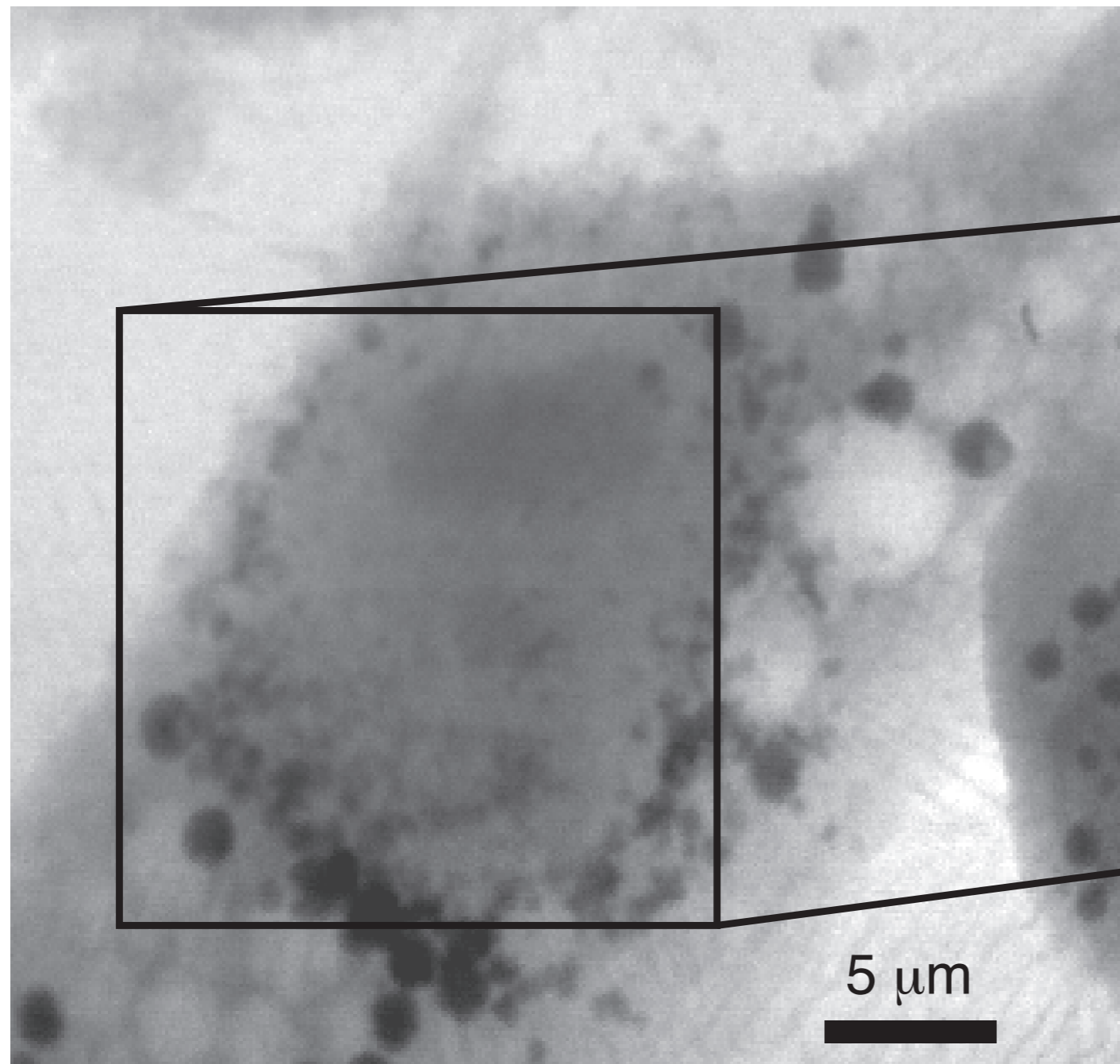
After warmup in microscope
(eventually freeze-dried): holes
at irradiated regions!

5 μm

Maser *et al.*, *J. Micros.* **197**, 68 (2000)

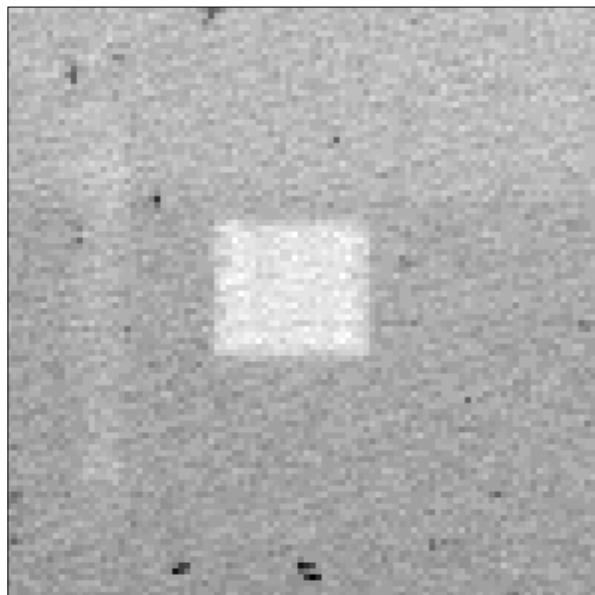# Radiation damage studies: poly (methyl methacrylate) or PMMA

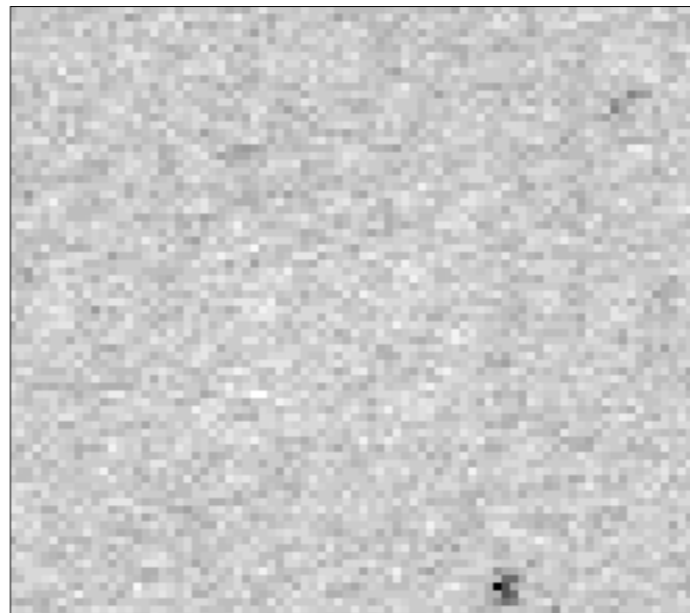Tinone *et al., Appl. Surf. Sci.* **79**, 89 (1994)

Tinone *et al., J. Electron Spect. Rel. Phen.* **80**, 117 (1996).
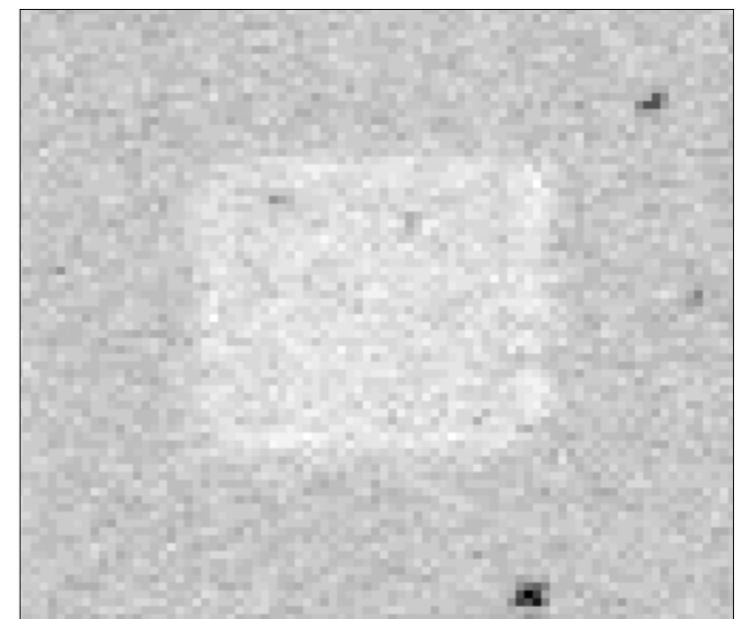
PMMA at room, LN2 temperature

- Beetz and Jacobsen, *J. Synchrotron Radiation* **10**, 280 (2003)
- Repeated sequence: dose (small step size, long dwell time), spectrum (defocused beam)
- Images: dose region (small square) at end of sequence

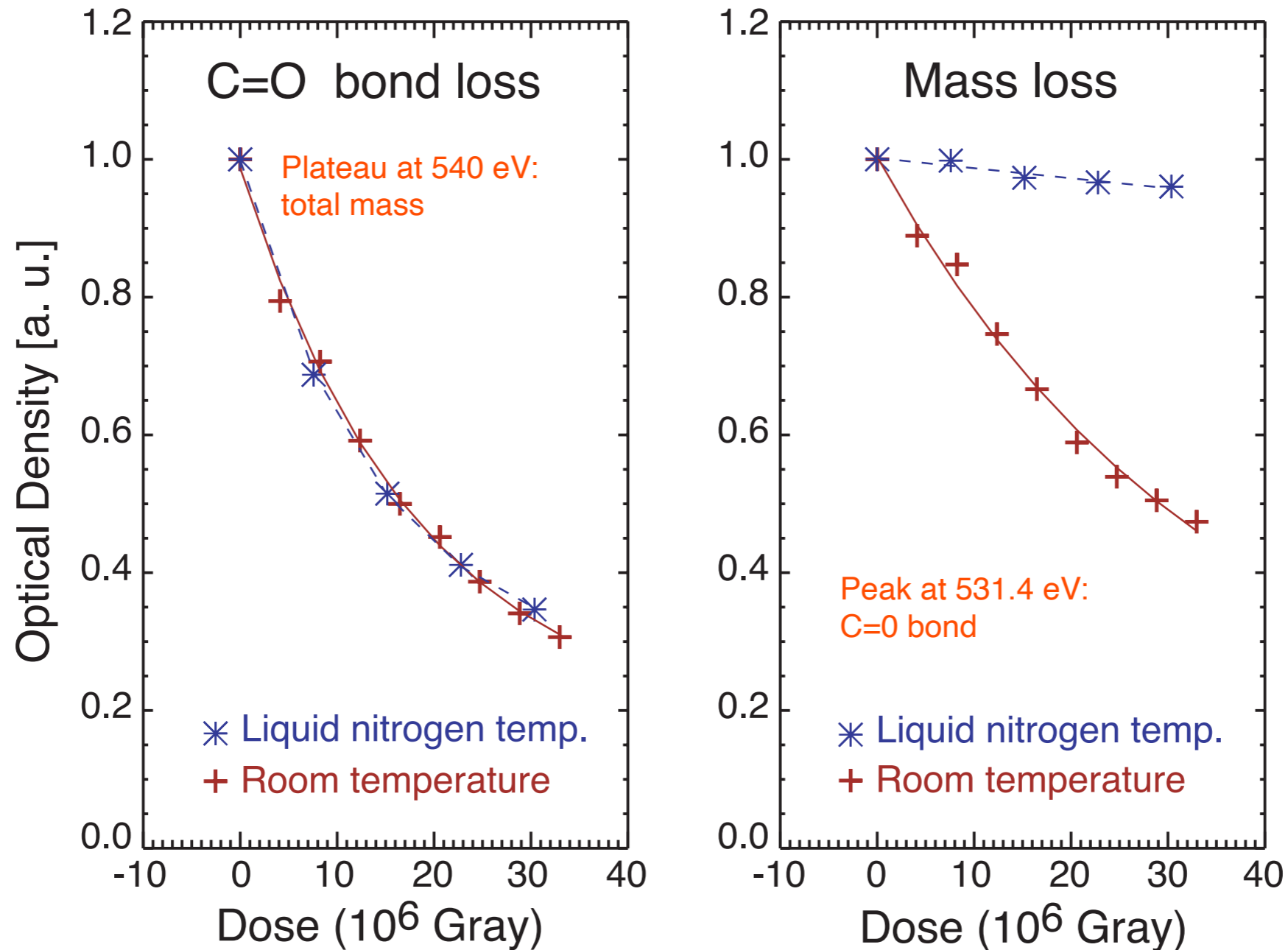Room temperature: mass loss immediately visible

LN$_2$ temperature: no mass loss immediately visible

After warm-up: mass loss becomes visible

PMMA at 300 K and 110 K: chemistry and mass

LN$_2$ temp: protection against mass loss, but not against breaking bonds (at least C=O bond in dry PMMA)

Beetz and Jacobsen, *J. Synchrotron Radiation* **10**, 280 (2003)

The Ramen noodle model of radiation damage

Macromolecular chains with no "encapsulating" matrix
(dry, room temperature wet)

The Ramen noodle model of radiation damage

Macromolecular chains in an "encapsulating" matrix
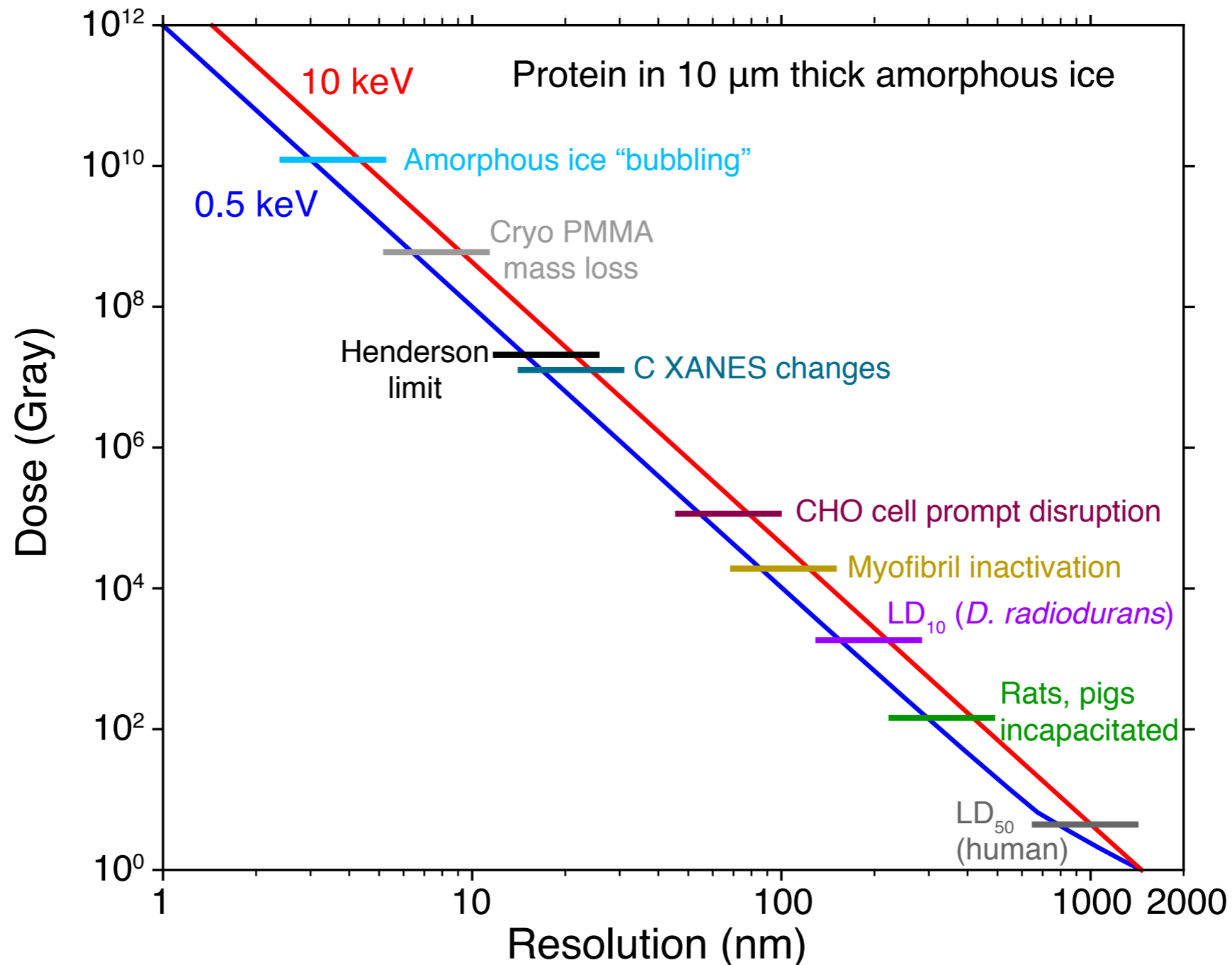(frozen hydrated)

The Ramen noodle model of radiation damage

Actual noodles *were* harmed during the filming of this movie

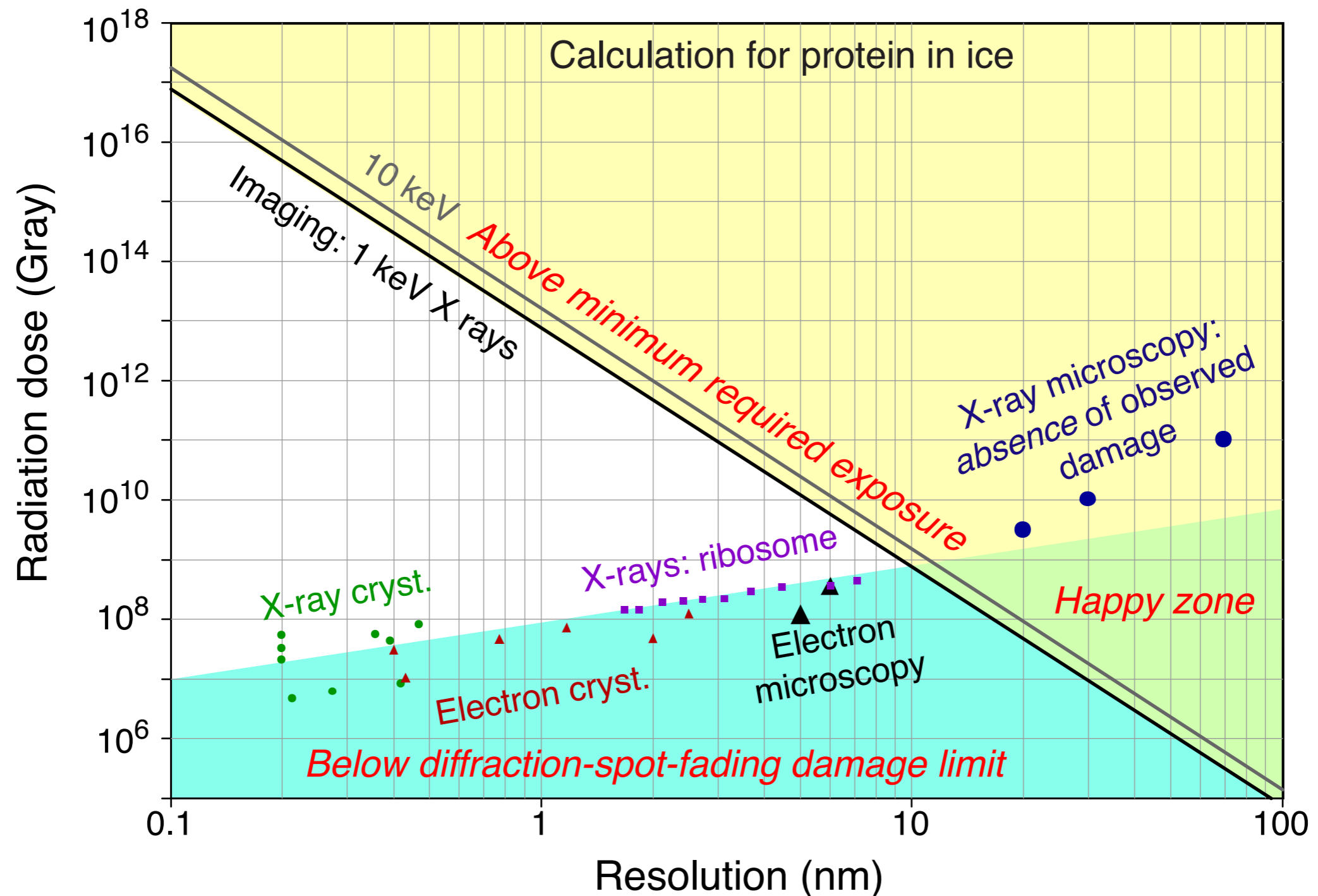# Dose versus resolution for transmission x-ray imaging

- Calculation of radiation dose using best of phase, absorption contrast and 100% efficient imaging

Du and Jacobsen, *Ultramicroscopy* **184**, 293-309 (2018).

Achievable resolution?

- Howells *et al., J. Electron Spectroscopy and Related Phenomena* **170**, 4 (2009)

Lecture feedback:

https://forms.office.com/g/wTcKEdinUZ

NXS Lecture - Chris Jacobson: "X-ray Imaging"